A STUDY OF DENSITY FLUCTUATIONS OF PARTICLES PRODUCED IN SI-EMULSION COLLISIONS AT 14.6 AGeV

ABSTRACT

THESIS

SUBMITTED IN PARTIAL FULFILMENT OF THE REQUIREMENTS
FOR THE AWARD OF THE DEGREE OF

Doctor of Philosophy

IN

PHYSICS

BY

MALIK MOHIB-UL-HAQ

Under the Supervision of

DR. RASHID HASAN

DEPARTMENT OF PHYSICS
ALIGARH MUSLIM UNIVERSITY
ALIGARH (INDIA)

2003

Relativistic heavy ion collisions are being studied with the intention of investigating the properties of hot, ultra-dense and strongly interacting matter. Theoretical physics demonstrates that the collisions of these high energy nuclei with target material may provide us matter with high temperature and energy density. This in turn may lead to a new phase of matter known as quark gluon plasma (QGP), which is expected to have existed in the early universe and be present in the heart of neutron stars. Although this field has seen a lot of activity during the last decade, no consensus could be built till date. It has, however, been demonstrated that in order to find unambiguous signals regarding the processes involved in such relativistic collisions, it is essential to have a clear understanding of the multiparticle production and fragmentation processes in these collisions.

It has been suggested that the QGP formation could cause large fluctuations in phase space, which in turn may result in large fluctuations in the measured particle densities. In order to disentangle information regarding these dynamical fluctuations in particle densities, various methods of analysis have been developed.

In the present investigation, an attempt has been made to gain some insight into these density fluctuations of multiparticle production seen in the heavy ion collisions through the examination of factorial moments. Emulsion experiments are well suited for this type of analysis as the production angles of the produced particles are measured with high precision. Emulsion experiments also have the advantage that the same detector design can be used at all the experimental sites, so that experiments which cover a wide range of energies can be used without the use of differing detector corrections, which could affect the required signals.

For this purpose, an emulsion stack of dimensions 16 ×10 × 0.06 cm^3, exposed to a silicon beam of energy 14.6 AGeV from the Alternating Gradient Synchrotron at Brookhaven National Laboratory (BNL AGS) has been used. The stack was line scanned by two independent observers to increase the scanning efficiency. A total of 1107 interactions were picked up. To reduce the loss of tracks and to reduce the error in angle measurement, only 796 interactions were picked up for the final analysis. In each event, particles emitted were classified as shower, grey, black and projectile fragments depending on the ionization power of the particle. Moreover, events were divided into different target groups: AgBr, CNO and H according to the standard emulsion terminology, that is,

AgBr events: (i) $N_h \geq 8$

(ii) $N_h < 8$ and at least one track with range $R \leq 10\ \mu m$ and no track with $10 \leq R \leq 50\ \mu m$.

CNO events: $2 \leq N_h \leq 7$ and no track with $R \leq 10\ \mu m$.

H events: (i) $N_h = 0$

(ii) $N_h = 1$ but not falling in above categories.

In each event the space angle of each particle emitted from the collision vertex with respect to the forward direction of the primary beam was calculated using the expression: $cos\theta = cos\theta_p \times cos\theta_d$. θ_p is the projected angle and θ_d the dip angle of each particle. Having measured the space angles of shower particles, the pseudorapidity ($\eta = -ln\ tan\ \theta/2$) value of each particle was determined.

The η values of all the particles thus obtained were transformed into a cumulative variable X so as to reduce the effect of non-uniform density distribution. The non-uniformity of particle spectra influences the scaling behaviour of factorial moments. The corresponding region of investigation $\Delta\eta$ in the new variable X then becomes 0 to 1. In terms of the variable X, the particle density $\rho(X)$ is constant. The cumulative variable $X(\eta)$ is related to the single particle rapidity distribution as

$$X(\eta) = \frac{\int_{\eta_1}^{\eta} \rho(\eta')\, d\eta'}{\int_{\eta_1}^{\eta_2} \rho(\eta')\, d\eta'}$$

where η_1 and η_2 are the two extreme limits of the considered pseudorapidity range $\Delta\eta$. The region (0-1) in X space was then divided into M bins, each of size $dX = 1/M$ and the values of the scaled factorial moments were calculated.

From our study of the scaled factorial moments of the pseudorapidity and azimuthal angle distributions of the secondary particles produced in silicon-emulsion collisions at 14.6 AGeV, a power law dependence of F_q on M, that is, an intermittency pattern is observed in both the spaces. A similar trend is followed in the two dimensional space. The values of the intermittency indices ϕ_q obtained from the slopes of the plots increase with the increase in q for all the three cases and the two dimensional ϕ_q are larger than the one dimensional ϕ_q for all values of q. Further, the values of ϕ_q/ϕ_2 for both one and two dimensional phase spaces show an increase with the increase in q, which means that the factorial moments follow a generalized power law.

On investigating the behaviour of λ_q as a function of intermittency index ϕ_q for various M ranges, a λ_q minimum is observed in both the pseudorapidity and azimuthal spaces. This means that there is a certain value $q = q_c$ at which the multiparticle system behaves as a mixture of two states. On either side of this critical value, the multiparticle system behaves differently, which is an indication of non-thermal phase transition in the multiparticle production process in ^{28}Si-AgBr collisions at 14.6 AGeV.

Moreover, on studying the two dimensional $(\eta\text{-}\phi)$ $ln\langle F_2\rangle$ versus lnM plots with different values of Hurst exponent H, we found that the two dimensional second order factorial moment exhibits an upward bending as a function of partition of space. This upward bending, however, vanishes at H = 2.5 or 3.0. This means that only when we use the right value of H, that is, the proper partition along the longitudinal and perpendicular directions, in the analysis can the superposition of the contributions from the elementary collisions in the nucleus-nucleus collisions be correctly accounted for. A parameter 'a' is introduced to characterize the degree of upward bending. Using this parameter, it is found that the heavier are the colliding nuclei, the stronger is the upward bending, in consistence with the fact that the number of elementary collisions is larger for heavier colliding nuclei. If QGP is formed, then there will be no elementary collisions. This in turn will lead to vanishing of the superposition effect due to the contribution of elementary collisions in nucleus-nucleus collisions. Under such conditions, the upward bending in the two dimensional second order factorial moment plots is not likely to be seen. Thus study of the nuclear effect in nucleus-nucleus collisions could be used as another indirect test for QGP formation.

We also studied the erraticity behaviour of multiparticle production process through the moment of moments $C_{p,q}$ analysis. Erraticity measure is a capture of fluctuations that have been lost in the normalized factorial moments while averaging over all the bins and events. From this study we find that our data exhibit large fluctuations of factorial moments from event to event. A comparison of results on moment of moments $C_{p,q}$ and other erraticity parameters with those obtained for the generated uncorrelated events indicates that the contribution of the statistical fluctuations to the observed fluctuations in our data is very small. Further, a comparison of our results with those obtained for the FRITIOF events suggests that only a part of the observed fluctuations could be explained by the FRITIOF generator. There are additional fluctuations, which the FRITIOF generator fails to explain. At present we do not know what mechanism causes these fluctuations in heavy ion collisions. However, the method used in the present work is very effective in studying the non-statistical fluctuations in the event factorial moments in relativistic heavy ion collisions.

The fact that the values of the entropy index for different samples of our data are positive and very large as compared to the values obtained for the generated uncorrelated events indicates that the multiparticle production in ^{28}Si-emulsion collisions at 14.6 AGeV is chaotic in nature.

On studying the erraticity of rapidity gaps, the method proposed for low multiplicity events, we observe that both the erraticity measures S_q and Σ_q deviate significantly from 1 for both the pseudorapidity and azimuthal angle spaces and that both S_q and Σ_q increase linearly with the increase in q. This means that significant event-to-event fluctuations are present in the multiparticle production in ^{28}Si- AgBr collisions at 14.6 AGeV. The values of

erraticity measures obtained in the present investigation would provide valuable input to fine tune various event generators.

We also dealt with the non-statistical fluctuations in the angular distribution of target associated knockout protons. These particles are produced soon after the pions are produced and are believed to carry relevant information about the collision mechanism. By using the scaled factorial moment F_q and Takagi moment methods, fractal structures are observed in our data for both cosine and ϕ spaces. This in turn reflects a self-similar behaviour in the production of target protons. The generalized dimension D_q and the multifractal specific heat 'c' have been determined from both the analyses for both the spaces. Differences in the values of D_q and c from the two methods used in our analyses are mainly due to the difference in the definitions of these moments.

Finally, we conclude that moment analyses of particle density in one dimensional pseudorapidity space and two dimensional combined pseudorapidity - azimuthal angle space provide useful information about the mechanism of multiparticle production process. Experiments at RHIC and LHC will provide us interacting systems with much higher energy densities and larger formation times. If then large fluctuations induced in particle densities from the phase transition from QGP to hadronic matter are observed, then the comparison of moment analyses at RHIC and LHC energies with those at AGS and SPS energies may provide us one of the signals needed to establish the existence of the phase transition to a QGP state.

A STUDY OF DENSITY FLUCTUATIONS OF PARTICLES PRODUCED IN SI-EMULSION COLLISIONS AT 14.6 AGeV

THESIS

SUBMITTED IN PARTIAL FULFILMENT OF THE REQUIREMENTS
FOR THE AWARD OF THE DEGREE OF

Doctor of Philosophy

IN

PHYSICS

BY

MALIK MOHIB-UL-HAQ

Under the Supervision of

DR. RASHID HASAN

DEPARTMENT OF PHYSICS
ALIGARH MUSLIM UNIVERSITY
ALIGARH (INDIA)

2003

CERTIFICATE

This is to certify that the thesis entitled "*A Study of Density Fluctuations of Particles Produced in Si-Emulsion Collisions at 14.6 AGeV*" which is being submitted by **Mr. Malik Mohib-ul Haq** in partial fulfillment of the degree of Doctor of Philosophy in Physics of Aligarh Muslim University, Aligarh is a record of his own research work carried out by him under my supervision. The research work presented in the thesis has not been submitted for the award of any other degree by him or by anyone else.

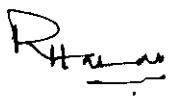

(**Dr. Rashid Hasan**)
Reader,
Department of Physics,
Aligarh Muslim University,
Aligarh 202 002
INDIA

Dated: 30.12.2003

Acknowledgements

Research is an intellectual pursuit and one needs to have an intelligent, honest, sincere and above all a diligent person as supervisor. I am fortunate to have Dr. Rashid Hasan as my supervisor whose mollycoddling saw me through this sensitive period. Although mere words are not sufficient to applaud his guidance, I avail this opportunity to express my deep sense of gratitude for his guidance, numerous suggestions and scholastic criticism. His erudite presence has been a constant source of inspiration and motivation during the course of this work.

It is my pleasure to thank Prof. A. K. Chaubey, Chairman, Department of Physics. A. M. U. Aligarh for providing me the necessary facilities in carrying out my research.

I am highly indebted to Prof. Mohammad Irfan and Prof. Mohammad Zafar for their encouragement and healthy suggestions on different aspects of this work.

I am grateful to Prof. P. L. Jain, Department of Physics, State University of New York at Buffalo, for sending us the processed emulsion plates used in the present investigation.

Special thanks are due to Mr. Habibur Rehman for his skillful scanning of emulsion stacks. His loving attitude and pat kept my spirits always alive.

I would like to thank to all the members of the high-energy physics group particularly Dr. Shakeel Ahmad, Dr. Nazeer Ahmad and Mr. Ayaz Ahmad for their sincere help. I also appreciate the help of Dr. Shahid Hussian.

My sincere thanks are due to my co-worker Saiful Islam and other friends for their valuable suggestions and encouragement.

I would like to thank Mr. Mushtaq Wani for his help while learning computer programming.

This acknowledgement would be incomplete without mentioning two of my cronies Farooq and Tariq. Intellectual discussions with them have been highly beneficial.

It is great pleasure for me to recognise the moral support and companionship of my uncle Mr. Ghulam Mustafa Khan and his family. Their love and generous behavior has been highly stimulating.

Last but not least, I would like to acknowledge the blessings and love of my parents and sisters. Their encouragement, understanding and patience have played a major role in bringing this work to the conclusion.

Finally, the financial assistance from the Aligarh Muslim University, Aligarh is acknowledged with thanks.

Malik Mohib-ul Haq

(M. Mohib-ul Haq)

Dedicated

To

My Father

Mr. Malik Ghulam Hassan

CONTENTS

List of Figures

List of Tables

List of Publications

Papers Published in International Journals

1. Multifractality in Multiparticle Production at High Energies.
   R. Hasan, **M. Mohib-ul Haq** and Saiful Islam
   Int. J. of Mod. Phys. (Singapore) vol. E9, No. 5 (2000) 417-429.

2. Chaoticity in Multiparticle Production in ^{28}Si-Emulsion Collisions at 14.6 AGeV.
   R. Hasan, **M. Mohib-ul Haq** and Saiful Islam.
   J. of Physics G: Nucl. and Part. Phys. (U.K) vol. 28 (2002) 2939-2949.

3. Multifractal Analysis of Multiplicity Fluctuations in ^{28}Si-AgBr Collisions at 14.6 AGeV.
   R. Hasan, Saiful Islam and **M. Mohib-ul Haq**.
   Accepted for publication: *Mod. Physics Lett. B* (Singapore).

4. Erraticity Analysis of Silicon-Emulsion Collisions at 14.6 AGeV.
   R. Hasan, **M. Mohib-ul Haq** and Saiful Islam
   Communicated: *Int. J. of Mod. Phys. A.* (Singapore).

Papers Presented at National and International Conferences:

1. Event-by-Event Fluctuations of Rapidity Distribution in ^{28}Si – Emulsion Collisions at 14.5 AGeV/c
   R. Hasan, Saiful Islam and **M. Mohib-ul Haq**.
   International Symposium on Nuclear Physics held at BARC (Mumbai) India, Dec. 26-30, (2000).

2. Chaoticity in Multiparticle Production in ^{28}Si-Emulsion Collisions at 14.6 AGeV/c.
   M. Mohib-ul Haq, Saiful Islam and R. Hasan
   High Energy Physics Symposium (Jammu) India, Nov.11-15 (2002).

3. Multifractality in ^{28}Si-AgBr Collisions at High Energies.
   Saiful Islam, **M. Mohib-ul Haq** and R. Hasan
   High Energy Physics Symposium (Jammu) India, Nov.11-15 (2002).

4. Log - Levy Stable Distribution and Intermittency in Nucleus-Nucleus Collisions at Relativistic Energy.
   M. Mohib-ul Haq, Saiful Islam and Rashid Hasan
   DAE-BRNS Symposium on Nuclear Physics held at BARC (Mumbai) India, Dec. 8-12, (2003).

5. Modified G_q-moment Analysis in Relativistic Heavy Ion Collisions.
   Saiful Islam, **M. Mohib-ul Haq** and Rashid Hasan
   DAE-BRNS Symposium on Nuclear Physics held at BARC (Mumbai) India, Dec. 8-12, (2003).

CHAPTER I

Introduction

1.1 Historical background

Experimental studies of heavy ion collisions at high energies were started in 1948 by Frier et al. [1] with the discovery of the presence of high energy heavy nuclei in the primary cosmic rays. Blau and Wambacher [2] were the first persons to study the interactions of cosmic rays in nuclear emulsion. Abraham et al [3], Andersson et al [4], Tsuzuki et al [5] and Jain et al [6] also studied the shower-particle production in cosmic ray collisions in nuclear emulsion. Initially these studies were carried out to determine the fragmentation cross-sections and the interaction mean free paths of the cosmic ray nuclei, required to understand the mechanism of interstellar propagation of cosmic rays. These studies provided some valuable results [7], but the experimental knowledge from these studies was limited and the reliability of the results remained always doubtful because cosmic rays provide low statistics (low intensity/flux) and the nature and energy of the primary nucleus taking part in the collision could be known only approximately. Hence it was difficult to disentangle information regarding the mechanism of multiparticle production in high energy nuclear collisions.

These problems, however, were overcome with the development of the giant particle accelerators. These huge machines with area of several square kilometers can accelerate the electrons. protons and other heavy nuclei until they travel nearly with the velocity of light. These subatomic 'bullets' when smashed into targets of nuclear material, interact with protons and neutrons within targets and enable us to study the mechanism of multiparticle production in greater detail.

Table 1.1 Various accelerator facilities operating at different laboratories.

Accelerator	*Location*	*Projectile*	Maximum Energy/nucleon (AGeV)	*Operation*
Alernating Gradient Synchrotron (AGS)	BNL	^{28}Si, ^{16}O	14.6	1986
Super Protron Synchrotron (SPS)	CERN	^{32}S, ^{16}O	200	1986
Alernating Gradient Synchrotron (AGS)	BNL	^{197}Au	10.6	1992
Super Protron Synchrotron (SPS)	CERN	^{208}Pb	160	1995
Relativistic Heavy Ion Collider (RHIC)	BNL	^{197}Au	100	1999
Large Hadron Collider (LHC)	CERN	^{208}Pb	3000	2007

It is worth mentioning that the first accelerator based fixed-energy heavy ion experiment was carried out in 1969 at Lawrence Berkeley Laboratory (LBL). Since then many more accelerator facilities at different laboratories have been developed. Some of the important accelerator facilities are listed in table 1.1. These accelerators can provide beams of any desired particle and nucleus with controlled energy. With these developments, interest in the study of high energy nuclear collisions has increased drastically.

1.2 Relativistic heavy ion collisions

In 1986, with the availability of heavy ion beams as heavy as ^{28}Si at 14.6 AGeV from AGS at BNL and ^{32}S at 200 AGeV from SPS at CERN, a new interdisciplinary field emerged from the traditional domains of nuclear and particle physics. Theoretical physics demonstrates that the collisions of these high energy nuclei with target material may provide us matter with high temperature (of the order of 10^5 times the temperature of the core of the sun) and high energy density (of the order of 20 times the energy density of nuclear matter). This in turn may lead to a new phase of matter known as quark gluon plasma (QGP), which is expected to have existed in the early universe and be present in the heart of neutron stars. Neutron stars have high baryon density of the order of 10 times the nuclear density and QGP may exist there. Since the phenomenon in neutron stars is very difficult to observe, the recreation of QGP through relativistic heavy ion collisions may contribute to astrophysics as well.

In the energy domain where relativity plays an important role, heavy ion collisions can be classified into two categories: relativistic heavy ion collisions and ultrarelativistic collisions. Collisions with center of mass energy range $\sqrt{s} \leq$ 50 GeV per nucleon have been referred to as relativistic heavy ion

collisions [8]. In such collisions, the formation of QGP is highly uncertain. However, the study of relativistic heavy ion collisions helps us in improving the accuracy of experimental data, to enlarge the variety of measured experimental characteristics and to accumulate data covering all aspects of particle production at different incident energies. Moreover, the study of these collisions allows us to make a comparative study of various observables such as impact parameter, multiplicity, particle ratio and fluctuations etc. at different energies and for different projectiles and targets, which in turn may be useful to have a thorough understanding of the background on which the signals regarding the QGP are expected to be found.

On the other hand, collisions with center of mass energy $\sqrt{s} > 50$ GeV per nucleon are called as ultrarelativistic heavy ion collisions [8]. These collisions are most likely to create the QGP state in the laboratory at small impact parameter (near head-on collision). Estimates are now available for the energy density 'ε' that could be achieved in such collisions. While these estimates are optimistic, collisions of high multiplicity may be more favorable for the QGP formation, a line of investigation that has not been explored so for, it deserves both theoretical and experimental attention.

1.3 Evolution of heavy ion collisions

High energy heavy ion collisions proceed through a number of stages as shown systematically in Fig. 1.1. The two colliding nuclei appear in the center-of -mass frame as two lorentz contracted pancakes with limited thickness ~ 1 fm [9,10] and fly towards each other at v ~ c. In the first stage, the two nuclei penetrate each other such that the nucleons of two nuclei collide and a large amount of energy is transferred from the projectile to the collision region. This

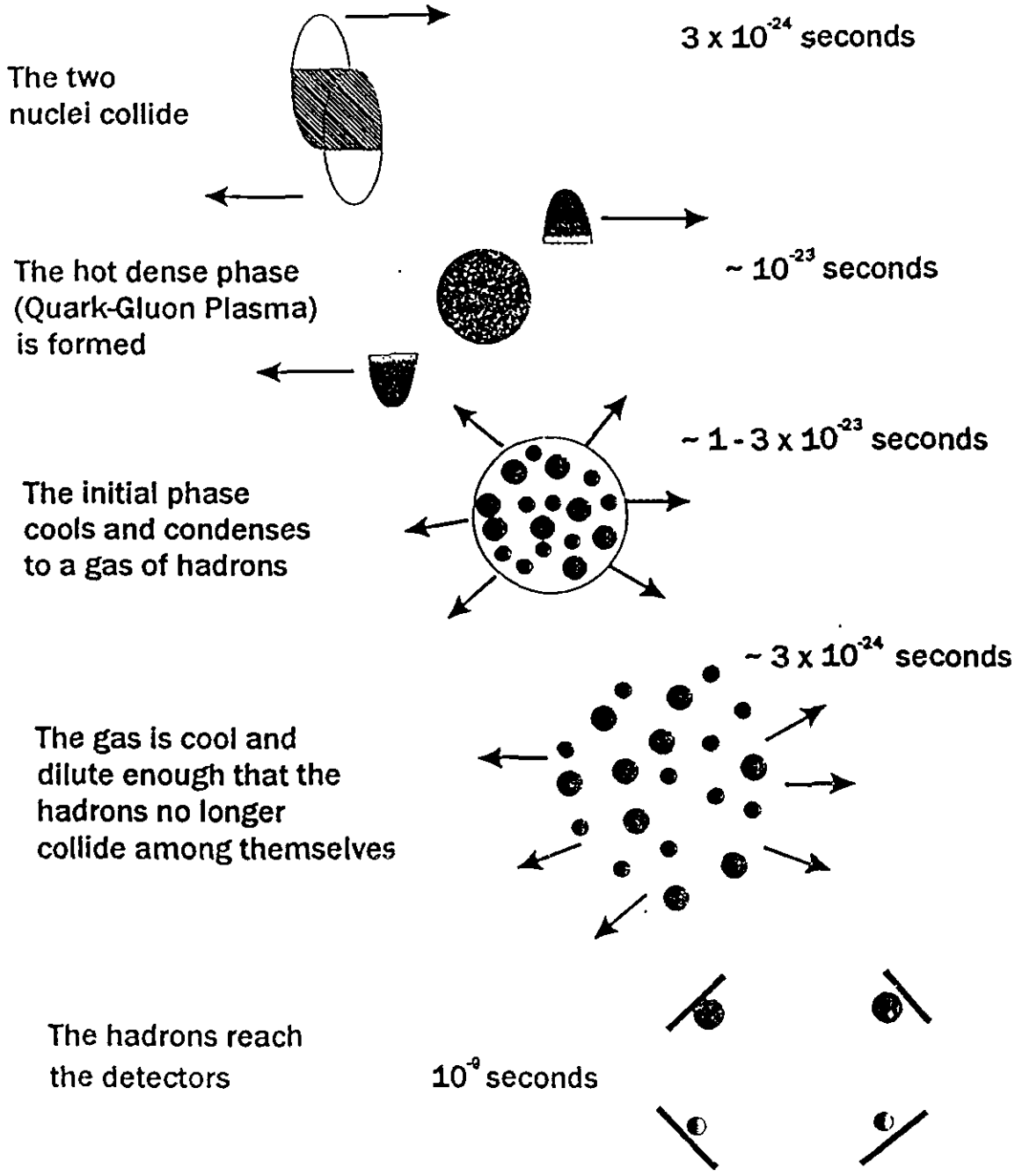

Fig. 1.1 Schematic illustration of the different stages in a heavy ion collision.

energy later on is converted into new particles. This stage lasts for about 3×10^{-24} seconds and is short because of relativistic contraction [11] of the nuclei moving nearly at the speed of light. After the collision, the remains of the colliding nuclei move along their respective forward directions, while the central rapidity region is occupied by energy-rich and highly excited participant matter. The energy deposited in the central rapidity region is transformed into matter with very high energy density [12,13].

The quanta, which carry the energy deposited, can be in the form of quarks, anti-quarks and gluons but not the hadrons. This is because the conditions are not suitable for the hadron phase or we can say that hadrons cannot survive at such high energy density [10]. Initially, the system is in pre-equilibrium state as the hard collisions among the quarks and gluons produce additional quarks and gluons. These newly produced quarks and gluons along with those present initially, undergo a cascade of further collisions. It is the presence of gluons that throws the system into an equilibrium condition. These gluons thermalize in less time than required for the nuclei to interpenetrate, sharing their energy equally among themselves. This process produces a quark gluon plasma state in local thermal equilibrium that lives long enough to generate the detectable signals [11].

This hot and dense phase (QGP) expands and cools rapidly with time, which lowers the de-confinement temperature and density so much so that the quarks and gluons condense into a gas of hadrons. The hadronization transition is expected to take place around 10 to 30×10^{-24} seconds after the nuclei begin to collide [11]. It is at this point that most of the produced particles come into existence. At this stage, the hadronic matter thus created is still highly excited. These hadrons scatter, causing further expansion and cooling. This multiple

scattering of hadrons tends to distribute the available energy equally among themselves. Eventually, the system may expand to very large dimensions (V ~ 10^4 – 10^5 fm^3) till freeze-out, that is, the interactions cease and the particles stream out freely without further disturbance [14]. The number of particles at the end reflects the energy deposited in the collision and rises with the beam energy. The detection of a large number of particles thus produced requires sophisticated and ingenious detectors with high resolution.

1.4 Signatures of QGP

The identification of formation of QGP is a major experimental challenge for the high energy physicists. Ideally, experiments must show that some features of the data cannot be present in the absence of QGP. The difficulty is that if QGP is formed, it will exist only for a fraction of the evolution time, so how one can know the QGP is formed in a heavy ion interaction. Does it leave any fingerprints of its existence? A number of such signatures has been predicted and some of them are briefly described here.

1.4.1 Direct photon production

The production of direct photons has been emphasized as one of the most relevant probes to detect the existence of QGP while studying the dynamics of the ultrarelativistic heavy ion collisions [15-19]. Interactions amongst the quarks and gluons in the plasma state give rise to the production of direct photons through the following processes

$$q + \bar{q} \rightarrow \gamma + g \qquad \text{Annihilation process}$$

$$\left.\begin{array}{l} g + q \rightarrow \gamma + q \\ g + \overline{q} \rightarrow \gamma + \overline{q} \end{array}\right\} \quad \text{Compton process}$$

Since photons interact electromagnetically and their mean free path is large compared to the size of the system formed in heavy ion collisions, they escape the colliding system virtually unaffected by the surrounding hadronic matter, that is, without re-scattering and thus carry information about the conditions and properties of the matter at the time of its production.

Secondly, the emission rate of photons is a strongly increasing function of temperature. Therefore, most of the direct photons are produced at the early stage of the collision when the temperature and energy density have their largest values. This allows them to provide information about the early stage of the collision. These two facts make the direct photons unique spectators of the exotic state of matter created in heavy ion collisions, thus making them a potential signature of the QGP formation.

1.4.2 J/Ψ suppression

A striking signature of the QGP existence is the suppression of $J/\Psi(c\overline{c})$. J/Ψ is formed in the scattering process of parton fusion such as

$$q\overline{q} \rightarrow c\overline{c}$$
$$g\overline{g} \rightarrow c\overline{c}$$

In the de-confinement state, the interaction between the quarks is screened by the presence of other quarks, so quark bound states such as J/Ψ cannot survive in the plasma. Bound states with larger radii are dissociated first, while the ones with smaller radii are dissociated later [20-22]. The observed J/Ψ production is currently under intense theoretical and experimental study for

finding whether it indicates QGP formation. Another test of this signature would be to see whether the upsilon ($b\bar{b}$) production probability is little changed. However, data on upsilon production in heavy ion collisions will not be available until LHC becomes operational. This is because higher energy is required for upsilon production.

1.4.3 Strangeness enhancement

The strangeness may work as another good signal for QGP, as the strangeness content in hadron matter and quark-gluon plasma is different [23-33]. In the nucleon-nucleon collisions, hadrons containing a strange quark are produced much less frequently than hadrons with light quarks (u and d). The formation of QGP should make it much easier to produce heavier strange quarks. Indeed, experiments at both SPS and AGS have observed a significant increase in the number of strange hadrons in nucleus-nucleus collisions in comparison to nucleon-nucleon collisions [34,35].

1.4.4 Fluctuations

Non-statistical fluctuations are associated with critical phenomena in the vicinity of phase transition. Analysis of one JACEE event (Si-AgBr) by Bialas and Peschanski [36] has drawn the attention of the high energy physicists for using fluctuations in rapidity distribution as a probe to search the formation of QGP.

A positive source of these fluctuations is known as turbulence and is now referred to as intermittency. Bialas and Peschanski [36] proposed that the particle production in a longitudinally expanding fluid of QGP has an underlying branching structure, which leads to clustering of particles in final

state. Therefore the fluctuations due to the branching structure can manifest in the form of sudden change in particle multiplicity in small phase space windows. However, these fluctuations are very sensitive and may get intermingled with statistical ones, which demands an attention on the resolution of measurement system.

The presence of non-statistical fluctuations in particle density is considered as a signal for phase transition. This is due to the fact that a dense medium has a long correlation length and at the critical point, this correlation length goes to infinity, resulting in divergent fluctuations in density. Such critical fluctuations can only be seen in individual events where the multiplicity is large enough [37-39].

1.5 Nuclear fragmentation

Various high-energy groups have already observed that the projectile and target fragmentation products in nuclear collisions are well separated on the pseudo-rapidity plot, thereby indicating that one should be able to observe the pure projectile and pure target fragmentation reactions. Experimental results on nucleus-nucleus collisions at different energies [40] have shown that the modes of fragmentation are independent of the mass of the target nucleus. With the help of these experiments, one can interpret the data in terms of high-energy concepts of limiting fragmentation. In the limiting fragmentation, the distribution of the products in the rest frame of projectile or target, approaches a limiting value as the incident energy increases, that is, the fragmentation distribution remains constant with increasing energy.

The information on projectile fragmentation could be accumulated from the single inclusive reaction. In a single particle inclusive reaction,

$$P + T \rightarrow F + X,$$

where P and T are the projectile and target nuclei, F is the detected (single) fragment and X refers to all other undetected reaction products. Consequently, the cross-section for the production of any particular projectile fragment may be written as a product of a factor r_T (depending only on the target mass) and a factor r_B^F (depending on the masses of the projectile and fragment) [41], that is,

$$\sigma_{BT}^F = r_B^F r_T$$

Similarly, to describe the target fragmentation, the projectile and target may be interchanged. Jaros et al. [42], Westfall et al. [43] and Chernov et al. [44] have made the calculations for σ_{BT} and it has been suggested that a study of projectile and target fragmentation process, gives a lot of information regarding the nuclear structure.

1.6 Classification of nucleus-nucleus collisions

In terms of geometry, the characteristics of nucleus-nucleus collisions at relativistic energies are determined by the size of the impact parameter. Heavy ion collisions can be classified into three different categories: peripheral, quasi-central, and central collisions. Fig.1.2 shows that the characteristic features of heavy ion reactions at relativistic energies depend sensitively on the value of the impact parameter of collisions.

If r_1 and r_2 are the radii of the two colliding nuclei and b is the impact parameter, then $b \approx (r_1 + r_2)$ for peripheral collisions, $(r_1 + r_2) > b \geq |(r_1 - r_2)|$ for quasi-central collisions and $0 \leq b < |(r_1 - r_2)|$ for central collisions.

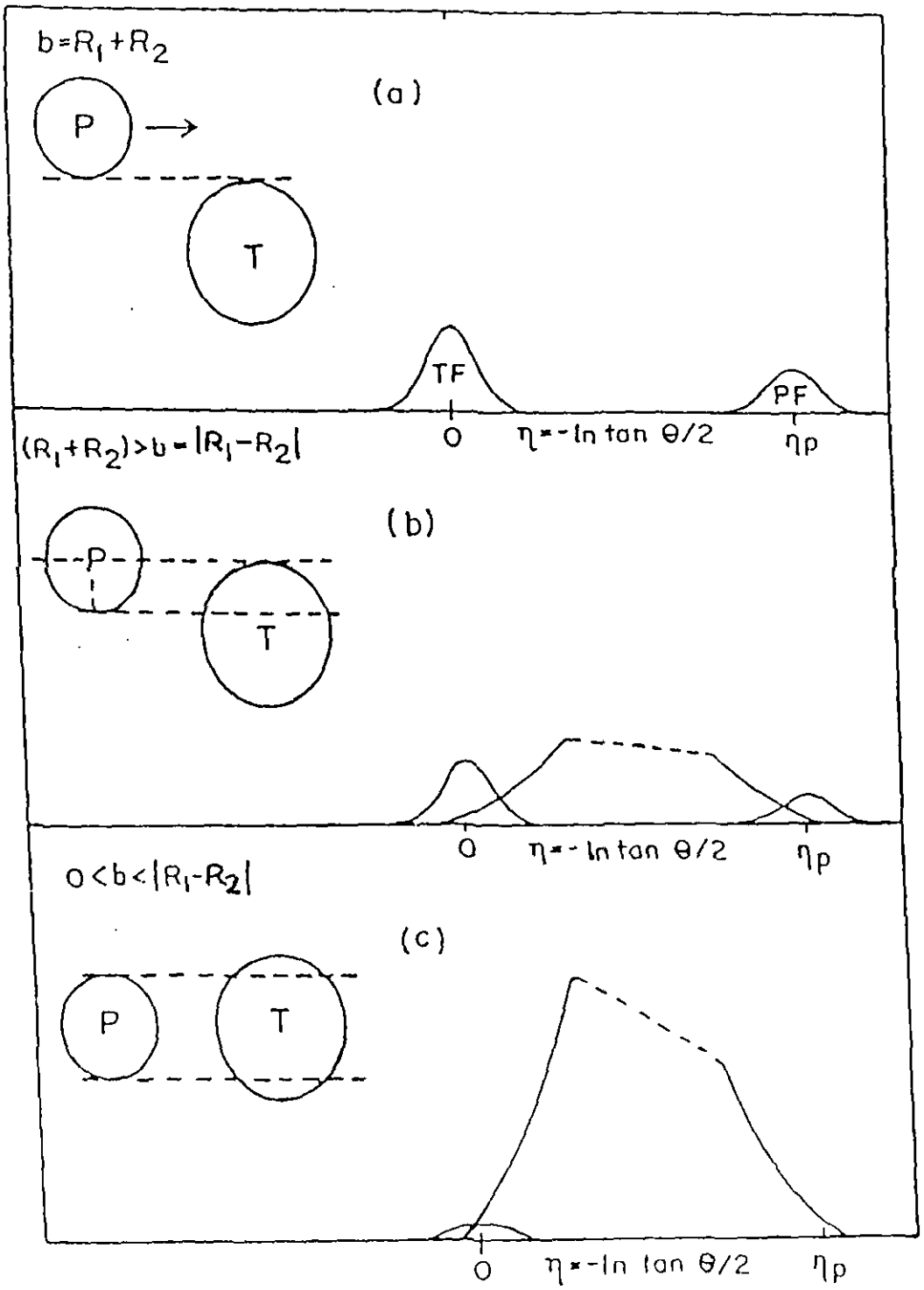

Fig.1.2 A schematic outline of pseudorapidity distributions in heavy ion collisions at high energy.

In the peripheral collisions, the centres of the two colliding nuclei are well separated. This allows only a small momentum transfer between the two nuclei. In these so–called peripheral collisions, one or both of the nuclei disintegrate through a fragmentation process leading to the observation of projectile nucleus and target nucleus fragments. The characteristics of the emitted fragments are determined by the intrinsic fermi momentum distribution of nucleons within the fragmenting nuclei [45]. These processes are illustrated in Fig.1.2a by the pseudo-rapidity distribution of projectile fragments (PF) and target nucleus fragments (TF), which are well separated at relativistic energies. The projectile fragments are emitted within a narrow cone around the beam direction, while the target fragments are nearly isotropically distributed in the laboratory frame.

When a nucleon is no longer a spectator, but participates in the reaction, it is scattered into the rapidity space between the projectile fragmentation region and target fragmentation region. Such collision may be either quasi-central or central type. Therefore in both quasi-central collisions and central collisions, the projectile and target nuclei are close to each other. However, in the central collisions both the nuclei overlap totally and the impact parameter could reach even zero value (Fig.1.2b and Fig.1.2c). The difference between the two types could be understood on the basis of number of nucleons taking part in the reaction. In both cases, the whole of the kinamatically allowed rapidity space is available for the produced particles, the difference being in the degree of population of the central region.

In the central collisions, which are more violent and complex, we expect almost complete extinction of projectile fragments for $r_1 < r_2$, that is, projectile nucleus fragmentation process is forbidden and the rapidity space available for

the produced particles is almost limited between the projectile fragmentation region and target fragmentation region (Fig.1.2c). In case the sizes of the interacting nuclei are comparable, the cross section for the total overlapping will be very small [46]. In the extreme case, when $r_1 = r_2$, the probability for the central collisions becomes zero. This indicates that a strict geometrical definition of central collisions is not appropriate. In fact, we do not have any strict definition for the centrality of collisions.

1.7 Organization of thesis

The main motivation behind the study of relativistic heavy ion collisions is to investigate the properties of hot, dense and strongly interacting matter experimentally [47]. Although this field has seen a lot of activity during the last decade, no consensus could be built till date. It has, however, been demonstrated that in order to find unambiguous signals regarding the processes involved in such relativistic collisions, it is essential to have a clear understanding of the multiparticle production and fragmentation processes in these collisions.

Studies of multiparticle production in relativistic heavy ion collisions are mainly carried out using the counter and emulsion techniques. The counter technique has an advantage of homogenous nature of the target material over the emulsion technique, thereby allowing one to study the dependence of different parameters on the target mass. However, this technique has a basic drawback of missing the large angle secondaries. On the other hand, the nuclear emulsion technique is considered a preferable one because of its wide range of sensitivity and high spatial resolution. Further, the same projectile–

target systems can be studied at different available energies with identical detectors.

It has been suggested that the strongly interacting matter at the energy densities produced in heavy ion collisions may undergo a phase transition to quark-gluon plasma [48]. Such a phase transition could produce large fluctuations in phase space, which may leave as a signature, large fluctuations in the measured particle densities [49,50]. In order to disentangle information regarding these dynamical fluctuations in particle densities, various methods of analysis such as F_q-moment, G_q-moment, Takagi-moment etc. have been developed. In the present investigation, these methods have been used to study fluctuations in the density of charged particles produced in collisions of 14.6 AGeV silicon nuclei in nuclear emulsion.

The second chapter of the thesis describes the details of the technique used. The scanning procedure, mechanism of track formation, various track parameters and their measurement are discussed. Besides, some theoretical models and event generators have also been described.

In chapter III, the fluctuations in the density of charged particles produced in ^{28}Si-AgBr collisions at 14.6 AGeV are studied by means of the normalized factorial moments F_q. The power law dependence of F_q on the bin size is known as intermittency [36]. The intermittency like fluctuations have been studied in the pseudorapidity space, in the azimuthal space and in the two dimensional (η-ϕ) space. The values of the intermittency indices ϕ_q for all the three cases have been determined. The ϕ_q values quantify the behaviour of the factorial moments which is of more interest than the actual magnitude of the moments.

It has been emphasized that the self-similar cascade mechanism in the multiparticle production is not consistent with one phase, but requires a non-thermal phase transition [51]. The behaviour of the function λ_q that quantifies this phase transition has been studied for our data. Moreover, the behaviour of two dimensional factorial moments $<F_2>$ as a function of phase space bin number M has also been investigated in order to throw some light on the superposition effect of the contributions from the elementary collisions in nucleus-nucleus collisions.

In chapter IV, event-to-event fluctuations in the densities of particles produced in ^{28}Si-AgBr and ^{28}Si-CNO collisions at 14.6 AGeV have been studied using a new observable $C_{p,q}$, the pth order moment of the normalized qth order factorial moment. The power law dependence of $C_{p,q}$ on the number of bins M is referred to as erraticity [38,39]. $C_{p,q}$ moments can probe the dynamics more deeply than the conventional observables such as multiplicity distribution and the normalized factorial moments. Therefore the behaviour of $C_{p,q}$ moments as a function of M has been investigated for different values of p and q. Various parameters that describe the spatial pattern of the final states of multiparticle production have been determined for our data so as to provide some valuable input for the models of multiparticle production.

In order to find the contribution of statistical fluctuations to those observed in our data, the behaviour of $C_{p,q}$ moments as a function of number of bins M has been studied for uncorrelated generated events also. These events are generated with the help of random number generator and FRITIOF event generator. The event-to-event fluctuations in our data have also been studied using another method, namely the erraticity of rapidity gaps. This method has

recently been proposed by R.C. Hwa [52] to study the event-to-event fluctuations in low multiplicity collisions.

In chapter V, the non-statistical fluctuations in the angular distribution of target-associated knockout protons (grey particles) produced in ^{28}Si-AgBr collisions at 14.6 AGeV are studied. Since both the shower and grey particles are produced in the first stage of the collision, it is speculated that the grey particles may also carry some important information on the spatial patterns from event-to-event. Moreover, the study of these particles will not only provide a unified description of the whole production process, but will also provide an additional parameter to understand the dynamics of particle-production-process.

Using the two most widely used methodologies, namely the scaled factorial moment method and Takagi method, the fluctuations in the distribution of grey particles have been studied in $cos\theta$ and azimuthal angle spaces. Values of the parameters that quantify the scaling behaviour have been calculated for both the spaces. Also the values of the generalized dimensions 'D_q' and multifractal specific heat 'c', which are the consequences of fractal structure, have been determined for both the spaces.

Finally in chapter VI, we give a brief summary of the results obtained in the present investigation and draw various conclusions.

References

[1] P. Frier et al., *Phys. Rev.* **74**, (1948) 213.

[2] M. Blau and H. Wambacher et al., *All* **146**, (1937) 623.

[3] Abraham et al., *Phys. Rev.* **159**, (1967) 1110.

[4] B. Andersson et al., *Ark. Fys.* **31**, (1966) 527.

[5] Y. Tsuzuki, *J. Phys Soc.* Japan **16**, (1961) 2131.

[6] P. L. Jain et al., *Phys. Rev.* **115**, (1959) 643.

[7] C. J. Waddington, *Prog. Nucl. Phys.* **8**, (1960) 1.

[8] L. Van Hove, *Proc. Bielefeld Workshop,* (1982) 349.

[9] J. D. Bjorken, *Proc. Int. Summer Inst. on Theor. Phys.* Hamburg, (1973) 93.

[10] C.Y. Wong, *Intro. to High Energy Heavy Ion coll.,* (1994) 271.

[11] Nucl. Phys.: *The Core of Matter, The Fuel of Stars, National Acadamy Press,* India (1999) 87.

[12] J. D. Bjorken, *Phys Rev.* **D27**, (1983) 140.

[13] S. Weinberg, *The First Three Minuets,* New York, (1977).

[14] R. C. Hwa and K. Kajantie, *Phys. Rev,* **D32**, (1985) 1109.

[15] E. V. Shuryak, *Phys. Lett.* **B78**, (1978) 150.

[16] K. Kajantie and H. I. Meittinen. *Z. Phys.* **C9**, (1981) 341.

[17] F. Helzen and H. C. Liu, *Phys. Rev.* **D25**, (1982) 1842.

[18] L.D. Mclerran and T. Toimela, *Phys. Rev.* **D31**, (1985) 545.

[19] S. Raha and B. Sinha, *Phys. Rev. Lett.* **58**, (1987) 101.

[20] T. Matsui and H. Satz, *Phys. Lett.* **B178**. (1986) 416.

[21] P. Abreu et al., *Phys. Lett.* **B247**. (1990) 137.

[22] T. Matsui, *Z. Phys.* **C38**, (1988) 245.

[23] J. Rafelski, *Phys. Rep.* **88**, (1982) 331.

[24] J. Rafelski, *Nucl. Phys.* **A544**, (1992) 279c.

[25] H. C. Eggers and J. Rafelski, *Int. J. Mod. Phys.* **A6**, (1991) 1067.

[26] P. Koch et al., *Phys. Rep.* **142**, (1986) 167.

[27] T. Matsui, B. Svetitsky and L. D. McLerran, *Phys. Rev.* **D34**, (1986) 783; *Phys. Rev.* **D34**, (1986) 2047.

[28] C. Greiner et al., *Phys. Rev. Lett.* **58**, (1987) 1825.

[29] T. S. Biro et al., *Phys. Rev.* **D42**, (1990) 3078.

[30] C. M. Ko and L. H. Xia, *Nucl. Phys.* **A498**, (1989) 561c.

[31] S. Nagamiya, *Nucl. Phys.* **A544**, (1992) 5c.

[32] Y. Pang et al., *Phys. Rev. Lett.* **18**, (1992) 2743.

[33] R. Matiello et al., *Nucl. Phys.* **B24**, (1991) 221.

[34] T. Abott et al., *Phys. Rev. Lett.* **64**, (1990) 847; *Phys. Rev. Lett.* **66**, (1991) 1567.

[35] T. Van Hecke et al., *Nucl. Phys.* **A525**, (1991) 227c.

[36] A .Bialas and R. Peschanski, *Nucl. Phys.* **B273**, (1986) 703; *Nucl. Phys.* **B308**, (1988) 857.

[37] R. C. Hwa, *Proc. Int. Conf. Part. Accel.,* Bombay, India (1988) 341.

[38] R. C. Hwa, *Proc. 7th Int. Workshop on Multiparticle Production, Correl. and Fluctuations,* Nijmegen, Netherlands (1996) 302.

[39] R. C. Hwa, *Proc. XXVI Int. Sympos. On Multiparticle Dynamics,* Fero, Portugal (1996) 189.

[40] P.J. Lindstrom et al., *LBL- Report* (1975) 3650.

[41] H. H. Heckman et al., *Phys. Rev.* **C17**, (1978) 1735.

[42] J. Jaros et al., *LBL – Report* (1977) 7509.

[43] G. D. Westfall et al., *LBL – Report* (1978) 7162.

[44] G. M. Chernov et al., *Nucl. Phys.* **A412**, (1984) 534.

[45] H. H. Heckman et al., *LBL- Report* (1977) 7509.

[46] I. Otterlund, Lund Univ. *Report LUIP* (1979) 7904.

[47] M. Jacob, *Nucl. Phys.* **A583**, (1995) 13.

[48] E.V. Shuryak, *Nucl. Phys.* **A525**, (1991) 3c.

[49] L. Van Hove, *Phys. Lett.* **B118**, (1982) 138.

[50] M.Gyulassy et al., *Nucl. Phys.* **B237**, (1984) 477.

[51] R. Peschanski, *Int. J. Mod. Phys.* **A6**, (1991) 3681.

[52] R. C. Hwa and Qing-hui Zhang, *Phys. Rev.* **D62**, (2000) 014003; nucl-th/0203022 (2002).

CHAPTER II

Experimental technique

2.1 Introduction

Photographic emulsion is a versatile instrument used for the detection of nuclear particles. It is capable not only of counting particles, but of giving precise information concerning their mass, energy and their modes of interaction and decay. In nuclear emulsion, as in bubble chamber the tracks of particles are visible and can be observed in detail. The emulsion is a continuously sensitive detector, able to record and store the information gathered over extended periods after the development. Moreover, rare events can be detected even in the presence of high background. The complete history of particles, from their production to their end through decay, interaction or loss of energy by ionization can be seen by means of tracks recorded in the emulsions and precise measurements can be made. The computer aided scanning has substantially enhanced the analyzing power of this technique.

The composition of the nuclear emulsion is heterogeneous. It consists of three basic components: (a) silver halide, mainly bromide with small admixture of iodine, (b) gelatine and glycerin and (c) water. The glycerin is incorporated as a plasticizer to avoid the brittleness. In the overall composition, the percentage of the three groups is such that about 71% of the collisions occur with heavy nuclei group, AgBr with average atomic mass 94, 25% with light nuclei group CNO with average atomic mass $< A > = 14$ and only 3.5% with hydrogen nuclei with average atomic mass 1 for p-emulsion collisions [1]. However, for nucleus-nucleus collisions, these numbers change with the mass of the projectile. In the present case, about 47% of the collisions are with AgBr group, 33% with CNO and 20% with H targets.

When a particle of charge Ze and mass M traverses a medium of atomic number z and mass number A, it excites and ionizes the atoms of the medium

due to coulomb interactions. This results in the loss of energy of the incident particle. The rate of energy loss dE per unit length dx traversed is given by the Bethe formula:

$$\frac{-dE}{dx} = \frac{4\pi^2 Z^2 e^4}{m_e v^2 A} N\left[z\left\{ \ln\left(\frac{2m_e v^2}{I(1-\beta^2)} \right) - \beta^2 \right\} - C_k \right], \qquad (2.1)$$

where minus sign means the loss of energy, v is the velocity of the incident particle, $\beta = v/c$, N is the number density of the medium, I is the ionization potential of the stopping material and m_e is the mass of the electron. C_k is the correction factor in case the velocity of the incident particle is comparable with that of the k-shell electron.

For a heterogeneous medium like emulsion, the above relation is modified to

$$\frac{-dE}{dx} = \frac{4\pi^2 Z^2 e^4}{m_e v^2 A} \sum N_i\left[z_i\left\{ \ln\left(\frac{2m_e v^2}{I_i(1-\beta^2)} \right) - \beta^2 \right\} - C_k \right], \qquad (2.2)$$

where I_i is the mean ionization potential of the medium. From the above relation, it is clear that the energy loss is directly proportional to the charge (Ze) of the incident particle, that is, only charged particles can be detected. Secondly the energy loss is inversely proportional to the square of the velocity of the incident particle, thereby indicating that as the velocity of the particle increases, the energy loss decreases or vice versa. Further, the logarithmic term varies slowly with velocity. However, the energy loss is independent of the

mass of the particle. Almost all the energy of a charged particle is lost through the ionization process while traversing through emulsion.

2.2 Advantages and disadvantages of nuclear emulsion

Because of the small size (*~0.6 μm*) of the developed grains of photographic material, the most important feature of the nuclear emulsion is its high spatial resolution. Particles going out closely can be easily separated. Secondly, it maintains a permanent record of the event. Interactions could also be studied after long time. Also, one can carry out event-by-event analysis in emulsion. Moreover, nuclear emulsion has a high stopping power, about 1700 times the stopping power of standard air. Particles, which might escape from the sensitive volume of a less dense medium, are quickly brought to rest in emulsion, where they can decay at their leisure. Muons decaying with a mean lifetime of 10^{-6} seconds and hyper-fragments with a mean iife of 10^{-10} seconds are easily detected. Through these properties, the use of nuclear emulsions has led to the discovery of many unstable particles and has contributed greatly to the analysis of their properties and behaviour.

Besides these advantages, the nuclear emulsion has some disadvantages also. In emulsion, the target identification and charge identification of different particles are not precise. These are considered as the main drawbacks of the emulsion. Also, the data collection is time consuming. A special dark room is required for the handling of emulsion. Shielding from the background radiation is necessary. In addition to this, low temperatures are required, so that the emulsions maintain their shape and rigidity. They must be kept at a temperature well below the melting point of gelatine, which is about 45°C. Moreover, at energies ~ 200 AGeV, the measurements become tedious.

2.3 Mechanism of track formation in emulsion

Photographic emulsion consists of grains of silver halide (AgBr), dispersed in gelatine. When a charged particle passes through nuclear emulsion, it interacts with the silver halide grains. This leads to the ionization of silver atoms and thereby the formation of latent image along the path of particle takes place. In other words, some of the halide grains are modified in such a way that on immersing the stack in a reducing bath called the developer, they are turned into black dots. The series of such black dots form the track of the particle. This is also called the signature of the particle, as it contains information about its mass, charge and energy. The mechanism by which the ionization of some of the atoms in AgBr grains can lead to the formation of the silver specks, which constitutes the latent image, was first explained by Gurney and Mott [2,3].

The chemical development process is considered to be a continuation of the process whereby the latent image is formed. Photographic developers are weak reducing agents, which require the presence of silver specks for their action. Electrons are transferred from the molecules of developer to the latent image; interstitial silver ions are then attracted from the body of the crystal and deposited on the latent image speck.

After the development, the emulsion is put in a fixer. The fixer dissolves all the undeveloped grains, but leaves the developed ones unaffected. Due to the removal of undeveloped grains, the thickness of the emulsion gets reduced. This is called the shrinkage and it has to be taken into account while making the calculations. After fixing, the emulsion is washed and then dried. The array of the developed black grains forms the track of the charged particle.

2.4 Scanning

The process of searching the position of collisions (events) in the emulsion pellicles is called the scanning. The scanning is generally done in two ways: (i) area scanning and (ii) line scanning.

2.4.1 Area scanning

Area scanning of an emulsion pellicle involves searching for events microscopically through a given volume of emulsion, field-of-view by field-of-view. Each field of view is scanned throughout its depth, from one surface to other, by rolling the fine focus of control (z-motion of the microscope). The fields may be overlapping, so as to leave no gaps. The area scanning is useful when the primary particles enter the pellicle over a wide solid angle; when they have a wide spread; when a population of certain easily noticed events is wanted.

Area scanning is considered faster than line scanning. However, the principal disadvantage of this scanning is the bias against the events with less number of prongs and against some directions of emission of secondary particles. When the area scanning is performed, these inefficiencies must be taken into account and corrected for.

2.4.2 Line scanning

This is the other mode of scanning carried out along the tracks. The line scanning is carried out, when a parallel beam of charged particles is showered on the emulsion stack, nearly parallel to the surface of the emulsion, such that the beam particles enter the leading edge, perpendicular to it and leave the opposite edge. By scanning across the beam direction near the leading edge,

the primary track is picked up on the scan line as it enters the stack and followed until the particle is found to interact or to leave the emulsion. The track is examined before picking it up to ensure that it does not interact before the scan line. This technique permits efficient study of the events occurring in flight and of small events both in flight and at rest. The line scanning is effective in the following conditions of exposure:

(i) The flux of the beam is not dense and it spreads up throughout the leading edge.

(ii) The available length for the traversal of the beam is large; that is, the beam does not dip much.

2.5 Track parameters and their measurements

2.5.1 Ionization

This is an important parameter used frequently in the emulsion technique. It can give information regarding the velocity and charge of a particle. Ionization caused by a charged particle may be estimated by measuring various quantities such as (i) grain density (ii) blob density (iii) blob and gap densities and (iv) delta ray density.

2.5.2 Grain density

The track of a particle in emulsion appears as small black trails of silver grains. The number of these black dots per unit path length is termed as grain density, which is found to be a reliable parameter for estimating the ionization caused by the particle. However, the grain density g in the track depends on the degree of development of the emulsion. To avoid the error, it is therefore necessary to determine the ratio g^* (relative grain density) of the observed

grain density g to the corresponding value of g_o, the minimum ionization caused by a relativistic singly charged particle over the same length in the same emulsion. The grain density g^* is proportional to the ionization loss per unit length, that is,

$$g^* or \frac{dN}{dr} \propto -\frac{dE}{dx} \propto \frac{Z^2}{\beta^2} f(\beta) \tag{2.3}$$

For singly charged particles $Z = 1$. Therefore,

$$g^* \propto \frac{1}{\beta^2} f(\beta). \tag{2.4}$$

Hence, the measurement of grain density gives some idea about the velocity of the particle.

2.5.3 Blob density

If the velocity of the particle is not too large, some of the grains in the track are clogged together to form blobs (compact groups of grains). The grain counting on such a track is difficult because the true number of grains is uncertain and may become the principal reason for the subjective error. In such circumstances, the number of individually resolved blobs is counted without estimating the number of grains in the clusters. The value of ionization [4] in such case is given by

$$B = g \, exp. \, (-\alpha \, g), \tag{2.5}$$

where B is the blob density, g is the grain density and α (~ 0.6 - $0.9 \mu m$) is a parameter depending largely on the average grain size and optical resolution of microscope.

2.5.4 Blob and gap density

When the velocity of the particle is small, the grains are frequently formed in clusters and the counting becomes really very difficult. In such cases, the blob and gap method [5-7] is used for estimating the ionization. The blob is a cluster of grains with no gap and the gap is defined as the distance between the edges of successive blobs.

The method is based on the fact that gap lengths have an exponential frequency distribution for widely different values of specific ionization. The density H of the gaps exceeding length L and blob density B are related as

$$H = B \exp.(-g L), \tag{2.6}$$

where H and B are obtained from their density per unit length. It was shown by Fowler and Perkins [4] that the coefficient g of the exponential is a good measure of the ionization of the track. The value of g can be determined from the equation

$$g = \frac{1}{L_2 - L_1} \log_e \left(\frac{H_1}{H_2} \right), \tag{2.7}$$

where H_1 and H_2 are the number of gaps of length exceeding L_1 and L_2 per unit length of the track.

2.5.5 Delta ray density

When a charged particle traverses a medium, it loses a very small fraction of energy $\eta \leq 5\ KeV$ in a single collision with an atomic electron. However, the collision in which the loss of energy is greater than the critical

value ($\eta \approx 5\ KeV$), results in the formation of δ-rays. The electrons, which take up these large energy losses, have ranges sufficient to carry them through several crystals, ionizing as they travel. The result is a series of short tracks called δ-rays, branching out from the main track. Thus δ-ray is another source of information concerning the identity and velocity of the moving particle. The number of collisions in which the energy transfer $\eta > 5\ KeV$ (delta ray density) is

$$n_\delta = \frac{Z^2}{\beta^2} f(\beta) \tag{2.8}$$

The δ-ray density is generally used in identifying the particles of projectile fragments. The δ-ray density depends on the criteria adopted to define a δ-ray. Usually a minimum length or a minimum total grain count (four grains in a row) is specified.

2.6 Classification of secondary particles

Secondary particles associated with each interaction are classified by determining their energy loss in the emulsion medium, that is, by calculating their grain density over a certain length (~100 μm). The normalized grain density is defined as $g^* = g/g_o$, where g is the observed grain density and g_o is the minimum ionization caused by the relativistic singly charged particles such as electrons or protons over the same length. Therefore particles in an event are classified into the following categories in accordance with the standard emulsion terminology.

- Singly charged particles with relative ionization $g/g_o < 1.4$. This ionization cut corresponds to particle velocities $\beta > 0.7$. These particles

include produced particles and protons from the colliding nuclei having energies greater than *400 MeV*. These are called shower particles or relativistic charged particles and their number is denoted by n_s.

- Singly charged particles with relative ionization $1.4 \leq g/g_o \leq 10$ and range in emulsion $L > 3mm$. This corresponds to velocities in the interval $0.23 < \beta \leq 0.7$. These particles are mainly protons from the target having energies in the range $(26 - 400)$ *MeV*. These are called grey particles and their number is denoted by n_g.
- Particles with relative ionization $g/g_o > 10$ and the range $L \leq 3mm$. These are the spectator target protons with energies less than *26 MeV* and multi-charged target fragments. These are called black particles and their number is denoted by n_b. The grey and black particles are together termed as heavy particles and are represented as $N_h = n_g + n_b$
- Multi-charged relativistic particles. These are solely projectile fragments with nearly the same energy per nucleon as that of the projectile. Their number is denoted by n_f. These particles are emitted within a narrow cone around the beam direction.

2.7 Angle measurements

2.7.1 Projected angle

To measure the space angle of a particle with respect to the primary direction, its projected angle in the X-Y plane with respect to the primary direction is measured. The projected angle can be measured directly with the help of a goniometer having least count of 0.25° under high magnification. The vertex of the collision is focused at the center of scale of the goniometer. The

track of the primary particle is aligned with the reference line of scale. Now the tracks of the secondary particles are aligned one by one with the reference line and the goneometer reading is taken for the projected angle θ_p with respect to the forward direction of primary particle.

2.7.2 Dip angle

This is the angle between the direction of emitted particle with the X-Y plane. If Δ_Z is the difference at two points on the track separated by a distance Δ_X, then the angle

$$\theta_d = tan^{-1}(\Delta_Z/\Delta_X), \tag{2.9}$$

is the dip angle of the track. Since the thickness of the emulsion stack gets reduced after the fixation (shrinkage), the dip angle is generally written as.

$$\theta_d = tan^{-1}(S.F \times \Delta_Z/\Delta_X), \tag{2.10}$$

where S.F is the shrinkage factor.

2.7.3 Space angle

Once the projected angle θ_p and dip angle θ_d are known, one can easily determine the space angle using the expression

$$cos\ \theta_S = cos\ \theta_p \times cos\ \theta_d \tag{2.11}$$

When the angular separation between the tracks in the forward cone is very small, it is difficult to measure the θ_p and θ_d directly due to the overlapping of tracks. In such cases, the co-ordinate method is used. According

to this method, the emission angle of each secondary track is measured by taking the co-ordinates (X_0, Y_0, Z_0) of the collision vertex, co-ordinates (X_1, Y_1, Z_1) at the end of the linear portion of the secondary track and the co-ordinates (X_i, Y_i, Z_i) of one point on the incident beam.

2.7.4 Azimuthal angle

This is the angle of projection of the secondary track in the Y-Z plane with respect to the Y-axis. The azimuthal angle is determined using the projected angle θ_p and dip angle θ_d. The azimuthal angle can also be determined by measuring the co-ordinates of the three points as mentioned above.

2.8 Rapidity variable

One of the most important variables used frequently to study the angular distribution of the charged particles produced in the relativistic heavy ion collisions is the rapidity variable. It is defined as

$$Y = \frac{1}{2}\ln\left[\frac{E + p_L}{E - p_L}\right] \tag{2.12}$$

where E and p_L are the total energy and longitudinal momentum of the outgoing particle respectively. However, it is quite tedious to determine the value of this variable for every particle because both energy as well as momentum are to be determined. In order to make it workable, an approximation, that is, the mass of a particle is negligible in comparison to its

momentum is made. This approximation is valid at high energies only and it leads to a new variable known as pseudo-rapidity variable 'η'

$$\eta = -ln\ tan\ \theta/_2, \tag{2.13}$$

where θ is the space angle of the secondary particle with respect to the incident direction of the primary particle. The transformation from Y to η can be readily obtained in the following way.

$$Y = \frac{1}{2}\ln\left[\frac{E + p_L}{E - p_L}\right]$$

$$= \ln\left[\frac{(E + p_L)^2}{(E + p_L)(E - p_L)}\right]^{\frac{1}{2}}$$

$$= \ln\left[\frac{E + p_L}{(E^2 - p_L^2)^{1/2}}\right]$$

The relativistic expression for the total energy is

$$E^2 = p^2c^2 + m_o^2 c^4$$

or $$E^2 = p^2 + m_o^2 \qquad \text{for } c = 1$$

At very high velocities, $p \gg m_o$. under this approximation, one can write $E = p$. It is because of this change that Y goes to η. Therefore,

$$\eta = \ln\left[\frac{p + p_L}{(p^2 - p_L^2)^{1/2}}\right]$$

$$= \ln\left[\frac{p + p\cos\theta}{(p_L^2 + p_T^2 - p_L^2)^{1/2}}\right]$$

$$= \ln\left[\frac{p(1 + \cos\theta)}{p_T}\right]$$

$$= \ln\left[\frac{1+\cos\theta}{\sin\theta}\right]$$

$$= \ln\left[\frac{2\cos^2\theta/2}{2\sin\theta/2\cos\theta/2}\right]$$

$$= \ln\cot\theta/2$$

$$or\ \eta = -\ln\tan\theta/2$$

The physical significance of the minus sign is that with the increasing angle, η decreases. The advantage of using the rapidity variable is that it is an additive quantity, that is, the results in one frame of reference can be readily transformed into other frame using the relation

$$Y_{Lab} = Y_{CM} + Y_{Boost} \tag{2.14}$$

where

$$Y_{Boost} = \frac{1}{2}\ln\left[\frac{1+\beta}{1-\beta}\right]$$

2.9 Present experiment

In the present investigation, an emulsion stack of dimensions 16 ×10 × 0.06 cm^3, exposed to a silicon beam of energy 14.6 AGeV from the Alternating Gradient Synchrotron (AGS) at Brookhaven National Laboratory (BNL), USA has been used. The tracks were picked up at 4mm from the entrance side of the stack and were followed backward in order to ensure that they are not secondary tracks. All the tracks thus picked up were then followed until they interacted or left the stack. Scanning was carried out through line scanning with almost 100 percent efficiency. A total of 1107 interactions (inelastic) of

silicon were picked up by following 12258.8 cm of the primary track length leading to a mean free path $\lambda = 11.07 \pm 0.48$ cm. Out of these, interactions that were within $20\mu m$ from the top or bottom surface of the emulsion pellicle, were not considered for the final analysis. Moreover, collisions caused by primaries making an angle greater than 2° with the mean beam direction were not recorded. In this way, 796 interactions were picked up for the final analysis.

Events were divided into different target groups: H, CNO and AgBr according to the standard emulsion criteria. Usually events with $N_h \leq 1$ are classified as collisions with hydrogen ($A_T = 1$), events with $2 \leq N_h \leq 7$ as collisions with light nuclei ($<A_T> = 14$) and events with $N_h \geq 8$ as collisions with heavy nuclei ($<A_T> = 94$). In this method the separation of events ($N_h \geq 8$) for AgBr target events is quite accurate in the sample, but in $N_h \leq 7$ events, there is an admixture of CNO target events and peripheral AgBr target events. To overcome this, the following criteria have been adopted for target identification:

AgBr events: (i) $N_h \geq 8$

(ii) $N_h < 8$ and at least one track with range $R \leq 10\ \mu m$ and no track with $10 \leq R \leq 50\ \mu m$.

CNO events: $2 \leq N_h \leq 7$ and no track with $R \leq 10\ \mu m$.

H events: (i) $N_h = 0$

(ii) $N_h = 1$ but not falling in above categories.

In each event the space angles of emission of all particles emitted from the collision vertex were measured under high magnification. To measure the space angle of a particle with respect to the primary, its projected angle (θ_p) in the X-Y plane with respect to the X-direction was measured with the help of a goniometer having a least count of 0.25° under 1000x magnification.

The dip angle (θ_d) of each particle was calculated using the relation: $tan\theta_d = (SF \times \Delta Z)/\Delta X$, where SF is the shrinkage factor of the emulsion, ΔZ is the difference between the z-coordinate at two points on the track of the particle separated by a distance ΔX. Knowing the projected angle and dip angle, the space angle of each particle was calculated using the expression: $cos\theta = cos\theta_p \times cos\theta_d$. Having measured the space angles of shower particles, the pseudorapidity ($\eta = -ln\ tan\ \theta/2$) of each particle was determined. The accuracy in the measurement of space angle was ~1 *mrad* and the corresponding accuracy in the calculation of pseudorapidity was ~ 0.1 unit.

At high energy, most of the shower particles lie in a narrow forward cone. These shower particles travel a large distance in an emulsion plate before crossing over to the adjacent plate. Tracks of all shower particles were followed over a large distance so that the double tracks, if any, were resolved. However, double tracks emitted with large dip angles have small projected lengths and thus it is difficult to resolve them. But the number of shower tracks having small projected lengths is small and therefore, the number of double tracks having small projected lengths is even smaller.

2.10 Models of nucleus-nucleus collisions

Since the search for the signatures of phase transition is extremely complicated and ambiguous, it is necessary to learn whether the proper conditions needed for the phase transition do really occur. Therefore, to study the reaction mechanism and to find out how the parameters of the system behave during the multi-particle production in the relativistic heavy ion collisions, various models have been proposed [8-20] so as to explain the experimental results. Besides, some event generators (simulations) have also been introduced. All these event generators assume no QGP formation and help in estimating the background signals. Some of these models and event generators are briefly described here.

2.10.1 Fireball model

The fireball model [21,22] is the most simple and promising model and shows a good agreement with the experimental data. In this model, the collision between two heavy ions is described as a two-step process. In the first step (10^{-23} seconds), both the projectile and target are assumed to make a clean cylindrical cut through each other (Fig 2.1). The projectile participants are assumed to transfer all their momentum to the effective center-of-mass system of all the participant nucleons forming a fireball, which moves forward in the laboratory frame at velocity between those of the target and projectile. This picture is referred to as nucleon fireball model and the three regions produced are the participant region, projectile spectator region and target spectator region. The energy density in the fireball is extremely high and consequently may be treated as an ideal gas, whose properties may be determined by the laws of thermodynamics. The fireball subsequently expands isotropically.

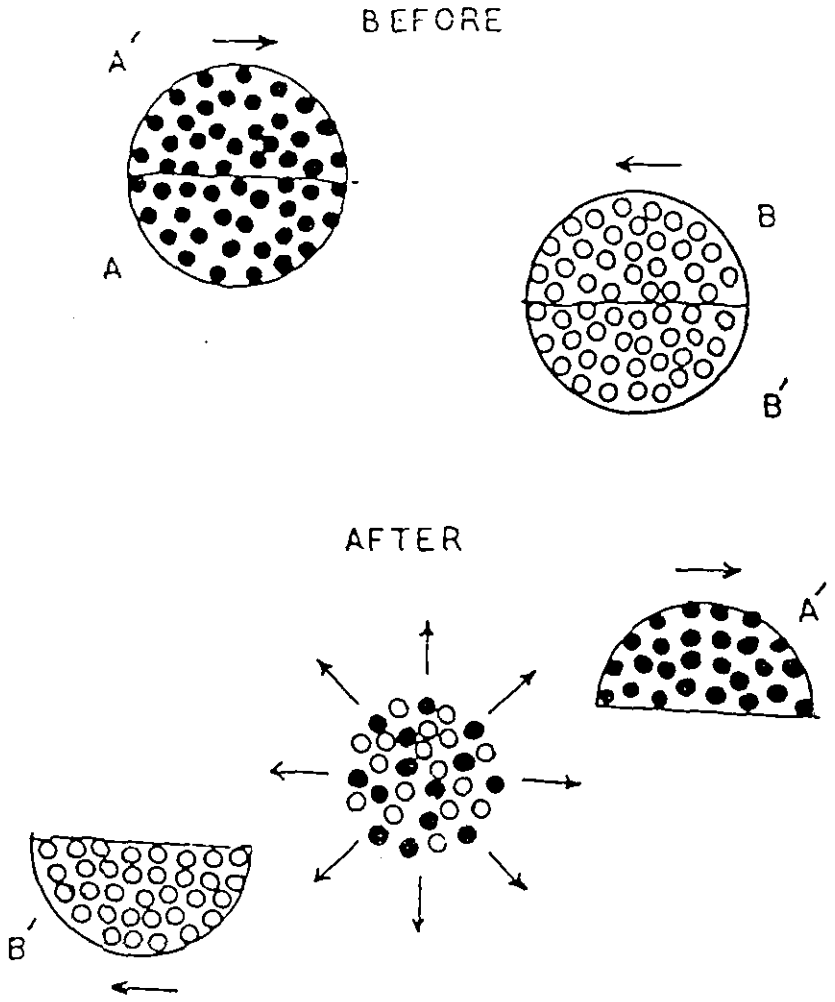

Fig. 2.1 Primary and secondary stages of two colliding nuclei in Fireball model. Parts A and B are the participants. Parts A' and B' are the spectators.

If A_t and A_p ($A_p = Z_p + N_p$, where Z_p is the number of protons and N_p the number of neutrons) are the number of nucleons in the target and projectile, the geometrical cross section is given by

$$\sigma = \pi r_0^2 \left(A_p^{1/3} + A_t^{1/3} \right)^2 , \tag{2.15}$$

where $r_0 = 1.0 - 1.2\,fm$. If a proton inside the projectile hits the target, it falls in the participant group, otherwise remains as a spectator. The average number of participant protons from the projectile nucleus is given as [23,24]

$$\left\langle Z_{proj}^{part} \right\rangle = \frac{Z_p \pi r_0^2 A_t^{2/3}}{\sigma}$$

$$= \frac{Z_p A_t^{2/3}}{\left(A_p^{1/3} + A_t^{1/3} \right)^2} \tag{2.16}$$

Similarly, the average number of target participants is

$$\left\langle Z_{tar}^{part} \right\rangle = \frac{Z_t A_p^{2/3}}{\left(A_p^{1/3} + A_t^{1/3} \right)^2} \tag{2.17}$$

The total number of participant protons Z_{eff}^{part} is thus given by

$$Z_{eff}^{part} = \left\langle Z_{proj}^{part} \right\rangle + \left\langle Z_{tar}^{part} \right\rangle$$

$$= \frac{Z_p A_t^{2/3} + Z_t A_p^{2/3}}{\left(A_p^{1/3} + A_t^{1/3} \right)^2} \tag{2.18}$$

Similarly, the total number of target and projectile spectators are respectively given by

$$Z_{eff}^{proj/spec} = Z_p - \left\langle Z_{proj}^{part} \right\rangle$$

$$= \frac{Z_p\left(A_p^{2/3} + 2 A_p^{1/3} A_t^{1/3} \right)}{\left(A_p^{1/3} + A_t^{1/3} \right)^2} \qquad (2.19)$$

$$Z_{eff}^{tar/spec} = Z_t - \left\langle Z_{tar}^{part} \right\rangle$$

$$= \frac{Z_t\left(A_t^{2/3} + 2 A_p^{1/3} A_t^{1/3} \right)}{\left(A_p^{1/3} + A_t^{1/3} \right)^2} \qquad (2.20)$$

The advantage of this model is its simplicity and non-involvement of the adjustable parameters. This model works nicely at low and medium energies.

2.10.2 Hydrodynamical models

Another type of models, which have been developed to describe the nucleus-nucleus collisions are the Hydrodynamical models [25,26]. These models assume that the mean free path for the interaction of a particle in a system is much less than the size of the system. In these models, when the two colliding nuclei collide, they instantaneously merge together, coming to equilibrium in the form of a drop of nuclear fluid. The characteristics of the resulting nuclear fluid are governed by the standard laws of thermodynamics. Generally these models consider two nuclear fluids corresponding to the

projectile and target nuclei. The behaviour of each of these fluids is determined by the fluid dynamics, conservation equations for nucleon number, energy and momentum.

The validity of the fluid model is subject to two constraints:

i) The collision must last for a sufficiently long time so that the local equilibrium is allowed to set in.

ii) The interaction strength between the two colliding nuclei must be large so that the formation of a single fluid droplet is ensured.

The resulting fluid drop corresponding to the projectile and target nuclei is the main source [27] of the secondary particles produced in the collision.

2.10.3 Wounded nucleon model

Wounded nucleon model is considered as one of the simplest models for explaining the phenomenon of multiparticle production in nuclear collisions. This model takes into account the total number of relativistic charged particles to determine the number of wounded nucleons W.

The particle multiplicity in nucleus-nucleus collisions at a given energy is given by

$$n_A = \frac{1}{2} W \times n_{PP}(E), \tag{2.21}$$

where n_{PP} is the number of particles produced at the same energy in pp collisions. W is the number of wounded nucleons and it depends on the nuclear radius, density and impact parameter [28,29]. The number of wounded nucleons in a nuclear collision is given by the relation [28]

$$W = A_T \frac{\sigma_{NP}}{\sigma_{PT}} + A_P \frac{\sigma_{NT}}{\sigma_{PT}} = W_T + W_P, \qquad (2.22)$$

where σ_{PT} is the total inelastic hadronic cross-section for the projectile nucleus interacting with the target nucleus. σ_{NP} and σ_{NT} are the corresponding nucleon-nucleus cross-sections. A_P and A_T are the mass numbers of two interacting nuclei respectively. The first term in equation 2.24 represents the number of wounded target nucleons W_T and the second one the number of projectile wounded nucleons W_P [30].

In the central nucleus-nucleus collisions, the number of total wounded nucleons is determined with the help of the maximum impact parameter. The value of b_{max} for the central nucleus-nucleus collisions may be estimated by the expression

$$\sigma_{par} = \pi b_{\max}^2 = \frac{N_{central}}{N_{total}} \sigma_{pt}, \qquad (2.23)$$

where $N_{central}$ is the number of central collisions from a sample of N_{total} events. N_{total} is obtained from a minimum bias scan of emulsions. The wounded nucleon model predicts that the cross-section for the excited nucleons due to various interactions is assumed to be the same as that for the unexcited ones. The number of target and projectile interactions may be estimated as

$$\upsilon_T = A_T \frac{\sigma_{NN}}{\sigma_{NT}} \qquad (2.24)$$

and

$$\upsilon_P = A_P \frac{\sigma_{NN}}{\sigma_{NP}} \qquad (2.25)$$

Further the total number of interactions caused by the projectile nucleons with the target nucleons may be obtained from the relation

$$\upsilon = W_P \upsilon_T = W_T \upsilon_P \tag{2.26}$$

It has been reported [29-31] that the predictions of wounded nucleon model are quite compatible with results obtained for experimental as well as FRITIOF data at SPS energies.

2.10.4 Bjorken model

This model is also called as inside outside cascade model of nuclear collisions [32]. In this model, it is assumed that the two nuclei collide at time $t = 0$, then at some time later, t, the system can be seen as composed of separate projectile and target remnant regions, with a cylinder of hot material stretching between them. The target and projectile fragmentation regions are moving apart at relativistic velocities, so that at some time after the collision, spatially separated regions along the axis of cylinder are causally separated. Fig. 2.2 shows the different stages of two nuclei in the Bjorken model.

The stretching cylinder can be parameterized in terms of a set of Lorentz frames interpolating between those of the target and projectile fragmentation regions. Further the model assumes that shortly after the collision, equal amounts of energy are deposited in each of those frames. The initial condition allows the evolution of the system to be described by simple hydrodynamic equations [33].

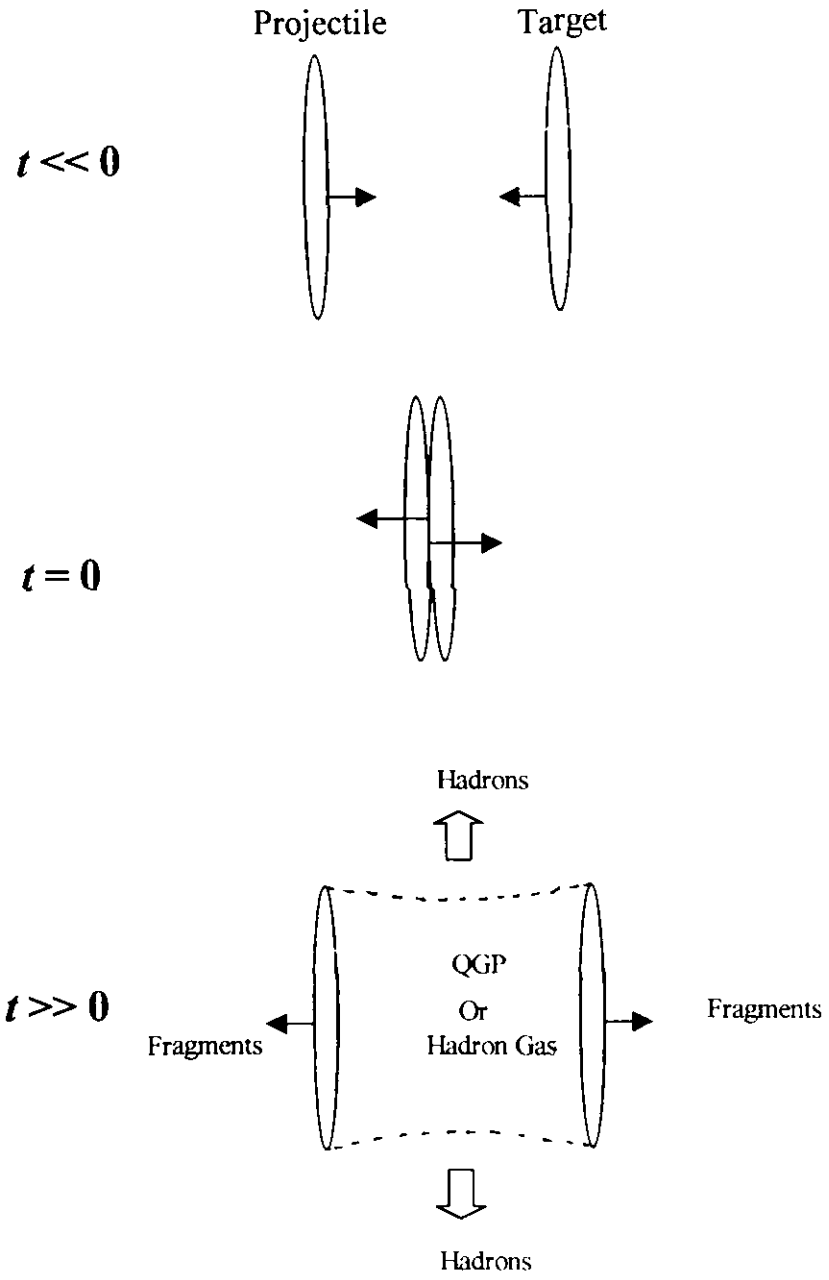

Fig. 2.2 Different stages of the two colliding nuclei in Bjorken model.

In the model the excited system, where the energy is deposited, is treated as a relativistic fluid. After the interaction, the two nuclei separate and at this time, the relativistic fluid is seen as uniformly expanding from the central position of the collision outward to the projectile and target regions. The material within the stretching cylinder is all moving at approximately the same velocity along the beam axis. With these assumptions Bjorken has shown that the entropy '*S*' remains constant, preserving a record of the early conditions in the collisions [32,33]. This model can provide an estimate of the energy density in the initial state with a few simplifying assumptions.

2.10.5 FRITIOF event generator

FRITIOF is a non-QGP event generator for hadron-hadron, hadron-nucleus and nucleus-nucleus collisions [34-38]. The basic idea of the model is that the hadron behaves like a relativistic string with confined colour field, that is, it consists of a hard core surrounded by an exponentially damped field.

In FRITIOF generator, when two nucleons interact, two excited string states are formed and then these excited states hadronize into final hadrons [39]. Interaction between the two nucleons is assumed to take place through the exchange of many small momenta between their constituent partons, however no net colour exchange takes place. The net colour exchange is assumed to be balanced by gluon exchanges. During the collision, two hadrons are excited due to momentum transfer and the highly excited string like objects (colour dipole) are formed, which emit gluons until a critical value of gluon emission is reached. The formed objects are then fragmented into final hadrons. The FRITIOF generator has also been developed to describe hadron-nucleus and nucleus-nucleus collisions by assuming that the reaction is a

superposition of hadron-hadron collisions in which geometry of nucleus plays an important role. FRITIOF model has succeeded in describing many experimental data in nucleus-nucleus collisions up to the highest SPS energy ranges [38]. In FRITIOF event generator, events are generated according to the Gaussian distribution with projectile energy, projectile mass and target mass as inputs. Moreover, if the number of participant nucleons is zero, then the interaction is rejected.

2.10. 6 VENUS event generator

VENUS is also a Monte Carlo procedure to simulate events at ultrarelativistic energies for hadron-hadron, hadron-nucleus and nucleus-nucleus collisions [40,41]. VENUS has some very important features. It allows secondary interactions to occur. In this model, each produced particle is allowed to re-interact with other produced particles or with spectators, which is very important for the hadron-nucleus and nucleus-nucleus collisions.

This model incorporates the participation of anti-quarks in the colour exchange mechanisms to form strings. It also has a sophisticated fragmentation procedure. Since the space-time evolution is an important issue concerning final state interaction, the VENUS fragmentation model has a right space-time description. This model uses the Feynmann field method for hadronization of the strings. In this method, one starts with a single quark 'a' with some initial momentum. In its colour field, a quark-antiquark pair $b-\bar{b}$ is formed. 'a' combines with $\bar{b}$ forming a meson with some momentum. b is left with the remaining momentum. In $b's$ field another pair $c-\bar{c}$ can form such that b and $\bar{c}$ give rise to another meson. This process continues until all the initial momentum is utilized. The end result is a chain of mesons among which many

decay if they are unstable. It is worth mentioning that this model is applicable at ultrarelativistic energies ($\geq 50\ GeV/n$) only.

2.10.7 HIJING event generator

Heavy Ion Jet INteraction Generator is another event generator for parton and particle production in high energy hadronic and nuclear collisions [42-45]. Based on QCD inspired models for multiple jet production, it is designed in particular to study jet and mini-jet production and associated particle production in high energy hadron-hadron, hadron-nucleus and nucleus-nucleus collisions. This model incorporates mechanisms such as multiple mini-jet production, soft excitation and jet interactions in dense hadronic matter. HIJING is written in FORTRON language, consisting of subroutines for physics simulation and common blocks for parameters and event records. In this model no secondary interactions are allowed, that is, rescattering of produced particles is not implemented.

HIJING model is the most thoroughly documented and tested heavy ion generator. It has been extensively compared to nucleon- nucleon and nucleon - nucleus data at collider energy and with the existing heavy ion data at SPS energies.

References

[1] B. Andersson et al., *Phys. Lett.* **B73**, (1978) 343.

[2] R. W. Gurney and N. F. Mott, *Proc. Roy. Soc.(London)* **A164**, (1938) 151.

[3] N. F. Mott and R. W. Gurney, *Elec. Proc. in Ionic Crys. 2nd ed., Clarendon Press*, Oxford (1948).

[4] Fowler and Perkins, *Phil. Meg.* **46**, (1955) 587.

[5] D. M. Ritson, *Phys. Rev.* **91**, (1953) 1572.

[6] G. Baroni and C. Castagoli, *Nuovo Cem.12, suppl.* **1**, (1954) 364.

[7] G. Tomasini et al., *Nuovo Cem.* **9**, (1958) 525.

[8] A. Z Mekjian, a) *Phys. Rev.* **C17**, (1978) 1051.
b) *Phys. Lett.* **B89**, (1980) 177.

[9] S. Das Gupta and A. Z Mekjian, *Phys. Report* **72**, (1981) 131.

[10] J. P. Bondrof et al., *Nucl. Phys.* **A296**, (1978) 320.

[11] P. J Siemens and J.O Rasmussen, *Phys. Rev. Lett.* **42**, (1979) 844.

[12] H. Stocker et al., *Phys. Rev. Lett.* **44**, (1980) 725.

[13] Y. Yariv and Z. Fraenkel, a) *Phys. Rev.* **C20**, (1979) 2277.
b) *Phys. Rev.* **C24**, (1981) 488.

[14] J. Cugnon, *Phys. Rev.* **C22**, (1980) 1885.

[15] J. Cugnon et al., *Nucl. Phys.* **A360**, (1981) 444.

[16] I. Otterlund and E. Stenlund, *Lund Univ. Report* (1978) 7806.

[17] M. Sandel et al., *Phys. Rev.* **C20**, (1979) 744.

[18] R. Hagedron and J. Rafelski, *Phys. Lett.* B 97, (1980) 136.

[19] A. Capetta et al., *LBL-Report* (1983) 16281.

[20] A. Bialas and W. Czyz, *Proc. Workshop on Future Relativistic Heavy Ion Experiments*, Darmstadt (1980).

[21] G. D Westfall et al., *Phys. Rev. Lett.* **37**, (1976) 1202.

[22] J. Gosset et al., *Phys. Rev.* **C18**, (1978) 844.

[23] R. J. Glauber and Matthial, *Nucl. Phys.* **B21**, (1970) 135.

[24] S. Nagamiya, *Nucl. Phys.* **A335**, (1980) 517.

[25] A. A Amsden et al., *Phys. Rev.* **C15**, (1977) 2509.

[26] V. S Barashenkov et al., *UPS Fiz Nauk* **109**, (1973) 93.

[27] A. A Amsden, *Phys. Rev. Lett.* **35**, (1975) 905.

[28] M. A. Nasr, *Ph. D. Thesis submitted to Aligarh Muslim University*, India (1995).

[29] A. Bialas, M. Bleszynski and W. Czyz, *Nucl. Phys.* **B111**, (1976) 461.

[30] H. Sumiyoshi, *Phys. Lett.* **131**, (1983) 241.

[31] A. Dabrowska et al., *Phys. Rev.* **D47**, (1993) 1751.

[32] David H. Skelding, *Ph. D. Thesis submitted to University of Washington,* USA (1996)

[33] J. D Bjorken, *Phys. Rev.* **D27**, (1983) 140.

[34] B. Andersson, G. Gustafson and B. Nilsson-Almqvist, *Nucl Phys.* **B281**, (1987) 289.

[35] B. Nilsson-Almqvist and E. Stenlund, *Comp. Phys. Comm.* **43**, (1987) 387.

[36] B. Andersson, G. Gustafson and B. Nilsson-Almqvist, *Nucl. Phys.* **34**, (1986) 451.

[37] B. Andersson et al., *Phys. Scripta* **B281**, (1987) 289.

[38] Ding Linkai and Evert Stenlund, *Phys Lett.* **B**, (1988) 204.

[39] B. Andersson et al., *Phys. Rep.* **97**, (1983) 31.

[40] K. Werner, *Phys. Rev.* **D39**, (1989) 780.

[41] B. Lorstadt, *Int. J. Mod. Phys.* **A4**, (1989) 2861.

[42] Xin-Nian Wang, *Phys. Rev.* **D43**, (1991) 104.

[43] Xin-Nian Wang and Miklos Gyulassy, *Phys. Rev.* **D44**, (1991) 3501.

[44] Xin-Nian Wang and Miklos Gyulassy, *Phys. Rev.* **D45**, (1992) 844.

[45] Xin-Nian Wang and Miklos Gyulassy, *Phys. Rev. Lett.* **68**, (1992) 1480.

CHAPTER III

Non-statistical fluctuations in multiparticle production in ^{28}Si-AgBr collisions at 14.6 AGeV

3.1 Introduction

Fluctuations of charged particle densities in phase space have a long history going back to early cosmic ray experiments. The phenomenon was first observed in Si-AgBr event of JACEE collaboration [1]. From the experimental point of view, there is little doubt that events with large local density fluctuations exist. The real question is whether these fluctuations are of dynamical or merely statistical origin. Early attempts made to answer this question were not conclusive. Therefore the problem was not followed up.

In the mid nineteen eighties, Bialas and Peschanski [2,3] proposed a new method of studying the density fluctuations in phase space by adopting the well known results obtained in the investigation of cascading phenomenon and turbulent behaviour. The method consists of a measurement of the scaled factorial moments F_q of the rapidity distribution at different values of the resolution $\delta\eta$. By taking several numerical examples, both for smooth and for fluctuating distributions, they showed that the measurement of the scaled factorial moments F_q removes the statistical fluctuations due to the finite number of particles in an event. Consequently, an observation of a variation of F_q with the resolution, that is, rapidity bin size would indicate the presence of genuine fluctuations of dynamical origin. Bialas and Peschanski reanalysed the Si-AgBr event of the JACEE [1] collaboration and observed a power law dependence of F_q on the size of the rapidity bin $\delta\eta$ ($F_q \propto \delta\eta^{-\phi_q}$). This power law dependence of F_q on $\delta\eta$ is known as intermittency.

The observation of power law behaviour of the scaled factorial moments in cosmic ray JACEE event has motivated many experimental groups in high energy physics to search for a similar effect, that is, intermittency in

studied for different values of ϕ_q in various M (number of bins) ranges for both the pseudorapidity and azimuthal spaces. The minimum of λ_q at certain critical value of $q = q_c$, the existence of which is an indication of non-thermal phase transition in multiparticle process, has been studied. In the regions $q > q_c$ and $q < q_c$, the system behaves differently.

Finally, the nuclear effect, which is a consequence of the superposition of elementary nucleon-nucleon collisions in nucleus-nucleus collisions, has been studied in the second order two dimensional factorial moment F_2. The slopes of $ln\langle F_2\rangle$ versus lnM curves for different H, 'Hurst Exponent', values have been determined. The parameter 'a' that characterizes the upward bending of $ln\langle F_2\rangle$ versus lnM curve plots has been investigated.

3.2 Factorial moments

The un-normalized factorial moments are defined as

$$F_q = \frac{1}{M}\sum_{m=1}^{M} n_m(n_m-1)\cdots(n_m-q+1) \tag{3.1}$$

where q = 1,2,3,..... is the order of the moments, n_m is the bin multiplicity and M is the number of partitions in which the phase space window is divided.

Different approaches have been adopted for normalizing the factorial moments. For events of fixed multiplicity N, the normalized or scaled factorial moments are defined as

$$F_q = \frac{1}{M}\sum_{m=1}^{M} \frac{n_m(n_m-1)\cdots(n_m-q+1)}{N(N-1)\cdots(N-q+1)} \tag{3.2}$$

However, in practice high energy collision data consist of collection of events of differing multiplicity, so a different approach is adopted for normalizing such events. If the single particle density distribution is uniform and fluctuation of particle density in a bin is independent of the location of the bin in the considered phase space window, then the factorial moments can be normalized by $\langle n_m \rangle^q = \left(\langle N \rangle / M\right)^q$, where $\langle N \rangle$ is the average multiplicity of particles for all events in the considered phase space window. $\langle n_m \rangle$ is, therefore, the average bin multiplicity for the whole sample. This normalization scheme has been termed as horizontal averaging. Thus the horizontal factorial moments for events of differing multiplicity are defined as

$$F_q = \frac{1}{M} \sum_{m=1}^{M} \frac{n_m (n_m - 1) \cdots (n_m - q + 1)}{\langle n_m \rangle^q} \tag{3.3}$$

or

$$F_q = M^{q-1} \sum_{m=1}^{M} \frac{n_m (n_m - 1) \cdots (n_m - q + 1)}{\langle N \rangle^q} \tag{3.4}$$

To obtain the normalized horizontal factorial moment $\langle F_q \rangle$ for an event sample, F_q values (equation 3.4) are determined for all the events and then averaged over the whole sample using the following equation

$$\langle F_q \rangle = \frac{1}{N_{ev}} \sum_{i=1}^{N_{ev}} F_{q,i} \ , \tag{3.5}$$

where N_{ev} is the total number of events in the sample.

In nuclear collisions, the single particle density distribution cannot be uniform because of the energy and momentum constraints [21]. Although

some models [22] predict a flat central region in the density distribution in the rapidity space at ultrarelativistic energies, the experimental distributions are found to have some shape even in the central region [21]. As the horizontal factorial moments are sensitive to the shape of the single particle density distribution, these moments should be corrected for the non-uniform shape of the single particle density distribution. Fialkowski et al. [23] proposed the following correction factor

$$R_q = \frac{1}{M}\sum_{m=1}^{M}\frac{M^q \langle n_m \rangle^q}{\langle N \rangle^q} \tag{3.6}$$

where $$\langle n_m \rangle = \frac{1}{N_{ev}}\sum_{i=1}^{N_{ev}} n_{m,i}$$

Therefore, the corrected qth order horizontal factorial moment is

$$\langle F_q \rangle^{cor} = \frac{\langle F_q^e \rangle}{R_q} \tag{3.7}$$

Another method to eliminate the effect of non-uniform density distribution has been proposed by Bialas and Gazdzicki [24]. In this method the original variable, say η, is transformed into a cumulative variable X. The corresponding region of investigation $\Delta\eta$ in the new variable X then becomes 0 to 1. In terms of the variable X, the particle density $\rho(X)$ is constant. The cumulative variable $X(\eta)$ is related to the single particle rapidity distribution as

$$X(\eta) = \frac{\int_{\eta_1}^{\eta} \rho(\eta')\, d\eta'}{\int_{\eta_1}^{\eta_2} \rho(\eta')\, d\eta'} \tag{3.8}$$

where η_1 and η_2 are the two extreme limits of the considered pseudorapidity range $\Delta\eta$. The region (0-1) in X space is then divided into M bins, each of size $dX = 1/M$ and the values of the scaled factorial moments are calculated using equations 3.4-3.5.

If the scaled factorial moments $\langle F_q \rangle$ exhibit a power law of the type

$$\langle F_q(\delta\eta) \rangle \propto (\delta\eta)^{-\phi_q}$$

$$\text{or} \qquad \langle F_q(M) \rangle \propto (M)^{\phi_q} \tag{3.9}$$

as $\delta\eta$ tends to zero or M tends to infinity, then it signals the presence of dynamical fluctuations in the data. The power law behaviour of $\langle F_q \rangle$ is referred to as intermittency and the exponents ϕ_q are known as intermittency indices which can be directly retrieved from the slopes of $ln\langle F_q \rangle$ versus lnM graphs.

It is worthwhile to mention that certain experimental biases can affect the experimental results. Factorial moments can be reduced by the limited two-track resolution and track loss. As mentioned in chapter two, nuclear emulsion has high spatial resolution; it is suitable for this kind of high resolution analysis. For minimizing the track loss effect, each event is measured by two

independent observers. Moreover, the factorial moments can be increased due to the γ-ray conservation effect. Gamma rays are produced by the decay of neutral pions (π°), which in turn get materialized into e^{+} e^{-} pairs in the vicinity ($\leq 1mm$) of collision. Since in nuclear emulsion, tracks could be followed along both the forward and backward directions, such conversions can be easily spotted by the scanner, unless they are obscured by a high density of tracks. However, the contribution of such conversions is negligible [21].

3.3 Intermittency

In this section, we study intermittency in our data. The present analysis was carried out for ^{28}Si-AgBr events only. Out of 784 inelastic collisions, 360 ^{28}Si-AgBr events were selected. To minimize the contribution of statistical fluctuations, only events with $N_s \geq 8$ were considered. In this way, 297 ^{28}Si-AgBr events were selected for the final analysis. Further, the analysis was restricted to the central region of the pseudorapidity distribution in the interval $\Delta\eta = \pm 2.0$ units from the central pseudorapidity value. This region covers almost the entire range of the produced particles. To eliminate the effect of non-uniformity of η-distribution, the pseudorapidity values of particles of each event were converted into X values using equation 3.8. In X space, the values of the cumulative variable X lie in the range 0-1. The range $\Delta X = 1$ was divided into M bins, each of size $\Delta X/M$. M was varied from 2 to 35. Using equation 3.4, the values of horizontal factorial moments F_q were calculated for all events and were then vertically averaged over all events to obtain $\langle F_q \rangle$. $\langle F_q \rangle$ were calculated for $q = 2, 3, 4, 5$ and 6.

$ln\langle F_q \rangle$ versus lnM graphs for our data for the pseudorapidity space are shown in Fig. 3.1(a). From the figure, it is clear that $ln\langle F_q \rangle$ increases linearly with lnM, thereby indicating a power law dependence of $\langle F_q \rangle$ on M.

We have also investigated intermittency in the azimuthal angle space. Here also, the azimuthal angle values of particles of each event were converted into X values. The values of the normalized factorial moments were calculated using equations 3.4 and 3.5. Since the distribution in the azimuthal space was almost isotropic, scaled factorial moments were determined for the entire range of ϕ (0-2π). Fig. 3.1(b) shows $ln\langle F_q \rangle$ versus lnM plots for our data for q = 2-6 in the azimuthal space. From these plots, we again observe a power law dependence of $\langle F_q \rangle$ on M. In Fig. 3.1(a & b) the moments of higher order show irregular behaviour. This is due to low statistics.

To obtain the intermittency indices ϕ_q, the graphs in Fig. 3.1(a & b) were fitted to the relation

$$\langle F_q \rangle = A + \phi_q \ln M \tag{3.10}$$

Straight lines in the plots represent equation 3.10. The slopes of these lines, that is, the values of the intermittency indices ϕ_q for both the pseudorapidity and azimuthal angle spaces are presented in table 3.1. From the table, it is clear that the values of ϕ_q increase with the increase in q in both η and ϕ spaces.

It has been pointed out that the scaled factorial moments follow a generalized power law of the type

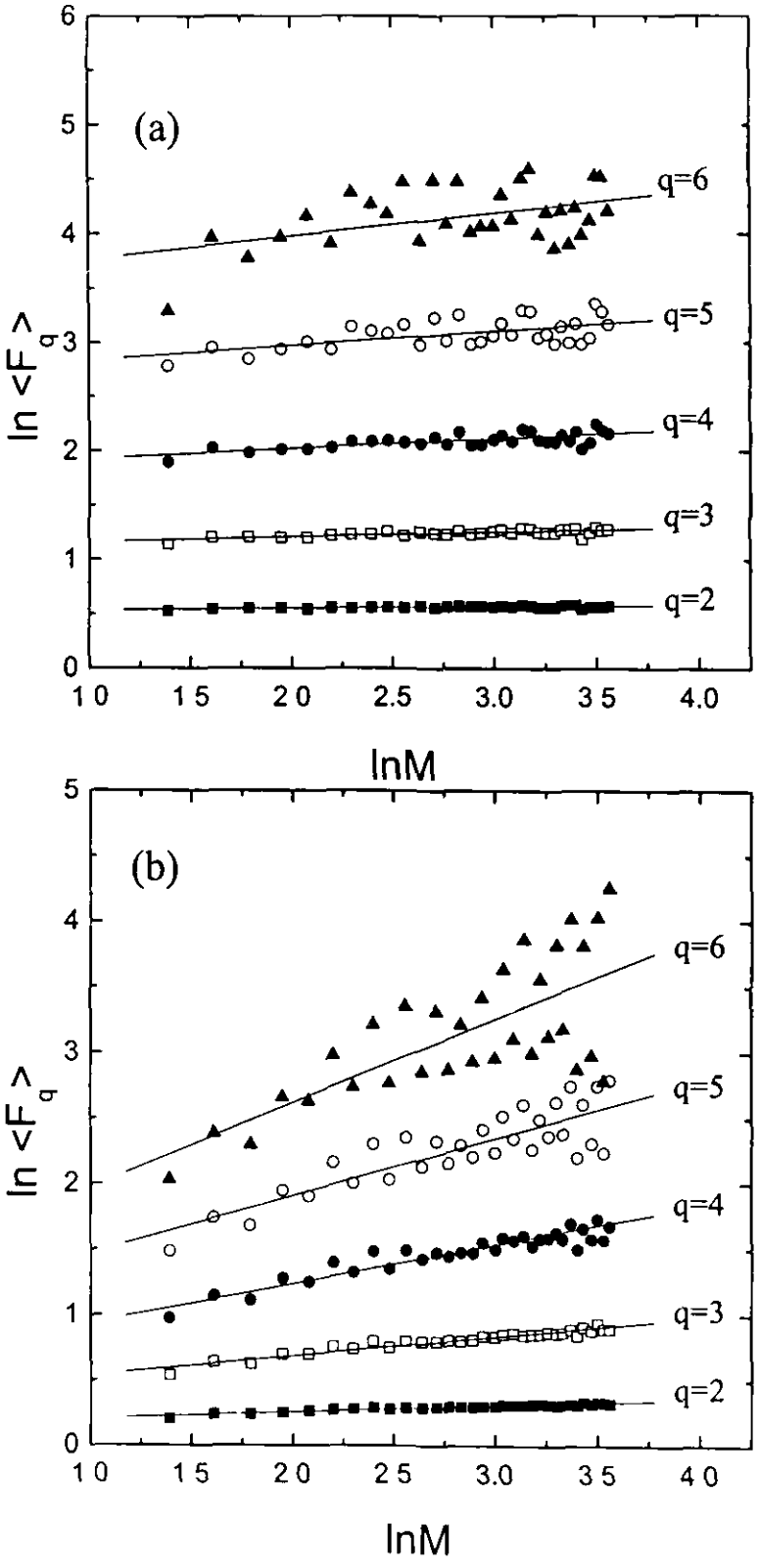

Fig. 3 1 Plots of ln<F_q> versus lnM for ^{28}Si-AgBr collisions at 14 6 AGeV
Solid lines represent the linear fits to the data (a) η- space (b) ϕ- space

Table 3.1 Values of the slopes ϕ_q of $ln\langle F_q \rangle$ versus lnM plots for ^{28}Si-AgBr collisions at 14.6 AGeV in one dimensional η - and ϕ -spaces and in two dimensional η -ϕ space.

q	$\phi_q(\eta)$	$\phi_q(\phi)$	$\phi_q(\eta$-$\phi)$
2	0.016 ± 0.003	0.050 ± 0.003	0.142 ± 0.007
3	0.043 ± 0.007	0.144 ± 0.007	0.303 ± 0.019
4	0.087 ± 0.015	0.273 ± 0.018	0.548 ± 0.049
5	0.133 ± 0.033	0.439 ± 0.048	0.852 ± 0.128
6	0.211 ± 0.074	0.642 ± 0.110	--

$$\langle F_q(M)\rangle \propto [g(M)]^{\phi_q} \tag{3.11}$$

in the multiplicative random models [20]. *g(M)* is a generalized function of *M*. Writing *g(M)* in terms of $\langle F_2\rangle$, the following relation can be obtained

$$\ln\langle F_q\rangle = C_q + \frac{\phi_q}{\phi_2}\ln\langle F_2\rangle \tag{3.12}$$

From equation 3.12, ϕ_q/ϕ_2 can be directly obtained by plotting $ln\langle F_q\rangle$ as a function of $ln\langle F_2\rangle$. To check the validity of equation 3.12 for our data, we plot in Fig. 3.2(a & b) $ln\langle F_q\rangle$ as a function of $ln\langle F_2\rangle$ in both the pseudorapidity and azimuthal angle spaces. The linear behaviour of the plots indicates the validity of equation 3.12 for our data. Values of ϕ_q/ϕ_2 for different q values are obtained by fitting equation 3.12 to the plots in Fig. 3.2 (a & b). Solid lines in Fig. 3.2 represent the fits and the values are shown in table 3.2. Again we see that ϕ_q/ϕ_2 values increase with increase in q.

We have also carried out the analysis in two dimensional (η-ϕ) space to investigate the intermittent behaviour for our data. The considered (η-ϕ) space was divided into M^2 ($M^2 = M_\eta \times M_\phi$) equal cells of area ($\delta\eta\delta\phi$). After converting the values of η and ϕ into X variable. as earlier, the two dimensional scaled factorial moments were then determined with the help of equations 3.4-3.5 with n_m representing the number of particles in the mth cell. The values of the two dimensional scaled factorial moments were determined

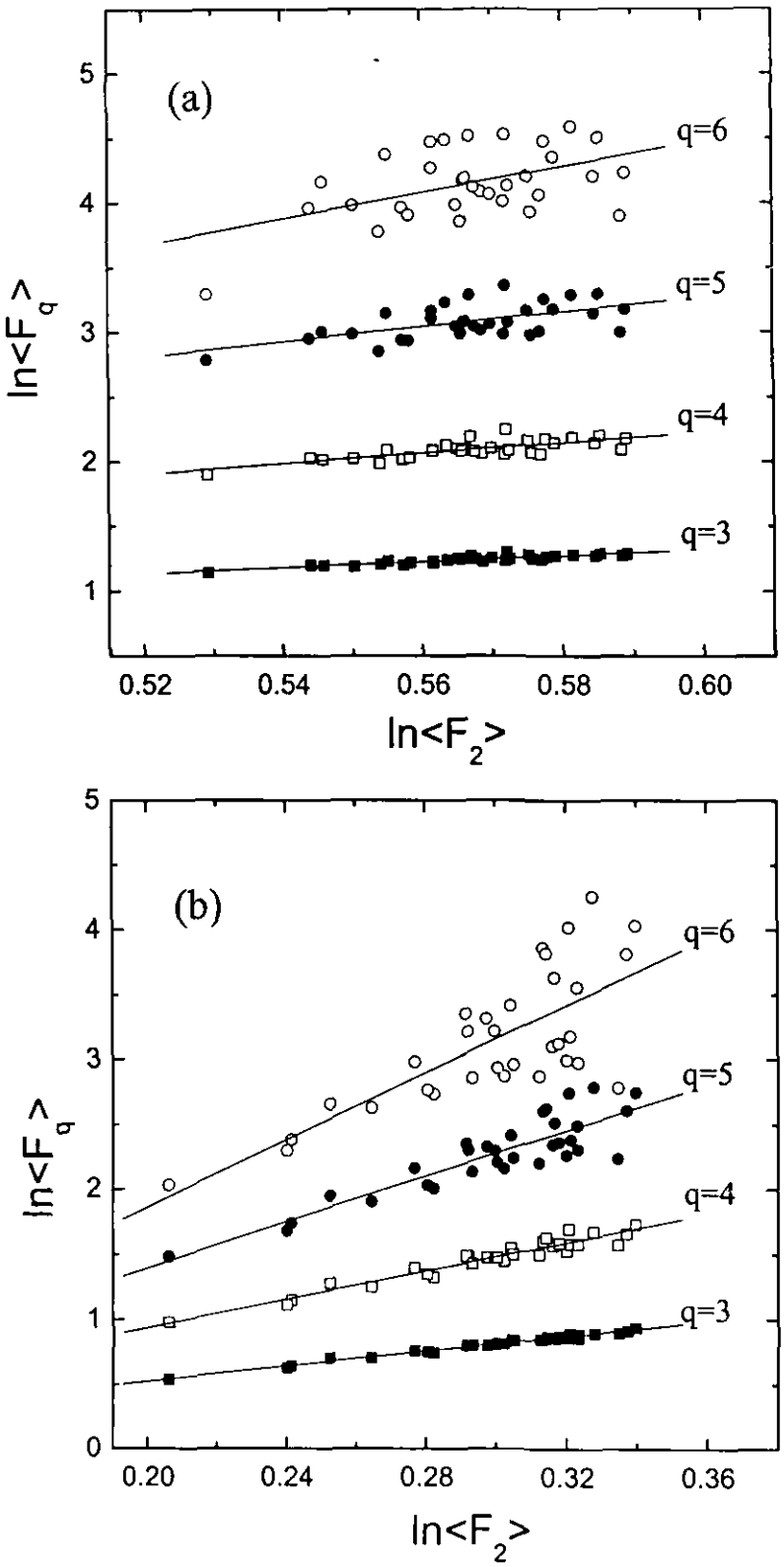

Fig. 3.2 Plots of $\ln\langle F_q \rangle$ versus $\ln\langle F_2 \rangle$ for ^{28}Si-AgBr collisions at 14.6 AGeV. Solid lines represent the linear fits to the data. (a) η- space (b) ϕ- space.

Table 3.2 Values of the slopes ϕ_q/ϕ_2 of $ln\langle F_q \rangle$ versus $ln\langle F_2 \rangle$ plots for ^{28}Si-AgBr collisions at 14.6 AGeV in one dimensional η - and ϕ -spaces and in two dimensional η -ϕ space.

q	ϕ_q/ϕ_q (η)	ϕ_q/ϕ_q (ϕ)	ϕ_q/ϕ_q $(\eta$-$\phi)$
3	2.290 ± 0.198	2.878 ± 0.069	2.143 ± 0.059
4	4.027 ± 0.638	5.452 ± 0.264	3.847 ± 0.305
5	5.793 ± 1.507	8.804 ± 0.851	5.923 ± 0.901
6	10.119 ± 3.238	12.964 ± 2.052	--

for the order 2, 3, 4 and 5 with $\Delta\eta$ = 0.2 - 4.2. The dependence of scaled factorial moments $ln\langle F_q \rangle$ on the number of cells lnM^2 is shown in Fig. 3.3(a). From the figure, it can be observed that $\langle F_q \rangle$ exhibits a power law dependence on M^2, which is an indication of intermittent behaviour in the two dimensional (η-ϕ) phase space also.

The two dimensional intermittency indices ϕ_q obtained from the best linear fits of log-log plots are also listed in table 3.1. From the table, it can be seen that the slopes in two dimensional space increase with increase in q and that the two dimensional intermittency indices are greater than the corresponding one dimensional values for all q values. Moreover, to see if equation 3.12 is valid in the two dimensional phase space also, we plot in Fig. 3.3(b) $ln\langle F_q \rangle$ versus $ln\langle F_2 \rangle$. Again, it is observed that $\langle F_q \rangle$ shows a linear behaviour with $\langle F_2 \rangle$. The ϕ_q/ϕ_2 values obtained from the best linear fits to the data points are presented in table 3.2. These values also increase with the increase in q.

Evidence of the two dimensional intermittency has been reported by several working groups for different relativistic heavy ion data with varying projectile nature and energy. Holynski et al. [9] investigated a multi-dimensional intermittency analysis of 200 AGeV ^{16}O and ^{32}S interactions with AgBr nuclei. They calculated the one and two dimensional intermittency indices for order 2-6 with $\Delta\eta$ = 2.0 - 5.0 and $\Delta\phi$ = 0 - 2π. Jain et al. [25] also studied multidimensional intermittency for 200 and 60 AGeV ^{16}O-AgBr collisions with $\Delta\eta$ = 4.0 and $\Delta\phi$ = 2π. Recently A. M. Tawfik et al. [26] have

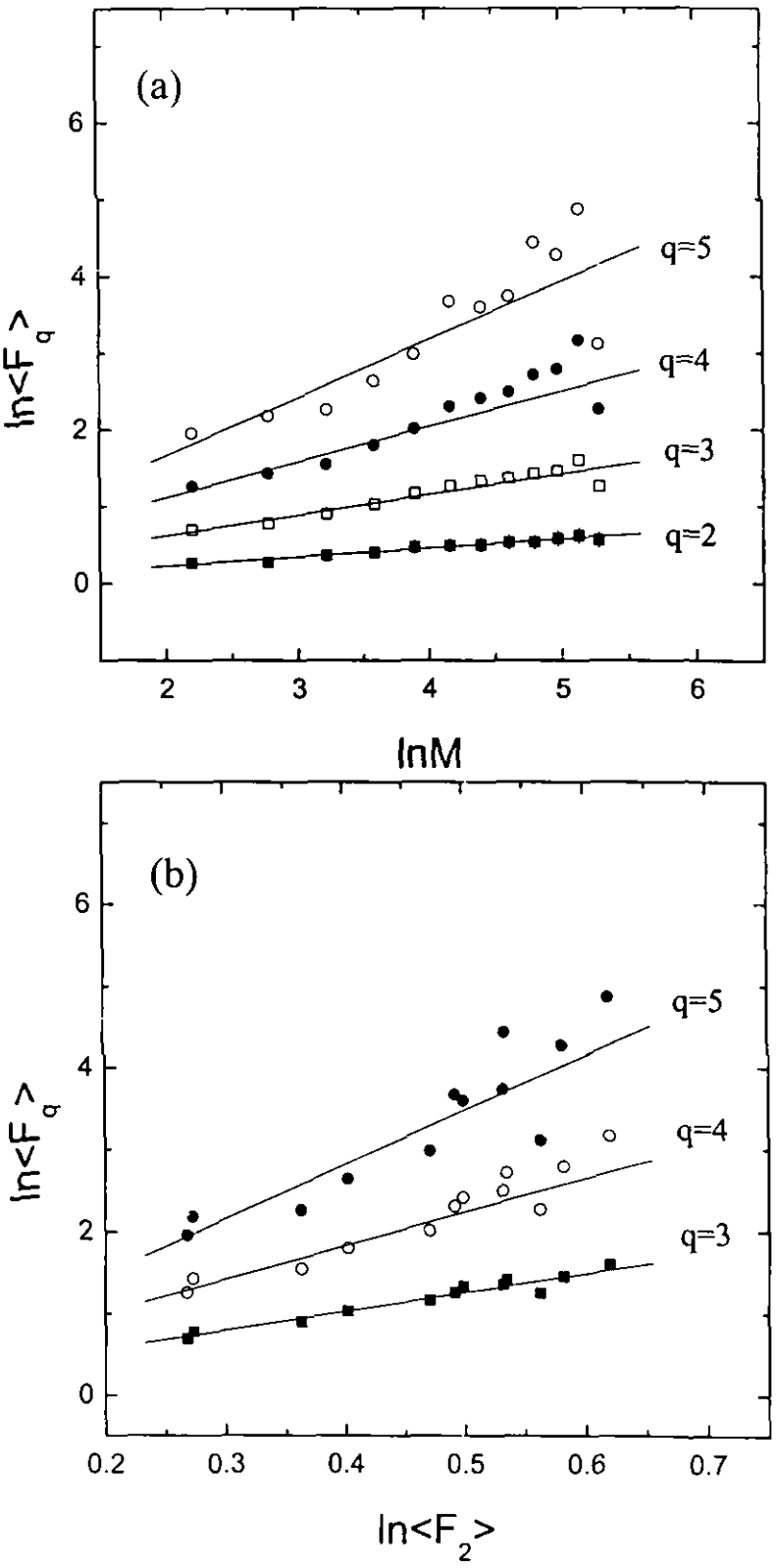

Fig. 3.3 Plots of (a) $\ln\langle F_q \rangle$ versus lnM and (b) $\ln\langle F_q \rangle$ versus $\ln\langle F_2 \rangle$ for ^{28}Si-AgBr collisions at 14.6 AGeV in two-dimensional ($\eta-\phi$) space. Solid lines represent the linear fits to the data.

analysed the data of Pb + Pb collisions at 158 AGeV/c for q = 2, 3, 4 with $\Delta\eta$ = 1.0- 4.0 and full ϕ space and obtained evidence of intermittency.

3.4 Non-thermal phase transition

The self-similar cascade mechanism in multiparticle production is not consistent with particle creation during one phase, but instead requires a non-thermal phase transition [27]. It has been argued [28] that the signals of non-thermal phase transition can be characterized with the help of a parameter λ_q. The function λ_q is related to the qth order intermittency index as

$$\lambda_q = \frac{\phi_q + 1}{q} \tag{3.13}$$

The condition for the existence of such different phases is that the function λ_q should have a minimum at certain critical value $q = q_c$ [29,30]. In the regions $q < q_c$ and $q > q_c$, the multiparticle system behaves differently. It has been observed that the region $q < q_c$ is dominated by numerous small fluctuations and the region $q > q_c$ is dominated by a small number of large fluctuations. The overall system is described [27] as a mixture of a 'liquid' of many small fluctuations and a 'dust' of a few grains of very high density. We see either the liquid phase or the dust phase, depending on whether we probe the system by a moment of order $q < q_c$ or $q > q_c$.

Although no final conclusions could be drawn yet regarding the non-thermal phase transition, a few working groups have reported observation of λ_q minimum for different data sets with varying types of projectile and energy. Jain

et al. [25] have reported that only some part of their heavy ion data had a minimum of λ_q. Sarkisyan et al. [31,32] have observed a λ_q minimum at $4 < q_c < 5$ in central C-Cu collisions at 4.5 AGeV/c. Ghosh et al. [27] have also observed a minimum at $3 \leq q_c \leq 4$, while analyzing the ^{16}O-AgBr collisions at 60 AGeV. Sarkisyan et al. and Ghosh et al. have carried out the analysis for q = 2-8.

We also studied the non-thermal phase transition in ^{28}Si-AgBr collisions at 14.6 AGeV for q = 2-6. We have determined the values of intermittency indices ϕ_q from the $ln\langle F_q \rangle$ versus lnM (Figs. 3.1& 3.2) graphs for the intervals $2 \leq M \leq 35$, $2 \leq M \leq 9$, $5 \leq M \leq 16$, $7 \leq M \leq 18$, $15 \leq M \leq 26$ and $27 \leq M \leq 35$ in both the pseudorapidity and azimuthal spaces. The values of the slopes in these intervals, ϕ_q are presented in table 3.3 and table 3.4. From these tables, it can be seen that ϕ_q increases sharply with the order of the moment in ranges $2 \leq M \leq 9$ and $27 \leq M \leq 35$ for η space, whereas in ϕ space, the sharp increase is observed in $2 \leq M \leq 9$ range only.

Using equation 3.13, the values of λ_q for all q values and M ranges have been calculated in both η and ϕ spaces. The variation of λ_q as a function of q for different M intervals for η and ϕ spaces is shown in Figs. 3.4 and 3.5 respectively. From Fig 3.4, it can be observed that a minimum of λ_q occurs between q = 4 and 5 for the interval $2 \leq M \leq 9$. For the interval $27 \leq M \leq 35$, it occurs around q = 4. However, for the other intervals, no significant minimum is observed. It may be pointed out here that due to low statistics, we could not determine the values of λ_q for orders greater than 6.

Table 3.3 The intermittency exponents ϕ_q for different bin ranges for ^{28}Si-AgBr collisions at 14.6 AGeV in the pseudorapidity space.

Bin range	$q = 2$	$q = 3$	$q = 4$	$q = 5$	$q = 6$
$2 \leq M \leq 35$	0.028 ± 0.004	0.072 ± 0.009	0.133 ± 0.018	0.200 ± 0.031	0.460 ± 0.081
$2 \leq M \leq 9$	0.067 ± 0.016	0.169 ± 0.041	0.286 ± 0.069	0.398 ± 0.087	1.269 ± 0.201
$5 \leq M \leq 15$	0.020 ± 0.004	0.040 ± 0.011	0.088 ± 0.022	0.198 ± 0.073	0.353 ± 0.164
$7 \leq M \leq 18$	0.025 ± 0.005	0.047 ± 0.015	0.097 ± 0.037	0.158 ± 0.105	0.213 ± 0.220
$15 \leq M \leq 26$	0.008 ± 0.012	0.051 ± 0.029	0.065 ± 0.088	0.049 ± 0.204	0.041 ± 0.389
$27 \leq M \leq 35$	0.034 ± 0.051	0.057 ± 0.133	0.333 ± 0.263	0.866 ± 0.465	1.754 ± 0.763

Table 3.4 The intermittency exponents ϕ_q for different bin ranges for ^{28}Si-AgBr collisions at 14.6 AGeV in the azimuthal space.

Bin range	$q = 2$	$q = 3$	$q = 4$	$q = 5$	$q = 6$
$2 \le M \le 35$	0.090 ± 0.005	0.249 ± 0.014	0.460 ± 0.027	0.719 ± 0.049	1.088 ± 0.096
$2 \le M \le 9$	0.128 ± 0.023	0.350 ± 0.064	0.642 ± 0.123	0.981 ± 0.193	1.657 ± 0.214
$5 \le M \le 15$	0.093 ± 0.006	0.258 ± 0.025	0.484 ± 0.059	0.757 ± 0.112	1.058 ± 0.189
$7 \le M \le 18$	0.074 ± 0.007	0.194 ± 0.023	0.340 ± 0.053	0.509 ± 0.111	0.682 ± 0.211
$15 \le M \le 26$	0.060 ± 0.010	0.188 ± 0.024	0.343 ± 0.056	0.513 ± 0.205	0.685 ± 0.530
$27 \le M \le 35$	0.871 ± 0.026	0.211 ± 0.115	0.262 ± 0.326	0.355 ± 0.978	0.582 ± --

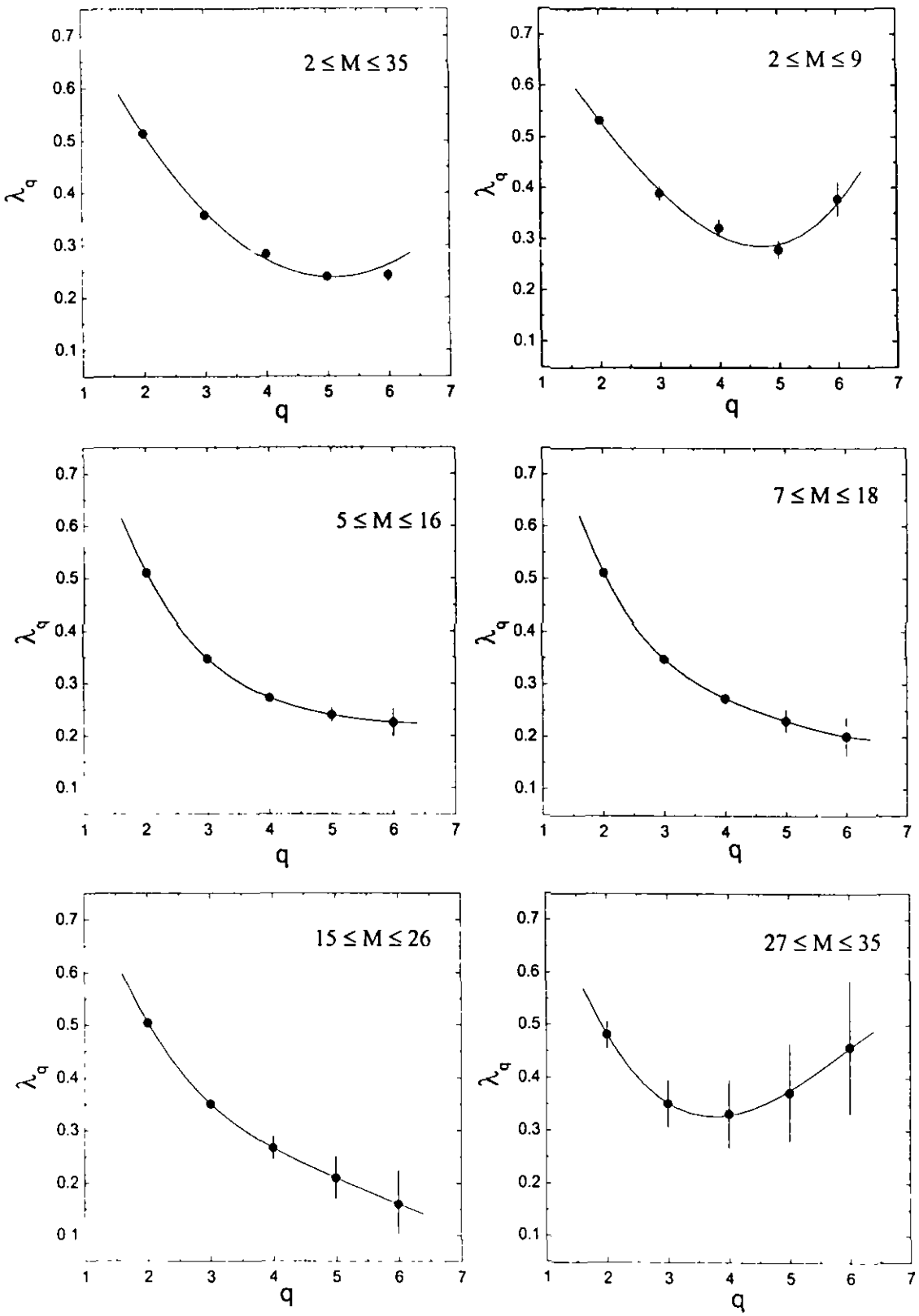

Fig. 3.4 Plots of λ_q as a function of q for different ranges of M for ^{28}Si-AgBr collisions at 14.6 AGeV in the pseudorapidity space.

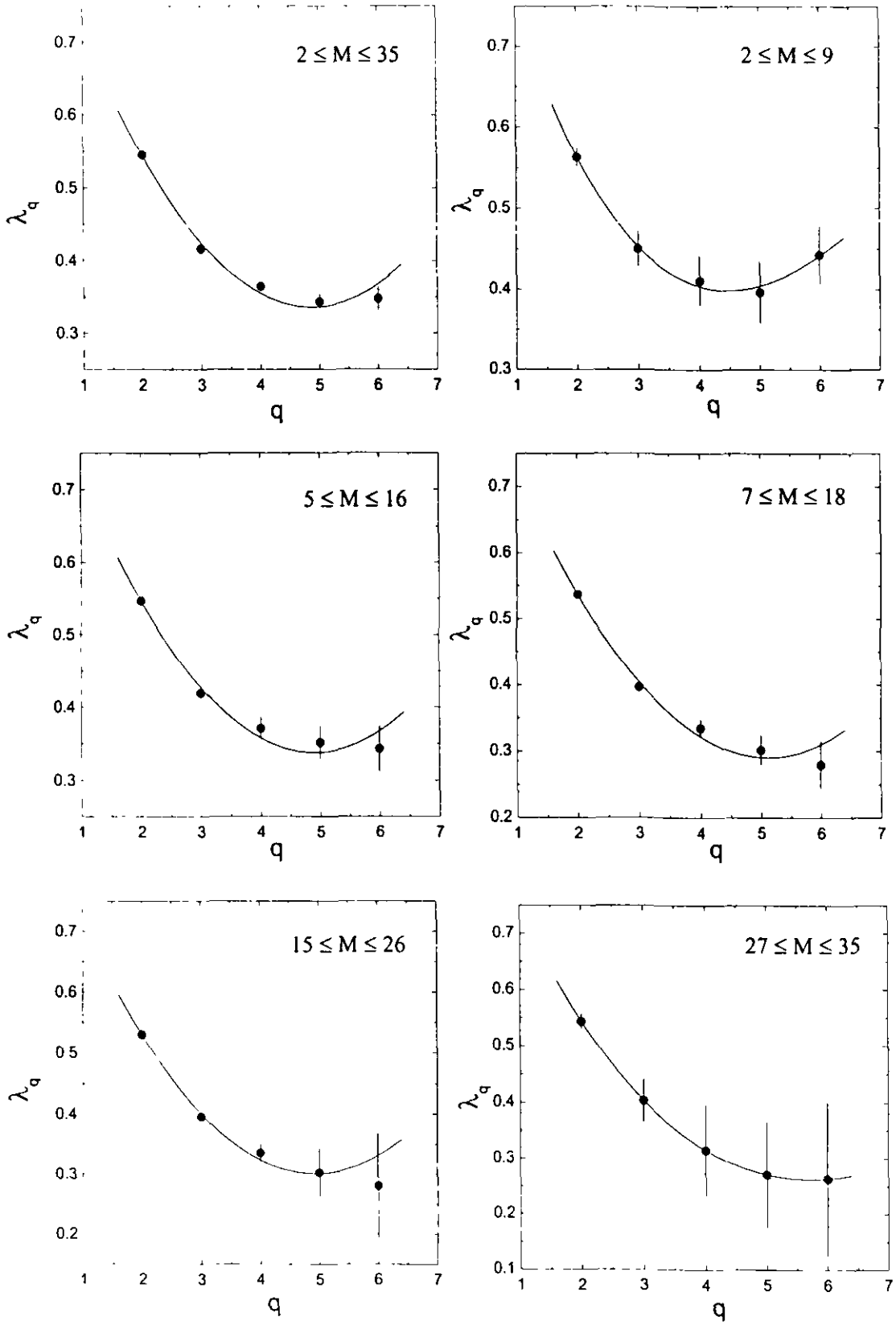

Fig. 3.5 Plots of λ_q as a function of q for different ranges of M for ^{28}Si-AgBr collisions at 14.6 AGeV in the azimuthal space.

In the azimuthal space (Fig.3.5), the minimum of λ_q exists between 4 and 5 for the range $2 \leq M \leq 9$. However, for other ranges, it occurs between 5 and 6.

Therefore, in both the pseudorapidity and azimuthal spaces, we observe a λ_q minimum and conclude that there is a certain critical value $q = q_c$ at which the multiparticle system behaves as a mixture of two states. On either side of this critical value, the system behaves differently, which is an indication of phase transition of non-thermal type in the multiparticle production process in ^{28}Si-AgBr collisions at 14.6 AGeV.

3.5 Nuclear effect

The primary goal for studying the scaled factorial moments $F_q(M)$ defined by equations 3.4 is to look for the possible existence of the dynamical fluctuations (intermittency) in relativistic nuclear collisions [2,3]. While studying the behaviour of factorial moments in hadron-hadron and nucleus-nucleus collisions, two different phenomena have been observed.

I In one dimension, the rise of $ln\langle F_q \rangle$ with the increasing phase space partition number M is much weaker for the nucleus-nucleus collisions than for hadron-hadron collisions and the heavier the colliding nuclei are, the weaker is the rising of $ln\langle F_q \rangle$ [33,34].

II In two or three dimensions, the $ln\langle F_q \rangle$ versus lnM plot for nucleus-nucleus collisions is bending upwards strongly, much stronger than for hadron-hadron collisions and the heavier the colliding nuclei are, the stronger is the upward bending of $ln\langle F_q \rangle$ versus lnM plot.

It has been shown [35] that these two apparently contradictory observations are due to the superposition effect of the contribution from the large number of elementary collisions in a nuclear collision process. In the superposition effect, due to the complexity of nuclear process, the rapidity centres of the individual collisions do not coincide but are scattered randomly within an interval on the rapidity axis. This arises due to the fact that each participant nucleon in the projectile nucleus interacts along the cylindrical tube in the target nucleus with more than one nucleon. Therefore, for each of these sub-nucleus interactions, there is a pseudorapidity distribution [36] with certain mid-rapidity depending on the typical characters of such interacting systems. In addition to these sub-interactions, the secondary particles produced within the target material cause further interactions with each other and with the target and projectile materials. These secondary interactions produce pseudorapidity distributions with their own mid-rapidity centres. Hence for each of these elementary collisions, a sub-pseudorapidity centre can be achieved.

The superposition of these elementary pseudorapidity values in sub-intervals $\delta\eta$, in which the original interval $\Delta\eta$ has been partitioned (Fig. 3.6), makes the total effective partition number, M^{eff}, much larger than M ($M^{eff} \gg M$) [36]. On the other hand, similar effect does not exist in the azimuthal space, where the phase space region is the same (0-2π) for all the elementary collisions and their superposition makes no change in the phase space partition, that is, $M_{\phi}^{eff} = M_{\phi}$

To characterize the phase space partition in two dimensions, a quantity known as 'Hurst exponent' [37] is used. It is defined as

$$H = \frac{\ln M_{\eta}}{\ln M_{\phi}} \tag{3.14}$$

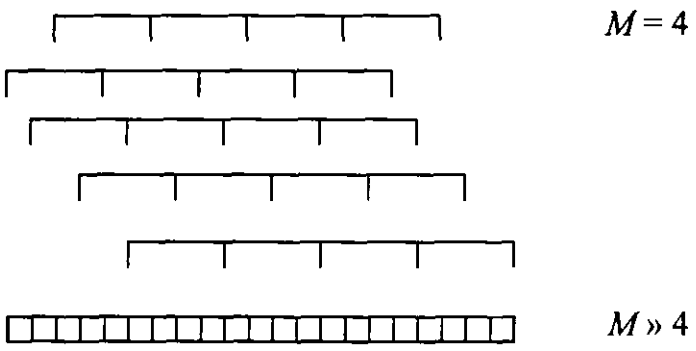

Fig. 3.6 Schematic plot of superposition effect on longitudinal phase space partition.

where M_η and M_ϕ are the number of partitions along the two perpendicular directions. The behaviour of factorial moments F_q depends on value of H. Therefore, to study the possible abnormal behaviour of factorial moments on the bin size, analysis should be performed with a suitable value of H. Otherwise, the observed trend of the calculated factorial moments will always be bending upwards [35,38-40], even if there is no fluctuation in particle production. The upward bending of the factorial moments can be weakened or totally removed if the exponents, H, are given a proper value.

In order to estimate the degree of upward bending of $ln\langle F_2 \rangle$ versus lnM curve, a simple quadratic equation $y = ax^2$ is fitted to the data. The second term 'bx' of the quadratic equation is neglected due to very small value of its coefficient b. Further, in the fitting the first few data points are omitted so as to reduce the effect of momentum conservation [40]. Momentum conservation tends to spread the particles in opposite directions and thus reduces the value of factorial moments. Therefore the origin of co-ordinates is shifted to the starting point $[M_0, F_2(M_0)]$ of the fitting and the variables are changed correspondingly to

$$\begin{aligned} x &= \ln M - \ln M_0 \\ y &= \ln\langle F_2(M)\rangle - \ln\langle F_2(M_0)\rangle \end{aligned} \tag{3.15}$$

The slope 'a' is taken as to be the characteristic parameter for the degree of upward bending of $ln\langle F_2 \rangle$ as a function of lnM.

To study the nuclear effect in ^{28}Si-emulsion collisions at 14.6 AGeV, we have used different values of Hurst exponent (H = 1.0, 1.5, 2.0, 2.5, 3.0). The intervals $\Delta\eta$ and $\Delta\phi$ have been divided into sub-cells with widths

$$\left.\begin{aligned}\delta_\eta &= \Delta_\eta / M_\eta \\ \delta_\phi &= \Delta_\phi / M_\phi\end{aligned}\right\} \tag{3.16}$$

The scale factors M_η and M_ϕ are connected to each other by the relation

$$M_\phi = M_\eta^{(1/H)} \tag{3.17}$$

It is clear from equation 3.17 that M_η and M_ϕ cannot be simultaneously integers. Therefore the size of elementary phase space cell cannot take continuously varying values. This problem can however, be circumvented by adopting the method proposed by L. Lianshou et al. [39]. According to this method, for each value of M_η, we get

$$M_\phi = N + \alpha \tag{3.18}$$

where N is the integer part and $0 \leq \alpha < 1$ represents the fractional part. When an elementary bin of width $\delta\phi$ is used as a scale to measure the region $\Delta\phi$, N of integer bins are obtained and a smaller bin of width α is left. Putting the smaller bin at the last place, the average is done with the first N bins only.

In the present analysis, we used $\Delta\eta$ = $-2 \leq \eta_{max} \leq +2$ and $\Delta\phi = 0 - 2\pi$. M_η was varied from 2 – 36. Further. to reduce the effect of non-flat particle density distributions, the cumulative variables X_η and X_ϕ were used. The

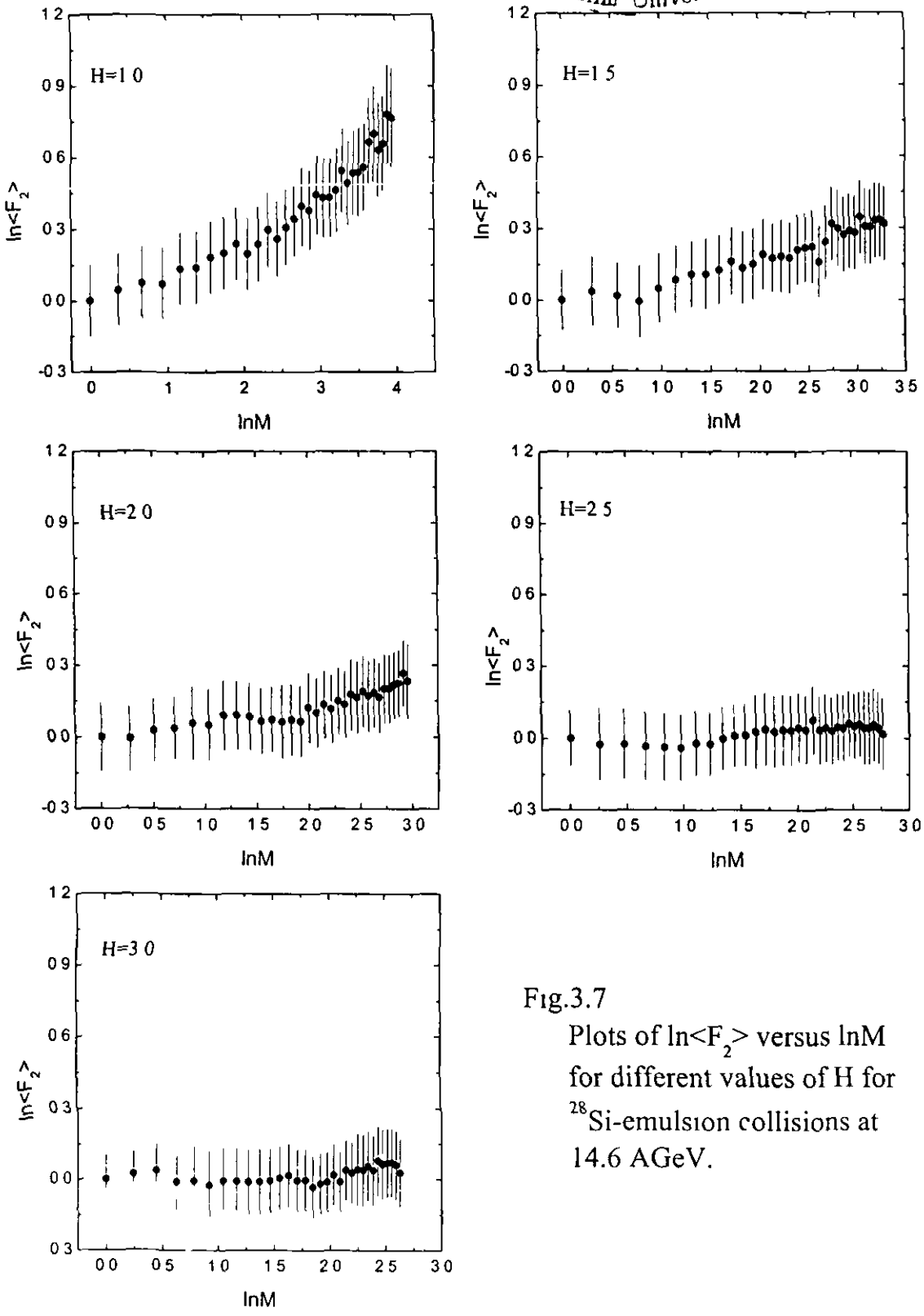

Fig.3.7
Plots of $\ln\langle F_2\rangle$ versus lnM for different values of H for ^{28}Si-emulsion collisions at 14.6 AGeV.

corresponding regions then became 0-1. Using the above partition scheme, the values of $ln\langle F_2\rangle$ were calculated with the help of equations 3.4 and 3.5. Fig. 3.7 shows $ln\langle F_2\rangle$ versus lnM plots for ^{28}Si-emulsion collisions at 14.6 AGeV for different values of H. From the figure, it can be seen that when $H = 1.0$, the curve bends upward strongly. However, when H increases, the upward bending is weakened and at $H = 2.5$ or 3.0, the curve becomes almost straight.

Next, we fit a quadratic equation $y = ax^2$ to the data points. This gives a quantitative description of the phenomenon. In order to see the quality of fitting, we plot in Fig. 3.8, the results of fitting for $H = 1$. In Fig. 3.8(a) all the points have been included and the origin is shifted to the first point. In Fig. 3.8(b), the first three points have been removed and the origin is shifted to the fourth point. Similarly, in Fig. 3.8 (c & d), the fourth and fifth points are omitted and the origin is shifted to the fifth and sixth point respectively. From the figure, it can be observed that the fitting is not good when all the points are included (Fig. 3.8(a)). This is due to the momentum conservation. The momentum conservation as already mentioned tends to spread the particles in opposite directions and thus reduces the value of the factorial moments. [36,40]. The effect, however, becomes weaker as M increases. When the origin is shifted to the sixth point (Fig. 3.8(d)), the fit becomes quite good.

The values of the fitting parameter 'a' ($y = ax^2$) for all the curves in Fig. 3.7, with the first three points omitted, as a function of H are presented in Fig. 3.9. The corresponding values of 'a' obtained by EMU-01 collaboration [36] for ^{197}Au-emulsion collisions at 11 AGeV and ^{16}O-emulsion collisions at 60 AGeV are also shown in Fig. 3.9. From the figure, it can be seen that in all the cases, the values of 'a' decrease as H increases, that is, $ln\langle F_2\rangle$ versus lnM

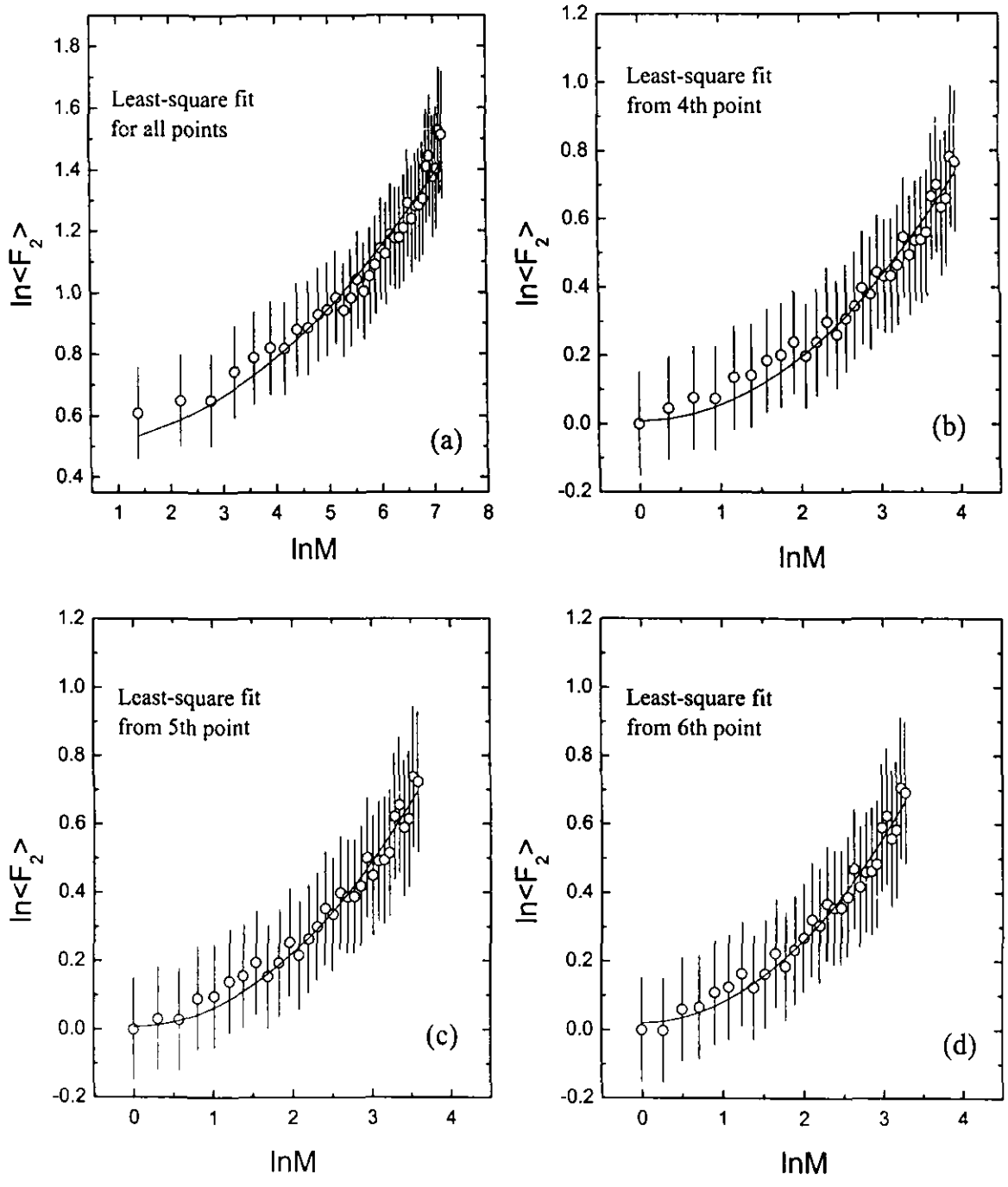

Fig. 3.8 Plots of $\ln\langle F_2\rangle$ versus lnM for H = 1 for ^{28}Si-emulsion collisions at 14.6 AGeV with different origins.

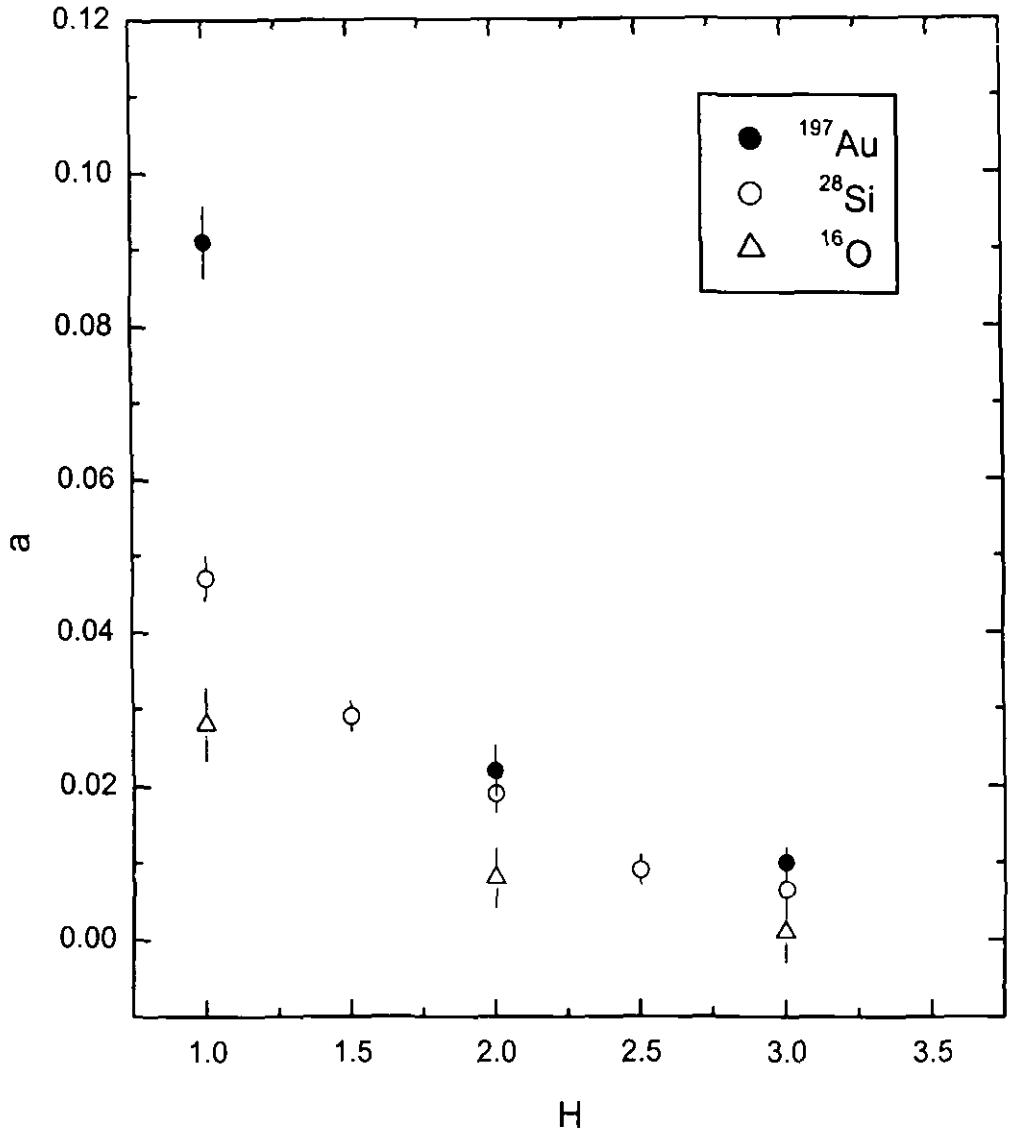

Fig. 3.9 Variation of slopes of the ln<F_2> versus lnM plots as a function of H for three types of heavy ion collisions.

curves bend upward stronger for smaller H and tend to become straight lines as H increases. Further, we find that the values of 'a' are greater for ^{197}Au-emulsion collisions than for ^{28}Si-emulsion collisions for all values of H. Moreover, the values of 'a' for ^{28}Si-emulsion collisions are greater than the corresponding values for ^{16}O-emulsion collisions. This means that the $ln\langle F_2 \rangle$ versus lnM curves bend upward stronger for heavier colliding nuclei than for the lighter ones at the same Hurst exponent. This is just what is expected, because for heavier colliding nuclei, the number of elementary collisions is large, thus making M^{eff} larger.

Therefore, we observe that the two dimensional second order factorial moment exhibits an upward bending as a function of partition of space, which in turn means the superposition of contributions from the elementary collisions in the nucleus-nucleus collisions. This upward bending could, however, be removed by choosing proper partition along the longitudinal and perpendicular directions, that is, the right value of Hurst exponent H. Moreover, it has been observed that heavier the colliding nuclei are, the stronger the upward bending is. It is consistence with the fact that the number of elementary collisions is more for heavier nuclei.

It is worth mentioning that if QGP is formed, then there will be no elementary collisions. This in turn will lead to vanishing of the superposition effect due to the contribution of elementary collisions in nucleus-nucleus collisions. Under such conditions, the upward bending in the two dimensional second order factorial moment plots is not likely to be seen. Thus study of the nuclear effect in nucleus-nucleus collisions could be used as another indirect test for QGP formation.

References

[1] T. H. Burnett et al., *Phys. Rev. Lett.* **50**, (1983) 2062.

[2] A .Bialas and R. Peschanski, *Nucl. Phys.* **B273**, (1986) 703.

[3] A. Bialas and R. Peschanski, *Nucl. Phys.* **B308**, 857 (1988).

[4] DELPHI Collaboration, *Phys. Lett.* **B247**, (1990) 137.

[5] TASSO Collaboration, *Phys. Lett.* **B231**, (1989) 548.

[6] I. Derado, G. Jansco, N. Schnitz and P. Stopa, *Z. Phys.* **C47**, (1990) 235.

[7] Wang Shaoshun et al., *Phys. Rev.* **D49**, (1994) 5785.

[8] UA1 Collaboration, *Nucl. Phys.* **B345**, (1990) 1.

[9] KLM Collaboration, R. Holynski et al, *Phys. Rev.* **C40,** (1989) R2449.

[10] D. Ghosh et al., *Phys. Rev.* **D49**, (1994) 3113.

[11] R. K. Shivpuri and V. K. Verma, *Phys. Rev.* **D47**, (1993) 123.

[12] EMU-01 Collaboration, *Phys. Rev. Lett.* **65**, (1990) 412.

[13] HELIOS Collaboration, *Phys. Lett.* **B252**, (1990) 303.

[14] K. Sengupta, P. L. Jain, G. Singh and S. N. Kim, *Phys. Lett.* **B236**, (1990) 219.

[15] EMU-01 Collaboration, *Z. Phys.* **C49**, (1991) 395.

[16] WA 80 Collaboration, R. Albrecht et al., *Phys. Lett.* **B221**, (1989) 427.

[17] P. L. Jain and G. Singh, *Mod. Phys. Lett.* **A7**, (1992) 93.

[18] A. Bialas and R.C. Hwa, *Phys. Lett.* **B253**, (1991) 436.

[19] R. Peschanski, *Nucl. Phys.* **B327**, (1989) 144.

[20] W. Ochs and J. Wosiek, *Phys. Lett.* **B214**, (1988) 617.

[21] D. H. Skelding, *Ph. D Thesis, Univ. of Washington* (1996).

[22] J. D. Bjorken, *Phys. Rev.* **D27**, (1983) 140.

[23] K. Fialkowski, B.Wosiek and J.Wosiek, *Acta Phys. Pol.* **B20**, (1989) 639.

[24] A. Bialas and M. Gazdzicki, *Phys. Lett.* **B252**, (1990) 483.

[25] P. L. Jain, and G. Singh, *Phys. Rev.* **C44**, (1991) 854.

[26] A. M. Tawfik and E. Ganssauge, hep-ph/0012008 (2000)

[27] D. Ghosh et al., *Euro Phys. Lett.* **41**, (1998) 371.

[28] R. Peschanski, *Int. J. Mod. Phys.* **A6**, (1991) 3681.

[29] A. Bialas and K. Zaleswski, *Phys. Lett.* **B238**, (1990) 413.

[30] P. Brax and R. Peschanski, *Nucl. Phys.* **B346**, (1990) 65.

[31] E. K. Sarkisyan and G.G Taran, *Phys. Lett.* **B279**, (1992) 177.

[32] E. K. Sarkisyan et al, *Phys. Lett.* **B318**, (1993) 568.

[33] X. Cai et al, Proc of 7^{th} Int. Workshop, Nijmegam, Netherlands (1996) 279.

[34] NA22 collaboration, N. M. Agababyan et al, *Phys. Lett.* **B382**, (1996) 305.

[35] Liu Lianshou, Hu Yaun and Deng Yue, *Phys. Lett.* **B388**, (1996) 10.

[36] EMU-01 Collaboration, M. I. Adamovich et al. *Z. Phys.* **C76**, (1997) 659.

[37] B. Mandelbrot, Die Fraktale Geometric der nature, 1, Sonderousgabe birkhauser, basel 1991 in German.

[38] W. Yuanfung and Liu Lianshou, *Phys. Rev. Lett.* **70**, (1993) 3197; *Science in China* **A24**, (1994) 1299.

[39] Liu Lianshou, Z. Yang and Wu. Yuanfung, *Z. Phys.* **C69**, (1996) 323.

[40] Liu Lianshou, Z. Yang and Deng Yue, *Z. Phys.* **C73**, (1997) 535.

CHAPTER IV

Erraticity analysis of multiparticle production in ^{28}Si-emulsion collisions at 14.6 AGeV

4.1 Introduction

Since the observation in 1983 of unexpectedly large local fluctuations in a single event of very high multiplicity recorded by the JACEE collaboration [1], extensive studies have been carried out to understand the non-linear behaviour of classical as well as quantum systems. For classical systems the description of non-linear behaviour is well established. In case of classical non-Abelion dynamics Matinyan et al [2] applied special simplifying conditions that reduce the equations of motion to manageable size and found chaotic solutions. But an exhaustive investigation of gauge equations has to be done on lattice. Recently, it has been shown by lattice calculations that the classical non-Abelion gauge theory exhibits deterministic chaos and that Lyapunov exponent that characterizes the divergent distances between trajectories can be computed numerically for lattices of different sizes [3,4].

The extension of the above investigation to quantum systems is very difficult because the notion of quantum chaos for dynamics is not well defined [5]. The first step in that direction was taken by Cao and Hwa [6], who explored the concept of chaos for systems that involve particle production through branching process. They considered two branching processes in particle production: One is pure gluon theory in perturbative QCD that was later extended to include quarks also [7] and the other is an Abelion cascade model. Characteristics of particle production were investigated by generating events according to the perturbative QCD and the cascade model. The temporal behaviour of the production process was studied by following the normalized variance V_i of the multiplicity distribution of each generation. The spatial behaviour was studied in terms of fluctuations of the normalized event

factorial moment F_q^e and the entropy index μ_q. Cao and Hwa [7,8] found that the branching process in perturbative QCD was chaotic.

Out of the different measures considered to describe the degree of fluctuations in the branching process, the normalized variance contains important information about the process from generation to generation, but it is not accessible to experiment. However, the other measures, the normalized event factorial moments F_q^e, the moment of moments $C_{p,q}$ and the entropy index μ_q can be determined in most high energy collisions.

It has been argued [9,10] that event-to-event fluctuations can probe the dynamics of multiparticle production more deeply than the variables such as the multiplicity distribution and the average factorial moments. In this chapter, we therefore study chaoticity or event-to-event fluctuations in the density of particles produced in ^{28}Si-emulsion collisions. The moment of moments $C_{p,q}$ that quantify these fluctuations have been determined. We also calculate the values of entropy index μ_q. The positivety of μ_q corresponds to large fluctuations of the spatial patterns from event-to-event. Further, the values of these parameters would provide valuable input to models of multiparticle production. In order to evaluate the contribution of the statistical fluctuations to the experimentally obtained event factorial moments, we generate a sample of uncorrelated Monte Carlo events and compare the values of moment of moments $C_{p,q}$ of the generated events with those obtained experimentally. Besides, we also study the erraticity of rapidity gaps. This method has recently been proposed by R. C. Hwa [11] to investigate event-to-event fluctuations in low multiplicity collisions. The values of S_q and Σ_q, which quantify event-to-event fluctuations in low multiplicity collisions have been determined for both the pseudorapidity and azimuthal spaces.

4.2 Moment of moments $C_{p,q}$ and entropy index μ_q

In order to study event-to-event fluctuations in multiparticle production, it is necessary to investigate the behaviour of the event factorial moment F_q^e in small bins. The q-th order factorial moment of an event is defined as

$$F_q^e = \frac{\frac{1}{M}\sum_{i=1}^{M} n_i(n_i - 1)....(n_i - q + 1)}{\left(\frac{1}{M}\sum_{m=1}^{M} n_m\right)^q}, \tag{4.1}$$

where M is the partition number and n_m the multiplicity of particles in the mth bin. Since F_q^e fluctuates from event-to-event, we get a distribution of F_q^e denoted by $P(F_q^e)$ after a large number of events. The normalized factorial moments of an event can now be defined as

$$\phi_q = \frac{F_q^e}{\langle F_q^e \rangle}, \tag{4.2}$$

where $$\langle F_q^e \rangle = \frac{1}{N_e}\sum_{e=1}^{N_e} F_q^e$$

It is worth mentioning here that the scaled factorial moment defined by Bialas and Peschanski [12] to study intermittency in multiparticle production is only an estimate of mean of the distribution $P(F_q^e)$. It should be realized that the averaging procedure, apart from its clear advantages, brings also a danger of losing some important information on spatial patterns from event-to-event. In particular, some interesting effects, if present only in a part of the sample of

events produced in high energy collisions, may be lost. A possible example of this kind is the quark-gluon plasma, which is expected to be characterized by specific intermittency exponents [13]. It is, therefore, essential to investigate the full shape of the distribution and the way it changes with the bin size. This task can be accomplished by studying the moments of the distribution of event factorial moments $C_{p,q}$ for varying bin size, up to the moment rank p allowed by the available statistics. $C_{p,q}$ quantify the fluctuations that are related to the chaotic behaviour of the system [6] and are defined as

$$C_{p,q} = \frac{1}{N_{ev}} \sum_{e=1}^{N_{ev}} (\phi_q)^p, \tag{4.3}$$

where N_{ev} is the total number of events in the sample. The exponent p can be any positive real number [9]. It should not be negative because F_q^e may vanish for some events. For $0 < p < 1$, it is the $F_q < 1$ region that is probed, while for $p > 1$ events with high F_q are described.

In principle the shape of $P(F_q^e)$ can exhibit many different behaviours as the scale changes, and so can its moments. However, since in intermittent systems, by definition, the mean shows a power law behaviour, we are quite naturally led to the search for a power law behaviour of the moments of any rank. Event-to-event fluctuations in multiparticle production are characterized by the power law behaviour of the normalized moments $C_{p,q}$ as a function of number of bins M. The power law behaviour of $C_{p,q}$ is referred to as erraticity.

$$C_{p,q} \propto M^{\Psi_q(p)} \tag{4.4}$$

where $\psi_q(p)$ is called the erraticity exponent and is determined from the slope of $lnC_{p,q}$ versus lnM plots. The information contained in the scaling function $\psi_q(p)$ can be alternatively displayed through the entropy index μ_q, which is related to the entropy of event space and is defined as [6]

$$\mu_q = \frac{d\Psi_q(p)}{dp} \quad \text{at} \quad p=1 \tag{4.5}$$

A positive value of μ_q would correspond to a broad $P(F_q^e)$ distribution which in turn would mean unpredictable large fluctuations of the spatial patterns from event-to-event. By applying this method to known classical chaotic systems, it has been shown [14] that μ_q can be used as a measure of chaoticity in systems where only the spatial patterns could be observed and a positive value of μ_q would signal the presence of chaos in the system.

4.3 Erraticity analysis

Since F_q^e depends on the shape of the single particle inclusive pseudorapidity distribution and also to compare the results from different experiments where the basic observable parameters are different, we shall continue to use the cumulative variable X. The advantage of working in the variable X has long been recognized [15]. To reduce the contribution of statistical fluctuation only events in which the number of shower particles was greater than seven ($N_s \geq 8$) were considered for the final analysis. Further, the analysis was performed in the central pseudorapidity region, that is, $\eta_{max} - 2 \leq \eta \leq \eta_{max} + 2$. This region covers most of the produced shower particles.

The rapidities of all shower particles produced in ^{28}Si-CNO and ^{28}Si-AgBr collisions were converted into X- variable using equation 3.8. The interval X = 0-1 was then divided into M bins and the values of the event factorial moment F_q and the moment of moments $C_{p,q}$ were calculated for q = 2 and p = 0.5, 0.7, 0.9, 1.1, 1.3, 1.5 and 2.0 using equations 4.1- 4.3. M was varied from 1 to 40. The $lnC_{p,q}$ versus lnM graphs for ^{28}Si-CNO and ^{28}Si-AgBr collisions with $N_s \geq 8$ are shown in Fig. 4.1(a) and Fig. 4.2(a) respectively. For the sake of clarity, graphs for p = 0.9, 1.1 and 1.3 are not shown. It should be pointed out here that when we calculate the average factorial moment for a sample of events, the average is performed over all events for a single bin. This process eliminates statistical fluctuations if the number of events is large. However, to study chaoticity, we have to calculate the average factorial moment of an event. In this case averaging is done over all bins in an event. As the number of produced particles N_s in an event is not very large for our data, the statistical fluctuations cannot be completely eliminated from the event factorial moments F_q^e and the moment of moments $C_{p,q}$. In order to find out the contribution of the statistical fluctuations to $C_{p,q}$ calculated for our data, we generate a sample of events. The generated events have the same multiplicity distribution and the same number of events as observed experimentally but do not have any correlations.

To generate uncorrelated events, we use a flat probability distribution in the region of pseudorapidity in which the fluctuations in F_q^e are being studied and also for the whole data sample. It means that the probabilities in all bins are equal and are the same for all events. The distribution of particles in the region of pseudorapidity under study can then be located by Bernoulli's distribution [16].

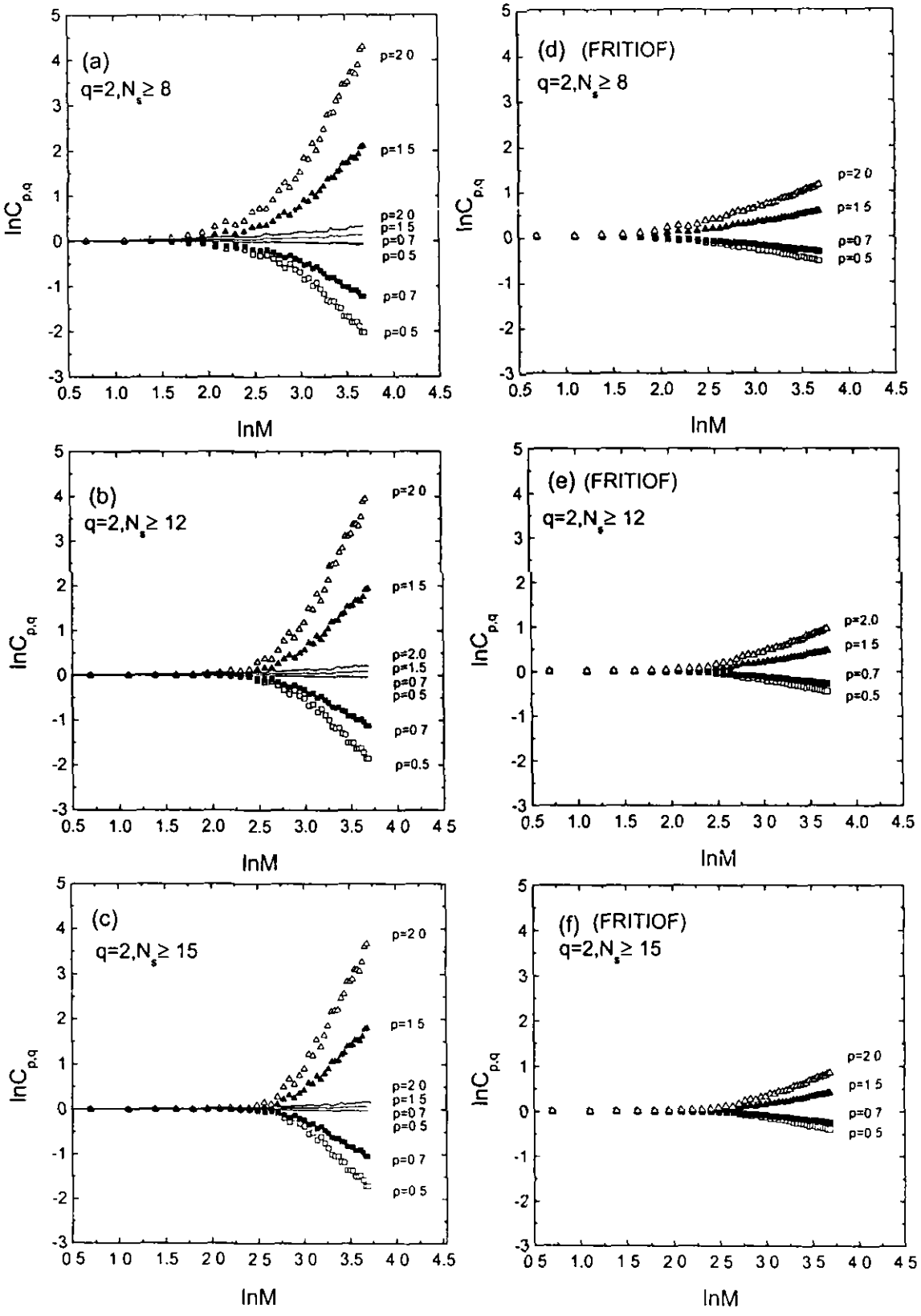

Fig. 4.1 (a)-(c) $\ln C_{p,q}$ versus lnM plots for different p values and for different data samples of ^{28}Si-CNO collisions. Points correspond to the experimental data and solid lines to the generated uncorrelated events. (d)-(f) $\ln C_{p,q}$ versus lnM plots for the corresponding FRITIOF events.

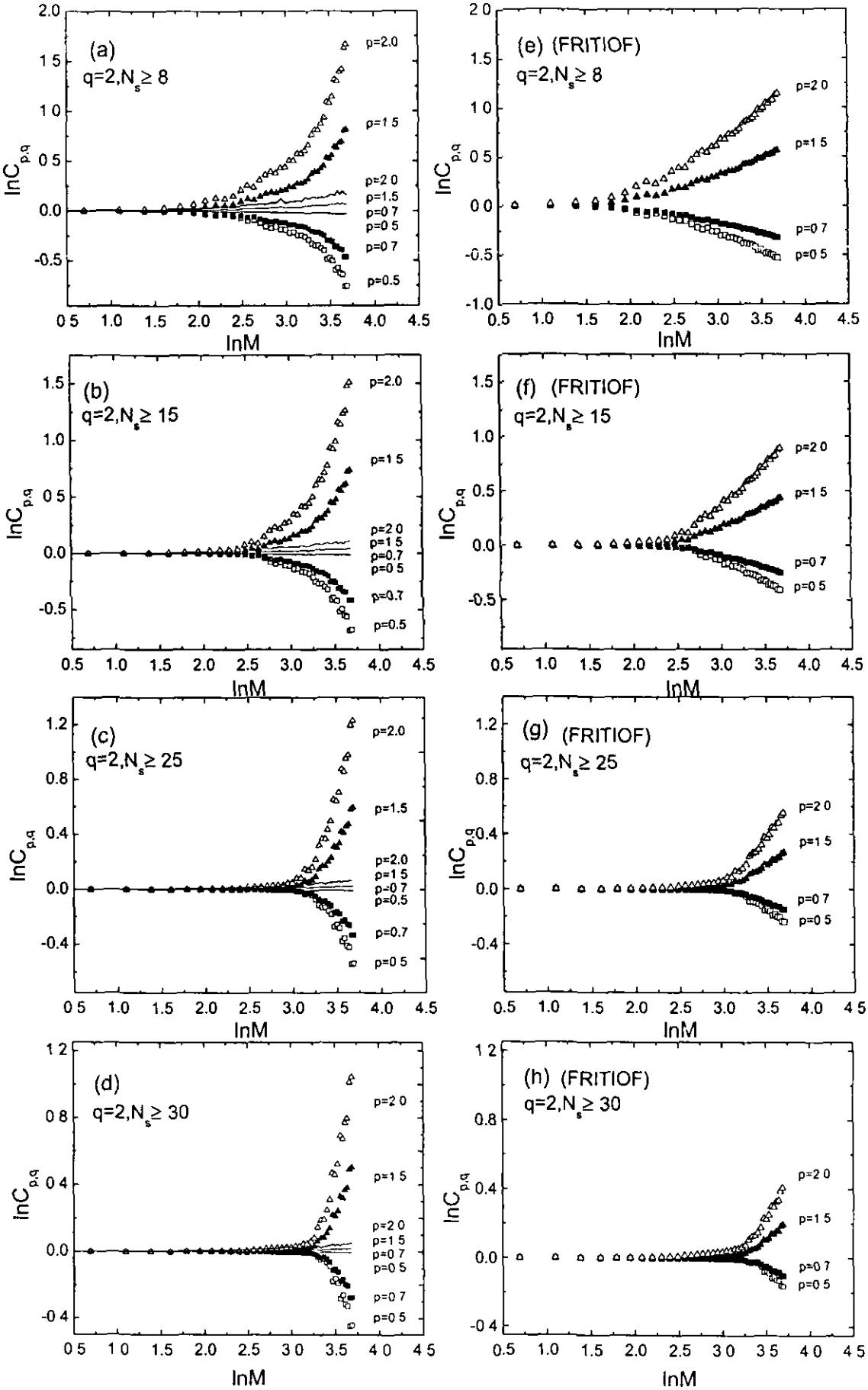

Fig. 4.2 (a)-(d) $\ln C_{p,q}$ versus lnM plots for different p values and for different data samples of ^{28}Si-AgBr collisions. Points correspond to the experimental data and solid lines to the generated uncorrelated events. (e)-(h) $\ln C_{p,q}$ versus ln M plots for the corresponding FRITIOF events.

$$B(n_1, n_2,....n_M \;/\; p_1,.....p_M) \;=\; \frac{N!}{n_1!...n_M!}\, p_1^{n_1}.....p_M^{n_M}\,, \qquad (4.6)$$

where $\sum_{m=1}^{M} n_m \;=\; N$

Events were generated according to the observed multiplicity distribution. In each event the pseudorapidity interval $\Delta\eta$ was divided into M bins and the particles of the event were distributed in these bins according to equation 4.6. The values of F_q^e and $C_{p,q}$ were then calculated using equations 4.1- 4.3. The values of $C_{p,q}$ for the generated uncorrelated events for $q = 2$ and for different values of p are shown in Fig. 4.1 and Fig. 4.2 as solid lines. It can be seen from these figures that the experimental values of $C_{p,q}$ lie well above those for the generated uncorrelated events in the region $M \geq 13$. It means that the contribution of the statistical fluctuations to $C_{p,q}$ values for our data is small.

In order to find whether the observed dependence of $C_{p,q}$ on M could be explained by the standard generators of particle production in heavy ion collisions, we simulated 10,000 ^{28}Si-emulsion collisions at 14.6 AGeV using the FRITIOF generator. The $lnC_{p,q}$ versus lnM graphs for these events are also shown in Figs. 4.1 and 4.2. It can be seen from these figures that for CNO events, in the ranges M = 13-25 and M = 26-40, the values of $C_{p,q}$ for FRITIOF events are much smaller than those for the experimental events. However, for AgBr events, in the range M = 13-25, the $C_{p,q}$ values for the experimental events are about the same as those predicted by the FRITIOF generator. But in the range M = 26-40, the $C_{p,q}$ values for the experimental events are higher than those predicted by the FRITIOF generator.

To study the effect of multiplicity of shower particles on chaoticity, we have truncated the multiplicity distribution at the lower end. The $lnC_{p,q}$ versus lnM graphs for CNO events with $N_s \geq 8$, $N_s \geq 12$ and $N_s \geq 15$ are shown in Fig. 4.1(a, b and c) respectively. Fig. 4.2(a, b, c and d) shows the $lnC_{p,q}$ versus lnM graphs for AgBr events with $N_s \geq 8$, $N_s \geq 15$, $N_s \geq 25$ and $N_s \geq 30$ respectively. Results from the corresponding generated uncorrelated events are shown in these figures as solid lines. $lnC_{p,q}$ versus lnM graphs for the corresponding FRITIOF events are shown in Fig. 4.1(d, e and f) and Fig. 4.2(e, f, g and h). From these figures we observe that for the experimental events $C_{p,q}$ values decrease as the average multiplicity increases. A similar trend is observed for the FRITIOF events.

Linear fits to the $lnC_{p,q}$ versus lnM graphs shown in Fig. 4.1 and Fig. 4.2, have been performed in two regions of M: M = 13-25, M = 26-40. For AgBr events, it is observed that in the range M = 13-25, the slopes $\psi_q(p)$ of the $lnC_{p,q}$ versus lnM graphs decrease sharply as the average multiplicity increases from 30.36 ± 1.77 for events with $N_s \geq 8$ to 41.61 ± 3.32 for events with $N_s \geq 30$. However, for CNO events the slopes $\psi_q(p)$ are almost the same for events with $N_s \geq 8$, $N_s \geq 12$, and $N_s \geq 15$. In the range M = 26-40, the slopes $\psi_q(p)$ are independent of the average multiplicity for both CNO and AgBr events.

In Fig. 4.3 and Fig. 4.4, the slopes $\psi_q(p)$ are plotted as functions of p for different data samples in the range M = 13-25 for CNO and AgBr events. We fit the points shown in these figures by a quadratic formula. The solid lines show the results. It can be seen from the figures that the fits are very good. Similarly, in the range M = 26-40. the slopes $\psi_q(p)$ are plotted as functions of p for different data samples for both CNO and AgBr events. These graphs are

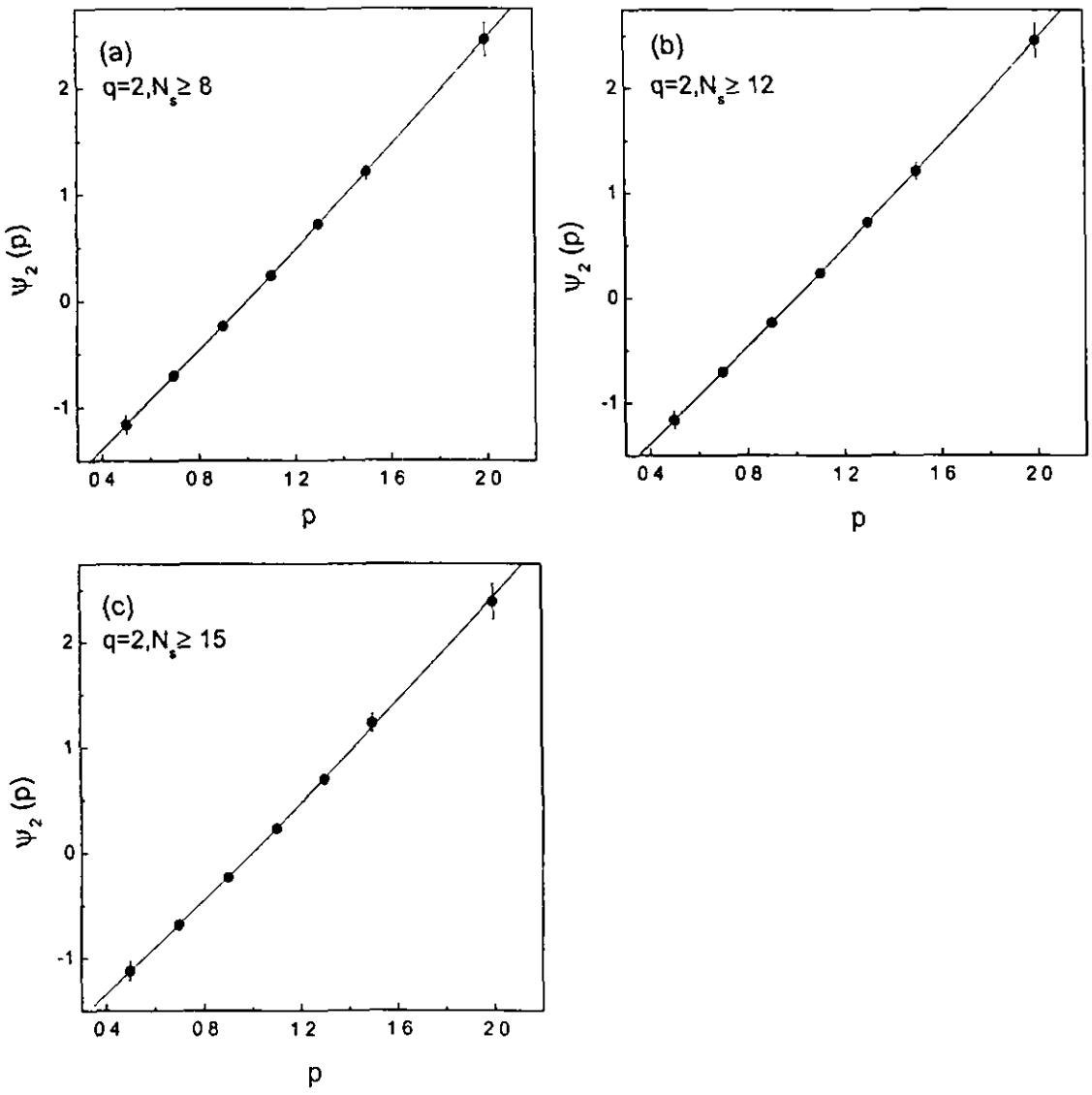

Fig 4 3 Plots of the slopes ψ_2 (p) versus p in the range M = 13-25 for different data samples of ^{28}Si-CNO collisions

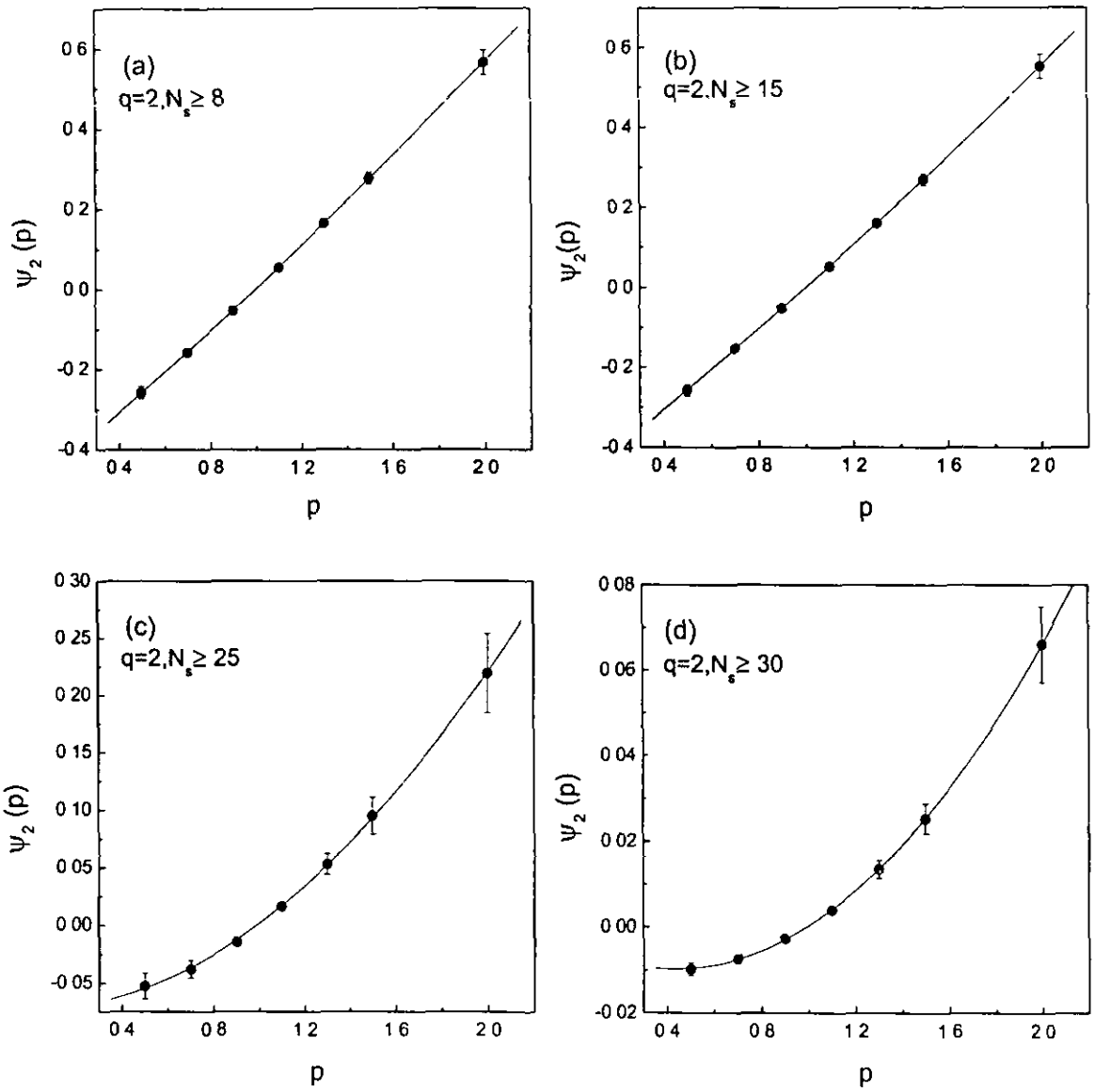

Fig. 4.4 Plots of the slopes ψ_2 (p) versus p in the range M = 13-25 for different data samples of ^{28}Si-AgBr collisions.

shown in Fig. 4.5 and Fig. 4.6 and again we see that the fits show a good agreement with the data points.

The values of the entropy index μ_2 can be obtained by finding the derivative of these curves at $p = 1$ (relation 4.5). The values of μ_2 thus obtained are given in tables 4.1 and 4.2. For AgBr events, in the range M = 13-25, the entropy index μ_2 decreases with increase in the average multiplicity whereas in the range M = 26-40, it is almost independent of the average multiplicity. However, for CNO events, the entropy index μ_2 does not depend on the average multiplicity in both ranges of M. A similar behaviour is observed for CNO events generated using the FRITIOF generator, but the values of the entropy index are smaller than those obtained for the experimental events in both the ranges of M. For AgBr events generated using the FRITIOF generator, the values of μ_2 in the range M = 13-25 are in agreement with those obtained for the experimental events. However, in the range M = 26-40 the values of μ_2 predicted by the FRITIOF generator are much smaller than those obtained experimentally (tables 4.1 and 4.2).

In tables 4.1 and 4.2 values shown within curly brackets are those of μ_2 for the corresponding generated uncorrelated events. As can be seen, these values are very small compared to the values of μ_2 obtained for the experimental data. This indicates that large event-to-event fluctuations of spatial patterns of the final states are present in our data.

Shaoshun and Zhaomin [17] have studied chaoticity in NA27 data on pp collisions at 400 GeV/c. In the range M = 5-25, they have also observed that the entropy index decreases as the average multiplicity increases. But they did not obtain μ_2 values in the range M = 25-40. It should be pointed out here that

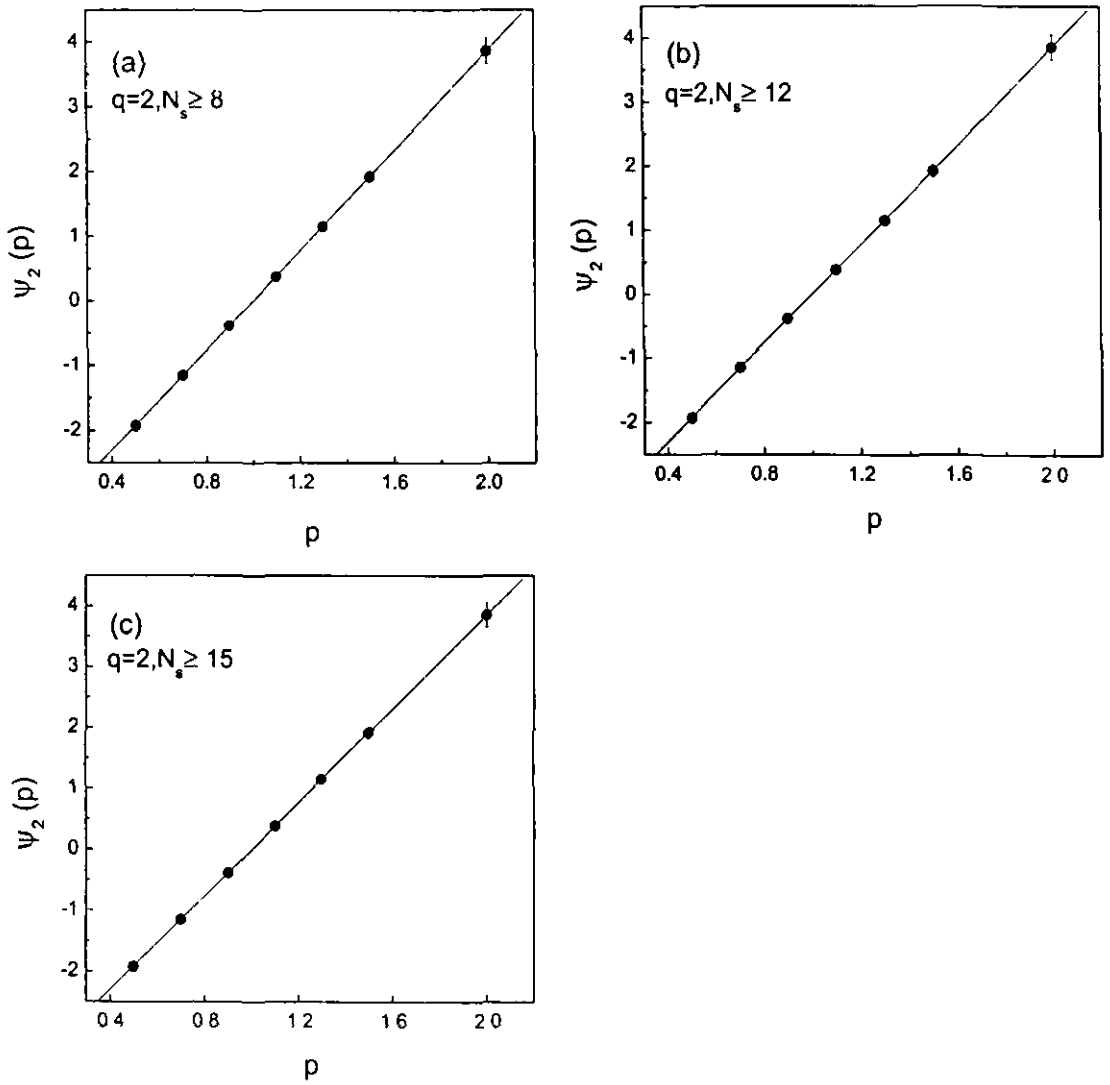

Fig. 4.5 Plots of the slopes ψ_2 (p) versus p in the range M = 26-40 for different data samples of ^{28}Si-CNO collisions.

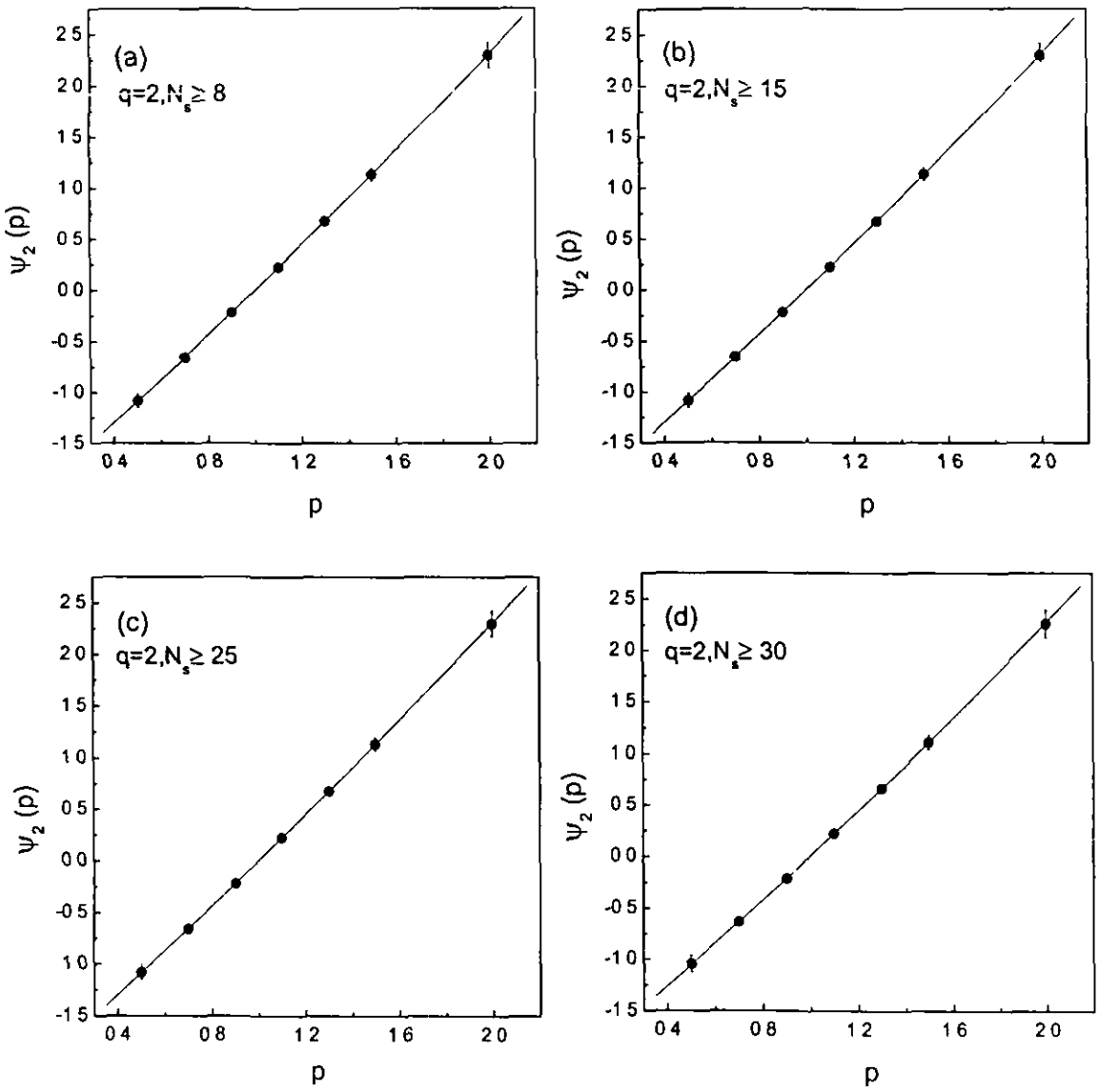

Fig 4 6 Plots of the slopes ψ_2 (p) versus p in the range M = 26-40 for different data samples of ^{28}Si-AgBr collisions

Table 4.1. Values of entropy index μ_2 for CNO events. The values within the curly brackets are those for the corresponding generated uncorrelated events. The values within the square brackets are those for the FRITIOF events.

Data sample	Number of events	Average multiplicity	Entropy index μ_2	
			M= 13-25	M=26-40
$N_s \geq 8$	209	16.29 ± 1.13	2.377 ± 0.016 {0.103 ± 0.002} [0.589 ± 0.003]	3.842 ± 0.018 {0.219 ± 0.006} [0.811 ± 0.006]
$N_s \geq 12$	148	19.44 ± 1.60	2.374 ± 0.023 {0.061 ± 0.004} [0.587 ± 0.002]	3.842 ± 0.014 {0.121 ± 0.006} [0.810 ± 0.003]
$N_s \geq 15$	112	21.77 ± 2.06	2.310 ± 0.115 {0.061 ± 0.004} [0.564 ± 0.003]	3.843 ± 0.015 {0.092 ± 0.007} [0.784 ± 0.107]

Table 4.2. Values of entropy index μ_2 for AgBr events. The values within the curly brackets are those for the corresponding generated uncorrelated events. The values within the square brackets are those for the FRITIOF events.

Data sample	Number of events	Average multiplicity	Entropy index μ_2	
			M= 13-25	M=26-40
$N_s \geq 8$	293	30.36 ± 1.77	0.533 ± 0.007 {0.050 ± 0.003} [0.589 ± 0.005]	2.218 ± 0.018 {0.098 ± 0.010} [0.805 ± 0.006]
$N_s \geq 15$	250	33.78 ± 2.14	0.526 ± 0.005 {0.025 ± 0.003} [0.591 ± 0.004]	2.219 ± 0.016 {0.038 ± 0.002} [0.831 ± 0.002]
$N_s \geq 20$	213	36.86 ± 2.53	0.344 ± 0.014 {0.017 ± 0.002} [0.380 ± 0.013]	2.219 ± 0.015 {0.023 ± 0.004} [0.839 ± 0.051]
$N_s \geq 25$	189	38.89 ± 2.83	0.148 ± 0.011 {0.018 ± 0.002} [0.125 ± 0.014]	2.220 ± 0.019 {0.027 ± 0.004} [0.826 ± 0.002]
$N_s \geq 30$	153	41.61 ±3.32	0.035 ± 0.001 {0.001± 0.001} [0.040 ±0.003]	2.164 ± 0.031 {0.001± 0.001} [0.744 ±0.004]

Fu et al. [16] have shown that the chaoticity observed by Shaoshun and Zhaomin in NA27 data could be reproduced by the statistical fluctuations only. But as has been shown in this section earlier, the chaoticity observed in the present investigation cannot be reproduced by the statistical fluctuations only. Thus the chaotic behaviour observed in our data has dynamical origin.

Very recently, Atayan et al (NA22 collaboration) [18,19] studied event-to-event fluctuations using a method based on event factorial moments in low multiplicity π^-p and K^+p collisions at 250 GeV/c. They have demonstrated that the observed fluctuations are dominated by statistical fluctuations. However, when Atayan et al analysed the same data in terms of recently suggested moments of rapidity gaps for low multiplicity events [18], they observed significant non-statistical event-to-event fluctuations. Ghosh et al [20] analysed ^{32}S-AgBr collisions at 200 AGeV in terms of entropy index μ_q and found evidence of event-to-event fluctuations.

4.4 Erraticity of rapidity gaps

The use of rapidity gap method has been proposed by R. C. Hwa [11] to study event-to-event fluctuations in low multiplicity events. It has been argued that the event factorial moments F_q^e receive a contribution from a bin in which $n_m \geq q$, but ignores where it is located. In other words, F_q^e is sensitive to the local height of the rapidity distribution in an event, not to the spatial arrangement in rapidity. When the particle multiplicity N in an event is low and the partition number M is high, many bins are empty. To have a bin with $n_m \geq q$ means that even more bins than the average would have to be empty. It then seems clear that the information about the fluctuations could be also collected by examining the rapidity gaps. When N is large, the rapidity gaps

are generally not very informative. However, when N is low, they characterize an event better than counting particle numbers (spikes). In our case, the average multiplicity for ^{28}Si-AgBr collisions is $\langle N_s \rangle = 30.36 \pm 0.18$, which is neither very low nor very large. In this section, we, therefore, use the method of rapidity gaps suggested by Hwa [11] to study erraticity or event-to-event fluctuations in our data. Working again in X variable [15], the rapidities of all the particles of each event have been distributed between 0 and 1.

One can consider an event with n particles labelled by $i = 1, 2, 3, \ldots\ldots n$ in X space at X_i, ordered in accordance to $X_i < X_{i+1}$, that is, from left to right. Now the distances between the neighboring particles are given by

$$x_i = X_{i+1} - X_i, \qquad i = 0, 1, 2, \ldots\ldots n \tag{4.7}$$

with $X_0 = 0$ and $X_{n+1} = 1$ being the boundaries of X space. Every event 'e' is thus characterized by a set S_e of $n+1$ numbers: $S_e = \{x_i \mid i = 0, 1, 2 \ldots n\}$, which clearly satisfy

$$\sum_{i=0}^{n} x_i = 1 \tag{4.8}$$

and these numbers are referred to as 'rapidity gaps'. To study the fluctuation of S_e from event-to-event, the moment of x_i for each event is defined as

$$\Gamma_q = \frac{1}{n+1} \sum_{i=0}^{n} x_i^q, \tag{4.9}$$

where q is the order of the moment. It is obvious from equations 4.8 and 4.9 that

$$\Gamma_0 = 1 \qquad \text{and} \qquad \Gamma_1 = \frac{1}{n+1}$$

At higher q, Γ_q are progressively smaller but are increasingly dominated by large x_i components in S_e, which in turn puts more emphasis on the large gaps than the small ones. A set of Γ_q for q ranging up to 7 or 8 is sufficient to characterize an event, better than S_e itself in the sense that Γ_q can be compared from event to event, whereas S_e cannot be compared due to the fluctuations in n. Since the moment Γ_q fluctuates from event-to-event, one can determine a distribution $P(\Gamma_q)$ of Γ_q after many events. It is the shape of $P(\Gamma_q)$ that characterizes the nature of event to event fluctuations of the gap distribution, and therefore of the spatial pattern of an event. Again we can describe the changes in the shape of the distribution by its moments, that is,

$$C_{p,q} = \frac{1}{N_{ev}} \sum_{e=1}^{N_{ev}} (\Gamma_q^e)^p, \tag{4.10}$$

where N_{ev} is the total number of events. Since $C_{1q} = \langle \Gamma_q \rangle$ is the mean of the distribution that gives least information on the degree of fluctuation, the derivative at $p = 1$ convey the broadest information on $P(\Gamma_q)$ [11]. Therefore, the event-to-event fluctuations of Γ_q can be quantified as

$$s_q = -\frac{d}{dp} C_{p,q}\bigg|_{p=1} = -\langle \Gamma_q \ln \Gamma_q \rangle, \tag{4.11}$$

where $\langle .... \rangle$ stands for the average over all events. The quantities s_q are the new measures of erraticity in terms of rapidity gaps.

Unlike the factorial moments F_q, Γ_q do not filter out statistical fluctuations. At low multiplicities, the factorial moments also fail to be effective in that filtering, thus there is no loss in considering Γ_q at low multiplicities. However, one can estimate how much s_q stands out above the statistical fluctuations by calculating

$$s_q^{stat} = -\left\langle \Gamma_q^{stat} \ln \Gamma_q^{stat} \right\rangle, \tag{4.12}$$

where Γ_q^{stat} is determined by using the distribution of the gaps from the generated events. Taking the ratio

$$S_q = \frac{s_q}{s_q^{stat}} \tag{4.13}$$

and examining the deviation of S_q from 1, one can observe the erraticity measure of an event sample.

In order to study the erraticity of rapidity gaps for ^{28}Si-AgBr collisions at 14.6 AGeV, we have calculated Γ_q moment for each event using equation 4.9 for both the pseudorapidity and azimuthal spaces. q has been varied from 2 to 9 in steps of 1. To probe the fluctuation of Γ_q from event-to-event, we have calculated the values of s_q by using equation 4.11. To eliminate the statistical part of this measure, we have calculated s_q^{stat} (equation 4.12) by generating random numbers between 0 and 1 for the pseudorapidity space and between 0 and 2π for the azimuthal space. The generated events have the same multiplicity distribution as that of the experimental events. Next we calculated S_q with the help of equation 4.13 for our data. The $ln S_q$ versus lnq plots for

both the spaces are exhibited in Fig. 4.7. It is evident from the figure that for both the pseudorapidity and azimuthal spaces, S_q deviates significantly from 1 and thus indicates the presences of event-to-event fluctuations in our data. The S_q values, as can be seen, increase linearly with the increase in q, thereby putting more weight on large gaps. Evidently the results show a power law behaviour in q, that is, $S_q \propto q^{\phi}$ where ϕ = 1.630 ± 0.015 for the pseudorapidity space and $\phi = 2.598 \pm 0.127$ for the azimuthal space.

Since x_i are less than one, Γ_q are usually much less than one (equation 4.9) and this may result in significant contribution of the statistical fluctuations to S_q, though not so large as to render the measures ineffective. To minimize this effect, Hwa and Zhang [11] defined different types of moments, that is,

$$H_q = \frac{1}{n+1}\sum_{i=0}^{n}(1-x_i)^{-q}, \tag{4.14}$$

where x_i are given by equation 4.7. The H_q moments like Γ_q receive dominant contribution from large x_i, but can become much greater than one. Substituting H_q in all foregoing equations, one can define

$$\sigma_q = \langle H_q \ln H_q \rangle \tag{4.15}$$

and

$$\Sigma_q = \frac{\sigma_q}{\sigma_q^{stat}} \tag{4.16}$$

as new measures of erraticity. Fig. 4.8 shows the plots of $ln\Sigma_q$ as a function of q for q = 2-9 for both the pseudorapidity and azimuthal spaces. The straight lines in the plots represent the linear fits of the type

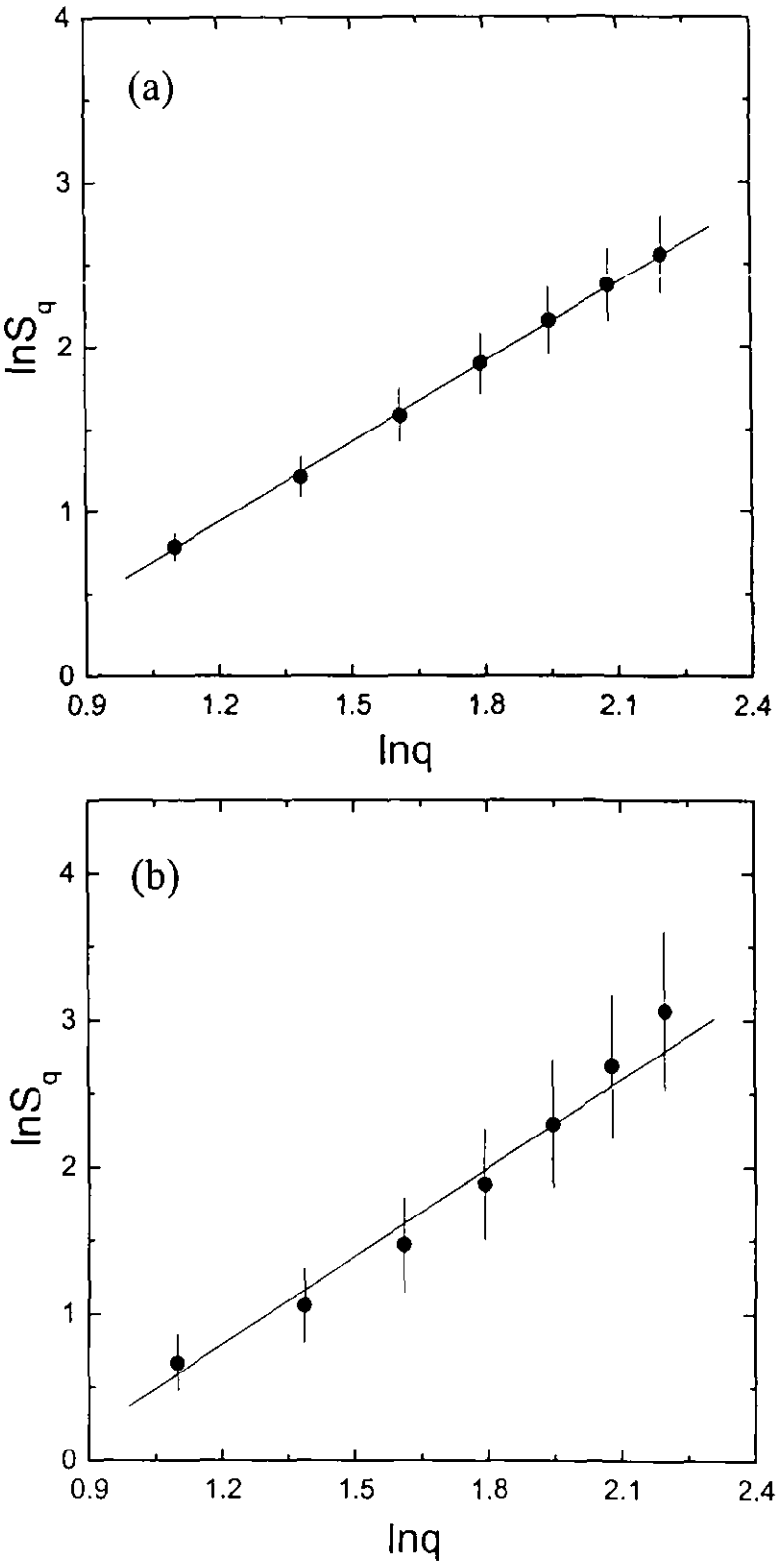

Fig. 4.7 Dependence of $\ln S_q$ on lnq for ^{28}Si-AgBr collisions at 14.6 AGeV. (a) η-space (b) ϕ-space.

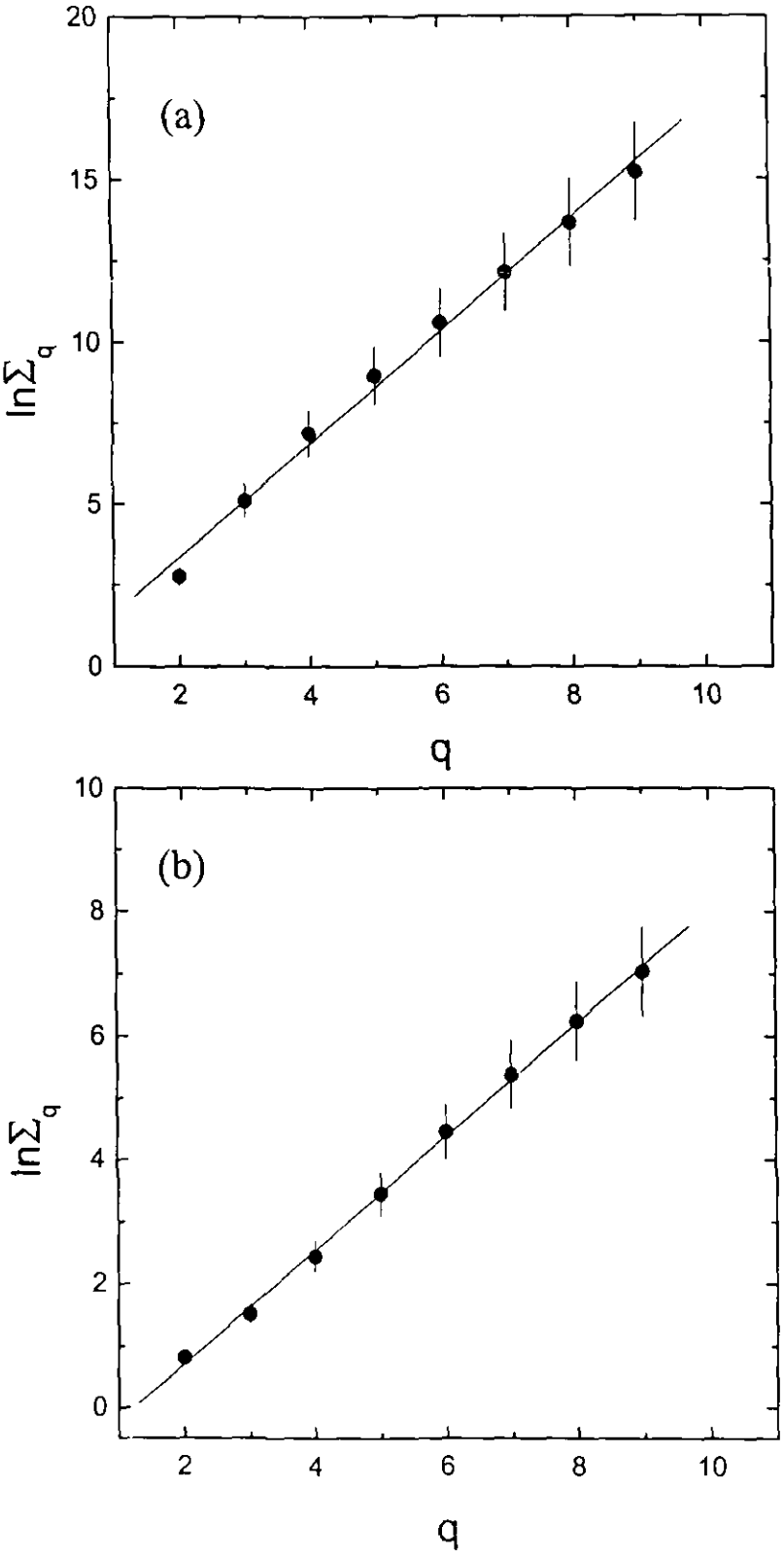

Fig. 4.8 Dependence of $\ln\Sigma_q$ on q for ^{28}Si-AgBr collisions at 14.6 AGeV. (a) η-space (b) ϕ-space.

$$\ln \Sigma_q = A' + \beta q , \qquad (4.17)$$

to the data points. From the figure, we again observe that Σ_q deviates from 1 and that Σ_q exhibits linear increase with the increase in q. The values of the slopes of the linear fits are β = 1.743± 0.057 and β = 0.917± 0.014 for the pseudorapidity and azimuthal spaces respectively.

Thus statistically significant measures of erraticity have been observed in the multiparticle production in ^{28}Si-AgBr collisions at 14.6 AGeV. Similar results have very recently been observed by M. R. Atayan et al (NA22 collaboration) [18] while analyzing the data on π^-p and K^+p collisions at 250 GeV/c and by Ghosh et al [20] analysed ^{32}S-AgBr collisions at 200 AGeV.

References

[1] T. H. Burnett et al., *Phys. Rev. Lett.* **50**, (1983) 2062.

[2] S G Matinyan et al. *Sov. Phys. JETP* **53**, (1981) 421.

[3] B Miller and A Trayanov *Phys. Rev. Lett.* **68**, (1992) 3387.

[4] C. Gong, *Phys. Rev.* **D49**, (1993) 2642.

[5] H. A. Cerdeira (ed.), Quantum Chaos, World Scientific Singapore. (1991).

[6] Zhen Cao and Rudolph C Hwa, *Phys. Rev. Lett.* **75**, (1995) 1268.

[7] Zhen Cao and Rudolph C Hwa, *Phys. Rev.* **D54**, (1996) 6674.

[8] Zhen Cao and Rudolph C Hwa, *Phys. Rev.* **D61**, (2000) 074011.

[9] R. C. Hwa, *Proc. 7th Int. Workshop on Multiparticle Production, Correl. and Fluctuations,* Nijmegen, Netherlands (1996) 302.

[10] R. C. Hwa, *Proc. XXVI Int. Sympos. On Multiparticle Dynamics,* Fero, Portugal (1996) 189.

[11] Rudolph C. Hwa and Qing-hui Zhang, *Phys. Rev.* **D62**, (2000) 014003; **nucl-th** / 0203022 (2002).

[12] A. Bialas and R. Peschanski, *Nucl. Phys.* **B273**, (1986) 703. *Nucl. Phys.* **B308**, (1988) 857.

[13] H. Leutwyler, *Proc. XXVI, Int. Conf. High Energy Phys.*, Dallas, (1992).

[14] Zhen Cao and Rudolph C. Hwa, *Phys. Rev.* **E56,** (1997) 326.

[15] A. Bialas and M. Gazdzicki. *Phys. Lett.* **B252**, (1990) 483.

[16] J. Fu, Y. Wu and L. Liu. *Phys. Lett.* **B472**, (2000) 161.

[17] Wang Shaoshun and Wang Zhaomin, *Phys. Rev.* **D57**, (1998) 3036.

[18] NA22 Collaboration. M. R. Atayan et al. *Phys. Lett.* **B558**, (2003) 29.

[19] NA22 Collaboration, M. R. Atayan et al. *Phys. Lett.* **B558**, (2003) 22.

[20] D. Ghosh et el, *Phys. Lett.* **B540**. (2002) 52.

CHAPTER V

Study of non-statistical fluctuations in the angular distribution of grey particles produced in ^{28}Si-AgBr collisions at 14.6 AGeV

5.1 Introduction

Unlike high energy elementary nucleon-nucleon collisions, where the produced shower particles are the only source to gather knowledge of collision dynamics, nucleus-nucleus collisions at relativistic energies offer further probes like the target nucleus and projectile nucleus fragments. However, the study of shower particles produced in relativistic nucleus-nucleus collisions has always been emphasized with a common belief that these particles are most informative about the collision dynamics and thus could be effective in revealing the underlying physics of high energy relativistic interactions. Since the physics of relativistic collisions is not conclusive, all the available probes need to be thoroughly studied towards the meaningful analysis of experimental data.

It has therefore been argued that the information about the non-statistical fluctuations could also be collected by studying the target associated knock out protons known as grey particles. The grey particles with range $L \geq 3$mm and velocity $0.7 > \beta \geq 0.23$ have energy 26 to 400 MeV. According to the evaporation model [1], these particles are the low energy part of the inter-nucleon cascade and they leave the nucleus during the passage of the incident nucleus. Since these grey particles along with shower particles are produced in the first stage of the collision, it is speculated that these particles may also carry some important information on the spatial patterns from event-to-event. Moreover, the study of grey particles will not only provide a unified description of the whole production process, but will also provide an additional parameter to understand the dynamics of particle production process.

The study of non-statistical fluctuations in the target associated particles was first carried out by Ploszajczak and Tucholski [2]. They investigated the

intermittent behaviour in nuclear fragmentation at intermediate energies by studying the bin size dependence of the normalized factorial moments. Takibaev et al. [3] analysed proton-nucleus interaction data at incident energies ranging from 67 to 400 GeV and demonstrated the existence of non-statistical fluctuations in the angular distribution of target associated particles. Similar observations have recently been reported by D. Ghosh et al [4] while studying the dynamical fluctuations in the azimuthal angle distribution of grey particles produced in ^{16}O-AgBr collisions at 60 AGeV and ^{32}S-AgBr collisions at 200 AGeV. In this chapter, we analyze the data related to the grey particles produced in ^{28}Si-AgBr collisions at 14.6 AGeV. Our objective is to see whether fluctuations of non-statistical origin exist in the angular distribution of these grey particles.

We have used two methods for this purpose: the scaled factorial moment method [5] and Takagi moment method [6]. These are the two most widely used methodologies for extracting information regarding the dynamical fluctuations. Using these two methods, the fluctuations in the angular distribution of grey particles in cosine and azimuthal spaces have been studied. Values of the parameters that quantify the scaling behaviour have been determined for both the spaces. Also the values of the generalized dimensions and multifractal specific heat, which are the consequences of the fractal structure, have been determined for both the spaces.

5.2 Takagi Method

The scaled factorial moment method has already been described in chapter III. Here we shall briefly discuss the Takagi methodology for studying the multifractal structure of multiplicity distributions [6]. Consider a process of

multiparticle production at some incident energy and the distribution in a phase space. A single event contains n grey particles distributed in the interval Δ. The particle multiplicity changes from event to event according to the distribution $Pn(\Delta)$. The interval Δ is divided into M equal bins, each of size $\delta = \Delta/M$. Let $Pn(\delta)$ be the multiplicity distribution in a single bin. It is assumed that $Pn(\delta)$ is independent of the location of the bin. Particles produced in Ω independent events are distributed in ΩM bins each of size δ. Let K be the total number of particles produced in Ω events and n_{ji} be the multiplicity of particles in the ith bin of the jth event. If the multifractal approach is applicable, then the quantity

$$T_q(\delta) = \ln \sum_{j=1}^{\Omega} \sum_{i=1}^{M} P_{ji}^{q} \qquad \text{for } q > 0 \tag{5.1}$$

behaves like a linear function of the logarithm of the resolution $R(\delta)$

$$T_q(\delta) = A_q + B_q \ln R(\delta), \tag{5.2}$$

where A_q and B_q are constants independent of q. P_{ji} is the normalized density defined as

$$P_{ji} = \frac{n_{ji}}{K} \tag{5.3}$$

If a linear behaviour is observed over a large range of $R(\delta)$, a generalized dimension may be defined as

$$D_q = \frac{B_q}{q-1} \tag{5.4}$$

When the number of events Ω is very large, Takagi [6] showed that the double sum of P_{ji}^{q} might be expressed as

$$\sum_{j=1}^{\Omega}\sum_{i=1}^{M} P_{ji}^{q} = \frac{\langle n^{q} \rangle}{\left(K^{q-1}\langle n \rangle\right)} \tag{5.5}$$

As the pseudorapidity distribution of the particles is assumed to be flat in the considered region, one can write

$$\langle n \rangle = \frac{K}{\Omega\Delta}\delta \tag{5.6}$$

On substituting equation 5.6 into equation 5.5 and taking log of both sides, we get

$$\begin{aligned} T_q(\delta) &= \ln \frac{\langle n^{q} \rangle}{\left(K^{q-1}(K/\Omega\Delta)\delta\right)} \\ &= \ln\langle n^{q}\rangle - \ln\delta - \ln K^{q-1}(K/\Omega\Delta) \\ &= \ln\langle n^{q}\rangle - \ln\delta + const. \end{aligned} \tag{5.7}$$

For the simplest choice of resolution $R(\delta) = \delta$, equation 5.2 becomes

$$T_q(\delta) = A_q + B_q \ln\delta. \tag{5.8}$$

On comparing relations 5.7 and 5.8, Takagi obtained the relation

$$\begin{aligned} \ln\langle n^{q}\rangle &= A_q + (B_q + 1)\ln\delta. \\ &= A_q + \{(q-1)D_q + 1\}\ln\delta. \end{aligned} \tag{5.9}$$

To check the validity of equation 5.9, Takagi plotted [6] $\ln\langle n^q \rangle$ as a function of $ln\delta$ for the experimental data [7-9]. Deviation from the linear behaviour was observed in the large pseudorapidity region. Takagi related the deviation to the non-flat behaviour of $dn/d\eta$ in the large η region (projectile and target fragmentation regions) and argued that $\langle n \rangle$ would be a better choice for $R(\delta)$ as $dn/d\langle n \rangle$ is flat by definition [10].

Choosing $R(\delta) = \langle n \rangle$, one can rewrite equation 5.9 as

$$\ln \langle n^q \rangle = A_q + \{(q-1)D_q + 1\} \ln \langle n \rangle. \qquad (5.10)$$

A linear behaviour of $\ln\langle n^q \rangle$ over a considerable range of $\ln\langle n \rangle$ would point towards a fractal structure. The generalized dimensions D_q for $q \geq 2$ can then be easily evaluated from the slopes of $\ln\langle n^q \rangle$ versus $ln\langle n \rangle$ plots. The generalized dimension D_1 for $q = 1$, which is known as the information dimension can be obtained from the relation

$$\frac{\langle n \ln n \rangle}{\langle n \rangle} = C_1 + D_1 \ln \langle n \rangle \qquad (5.11)$$

5.3 Results

Since the shape of the single particle density distribution is non-flat and the shape of the distribution influences the scaling behaviour of moments, we have used the cumulative variables $X_{cos\theta}$ and X_ϕ [10] instead of $cos\theta$ and ϕ. $cos\theta$ ranges from -1 to $+1$ and the azimuthal angle from is 0 to 2π. With the help of cumulative variable, the corresponding ranges for both $X_{cos\theta}$ and X_ϕ become 0 to 1.

5.3.1 F_q-moments

For the identification of intermittency pattern of fluctuations, if any, in the distribution of grey tracks obtained form ^{28}Si-AgBr collisions at 14.6 AGeV, we calculated the values of the scaled factorial moments for each event by using the following equation

$$F_q = M^{q-1} \sum_{m=1}^{M} \frac{n_m (n_m - 1) \cdots (n_m - q + 1)}{\langle N \rangle^q} \qquad (5.12)$$

for our data in $X_{cos\theta}$ and X_ϕ spaces. M, the number of bins into which the phase space interval is divided, varies from 2 to 20 for the present analysis. n_m is the multiplicity of grey particles in the mth bin and $\langle N \rangle$ is the average number of grey particles for all events. F_q values were calculated for all the events and were then averaged over to obtain $<F_q>$.

The plots of $ln<F_q>$ versus lnM for q = 2, 3 and 4 for both the cosine and ϕ spaces are shown in Fig. 5.1(a & b). From the figure, it is clear that $ln<F_q>$ exhibits a linear dependence on lnM in both the spaces. This implies that F_q-moments have a power law dependence on M. Values of the slopes ϕ_q known as intermittency indices determined from the least square fitting to the data points are listed in table 5.1. From the table it can be seen that ϕ_q values are significantly different from zero in both the spaces. Further. the ϕ_q values in both the cases increase with the increase in q. This indicates the presence of intermittent pattern and hence the non-statistical fluctuations in the distribution of grey particles. Ghosh et al [4,11] studied the behaviour of the scaled factorial moments of the distribution of grey particles produced in ^{16}O-AgBr

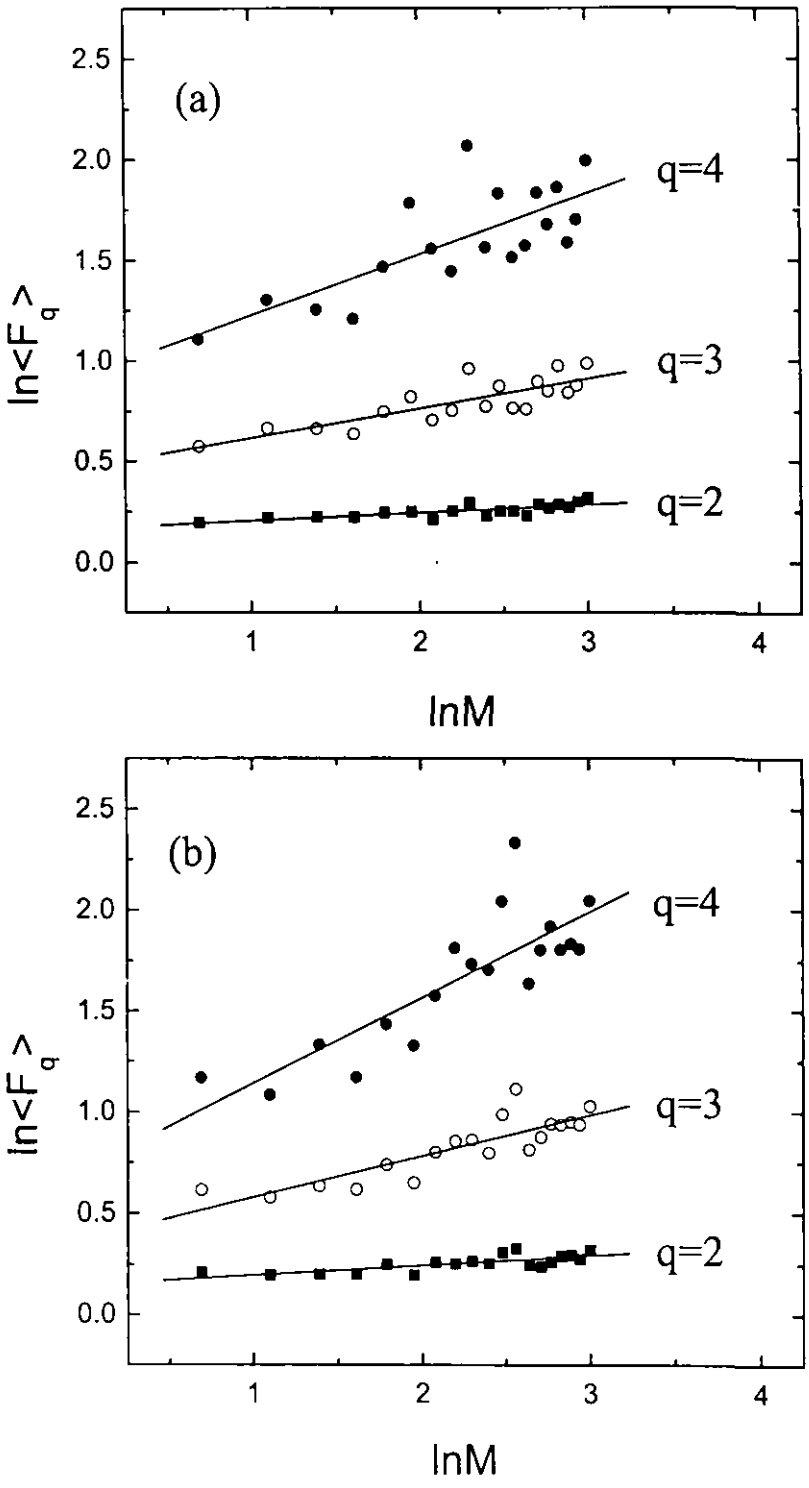

Fig. 5.1 Plots of $\ln\langle F_q \rangle$ versus lnM for grey particles produced in ^{28}Si-AgBr collisions at 14.6 AGeV. (a) cosine space (b) ϕ-space.

Table 5.1 Values of the slopes ϕ_q of $ln<F_q>$ versus lnM plots for grey particles for ^{28}Si-AgBr collisions at 14.6 AGeV in cosine and ϕ spaces.

q	$\phi_q(cos\theta)$	$\phi_q(\phi)$
2	0.039 ± 0.008	0.048 ± 0.009
3	0.148 ± 0.024	0.202 ± 0.029
4	0.303 ± 0.064	0.424 ± 0.068

Table 5.2 Values of the slopes K_q of $\ln\langle n^q \rangle$ versus $\ln\langle n \rangle$ plots for grey particles for ^{28}Si-AgBr collisions at 14.6 AGeV in cosine and ϕ spaces.

q	$K_q(cos\theta)$	$K_q(\phi)$
2	1.777 ± 0.012	1.785 ± 0.010
3	2.516 ± 0.021	2.549 ± 0.023
4	3.233 ± 0.031	3.302 ± 0.043

collisions at 60 AGeV and ^{32}S-AgBr collisions at 200 AGeV. They also found evidence of non-statistical fluctuations in the distribution of grey particles.

5.3.2 Takagi moments

To investigate the multifractal behaviour of grey particles produced in ^{28}Si-AgBr collisions at 14.6 AGeV through the method proposed by Takagi [6], the angular distribution interval $X_{cos\theta}$ (X_{ϕ}) ranging from 0 - 1 was subsequently decreased in steps of 0.05 and the values of $\langle n^q \rangle$ and $\langle n \ln n \rangle / \langle n \rangle$ were calculated for each interval. n is the multiplicity of grey particles in an event for the given interval. Fig. 5.2 (a & b) shows the dependence of $ln\langle n^q \rangle$ for q = 2, 3 and 4 on $ln\langle n \rangle$ in the cosine and ϕ spaces respectively. From the figure, we see that for the whole range of $\langle n \rangle$, a linear increase of $\ln\langle n^q \rangle$ with $\ln\langle n \rangle$ is observed in both the plots. This linear dependence is an evidence of self-similarity in the distribution of grey particles. The values of the slopes K_q for different values of q were obtained by fitting the relation

$$\ln\langle n^q \rangle = A_q + K_q \ln\langle n \rangle, \tag{5.13}$$

to the data points. These K_q values are listed in table 5.2. In both the spaces we observe that K_q increases with increase in q. In Fig. 5.3 (a & b), we plot $\langle n \ln n \rangle / \langle n \rangle$ as a function of $ln\langle n \rangle$ for both the spaces. The slopes of the plots give the values of D_1, the information dimension.

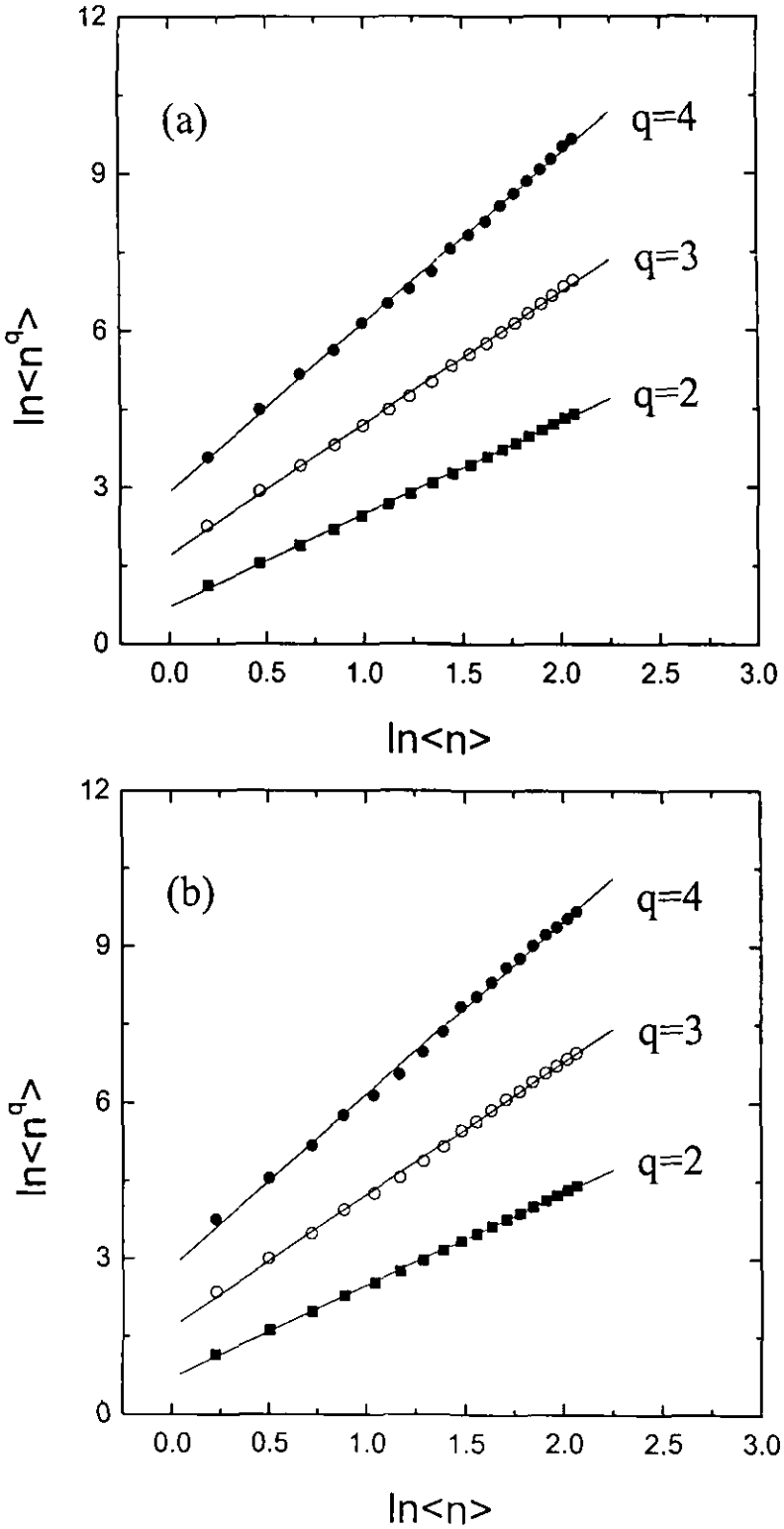

Fig. 5.2 Plots of $\ln\langle n^q\rangle$ versus $\ln\langle n\rangle$ for grey particles produced in ^{28}Si-AgBr collisions at 14.6 AGeV. (a) cosine space (b) ϕ-space.

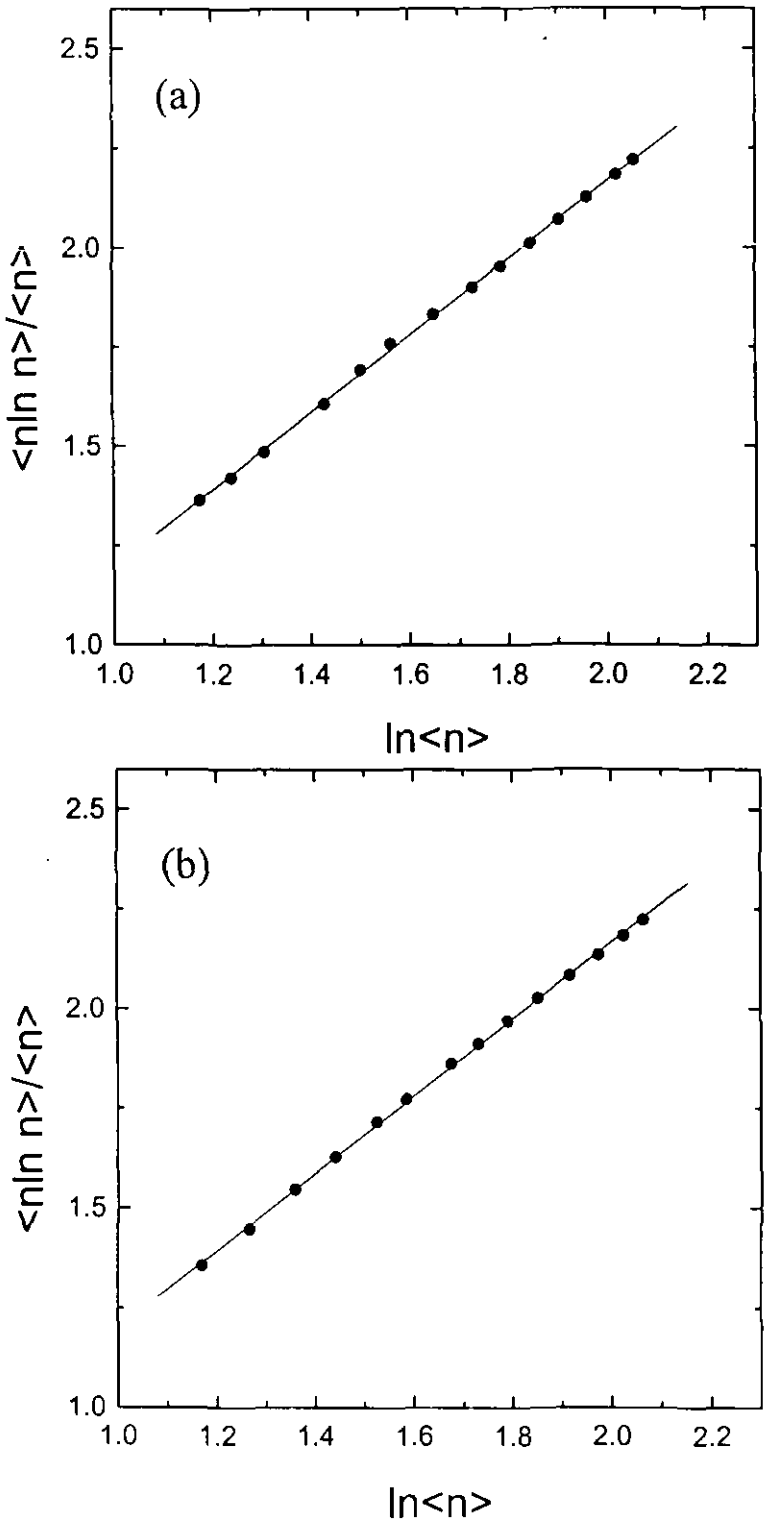

Fig. 5.3 Plots of <nln n>/<n> versus ln<n> for grey particles produced in ^{28}Si-AgBr collisions at 14.6 AGeV. (a) cosine space (b) ϕ-space.

5.3.3 Generalized dimensions

According to the theory of fractals, the self-similar systems are characterized by the generalized dimensions D_q. In the last section, we observed that the moments determined by the scaled factorial method and Takagi method exhibit power law dependences, thereby reflecting the self-similar property of multiparticle-production-process. This implies that the generalized dimensions can be obtained from both the analyses, using the following relations

$$D_q = 1 - \frac{\phi_q}{(q-1)} \tag{5.14}$$

$$D_q = \frac{K_q - 1}{(q-1)} \tag{5.15}$$

Values of D_q for our data were calculated from equations 5.14 and 5.15 in both the cosine and ϕ spaces. These values are presented in tables 5.3 and 5.4. In table 5.4, we also present the values of information dimension D_1 obtained from the slopes of $\langle n \ln n \rangle / \langle n \rangle$ versus $ln\langle n \rangle$ plots (Fig. 5.3 (a & b)). It is clear from table 5.3 that D_q values obtained from F_q-moment analysis in the cosine space are greater than the corresponding values in the azimuthal space. However, such a trend is not observed in D_q values obtained from the Takagi method. A similar result has been obtained by other investigators also [4]. D_q values not only depend on the space in which the analysis is carried out but also on the method of analysis. Further, it can be seen that D_q values in each case decrease with the increase in q. This is an evidence of multifractal structure in the distribution of target-associated knockout protons produced in ^{28}Si-AgBr collisions at 14.6 AGeV.

Table 5.3 Values of the generalized dimensions D_q determined from F_q –moment analysis for ^{28}Si-AgBr collisions at 14.6 AGeV in cosine and ϕ spaces.

F_q –moment analysis		
q	$D_q(cos\theta)$	$D_q(\phi)$
2	0.961 ± 0.008	0.952 ± 0.009
3	0.926 ± 0.012	0.891 ± 0.015
4	0.899 ± 0.021	0.859 ± 0.023

Table 5.4 Values of the generalized dimensions D_q determined from Takagi–moment analysis for ^{28}Si-AgBr collisions at 14.6 AGeV in cosine and ϕ spaces.

Takagi –moment analysis		
q	$D_q(cos\theta)$	$D_q(\phi)$
1	0.968 ± 0.007	0.967 ± 0.006
2	0.777 ± 0.012	0.785 ± 0.010
3	0.758 ± 0.011	0.775 ± 0.012
4	0.744 ± 0.010	0.767 ± 0.014

5.3.4 Multifractal specific heat

Recently Bershadskii [12] showed that Bernoulli distribution appears in natural way when transition from mono-fractality to multifractality is studied. Starting from the definition of G_q-moments [13], he derived the following relation

$$D_q = D_\alpha + c\frac{\ln q}{q-1} \tag{5.16}$$

for the multifractal Bernoulli fluctuations. In the above relation, D_q is the generalized dimension of order q and c is a constant. The mono-fractality to multifractality transition corresponds to $c = 0$ to a finite non-zero value of c. If the thermodynamical interpretation of the multifractality is used, then c can be interpreted as the multifractal specific heat of the system [14]. Bershadskii [12] analysed the data on nucleus-nucleus collisions at various energies and found that equation 5.16 gives a good fit to the data. We have also determined the multifractal specific heat for our data on grey particles produced in ^{28}Si-AgBr collisions at 14.6 AGeV using different sets of D_q values. Fig. 5.4 (a & b) shows the plots of D_q, obtained from F_q-analysis as a function of *lnq/(q-1)* for both the cosine and ϕ spaces. Straight lines are the linear fits to the data points and these fits indicate a good agreement between our data and the multifractal Bernoulli representation. The slopes of the fitted lines, which give the values of the multifractal specific heat c for our data are 0.266 ± 0.018 and 0.401 ± 0.025 for the cosine and ϕ spaces respectively.

Fig 5.5 (a & b) shows the plots of D_q, obtained from Takagi method as a function of *lnq/(q-1)* for both the cosine and ϕ spaces. The values of c, the slopes of fitted lines, in this case are 0.141 ± 0.007 and 0.076 ± 0.002 for the

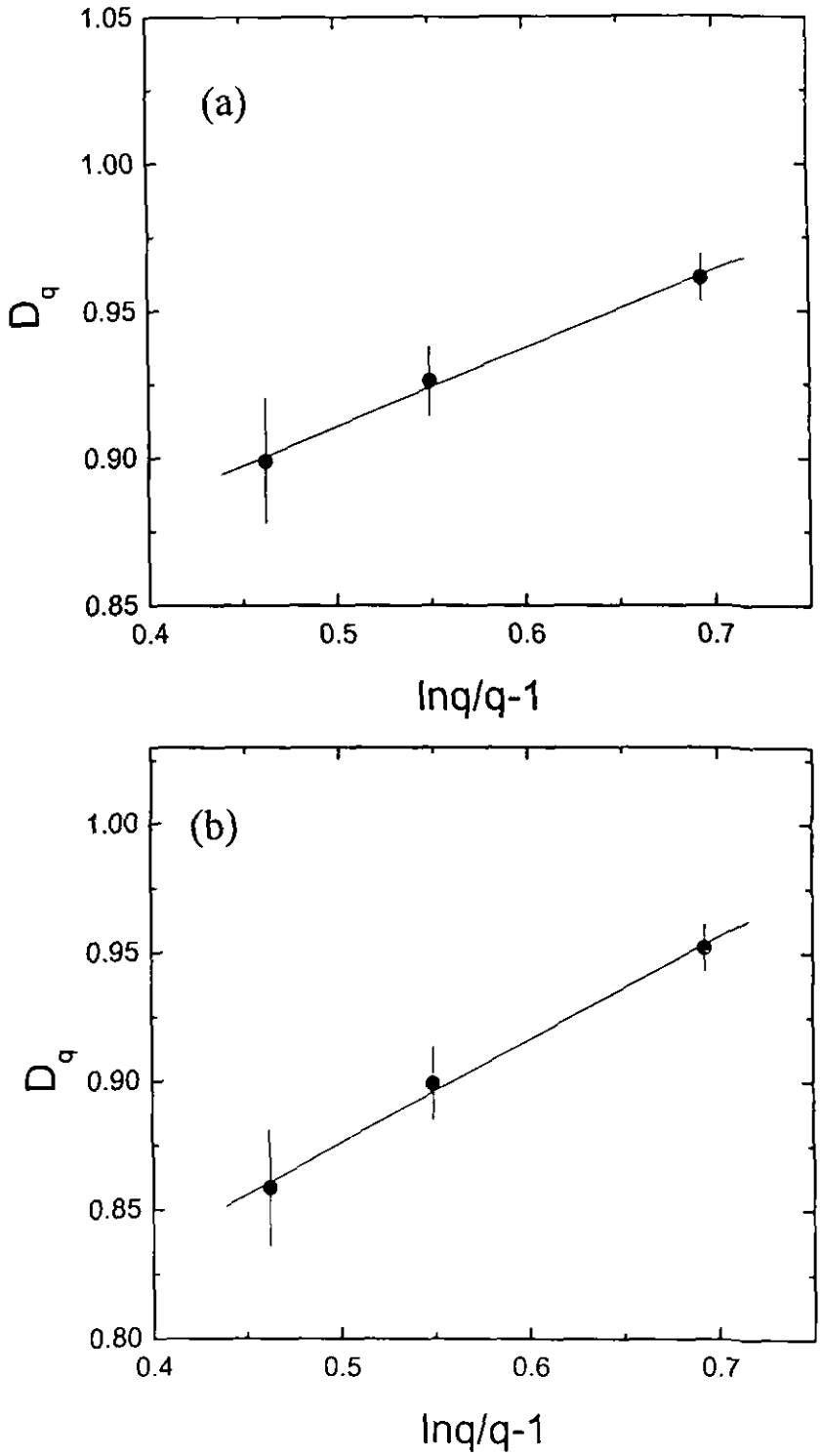

Fig. 5.4 Dependence of the generalized dimension D_q determined by F_q-moment method on lnq/(q-1) for ^{28}Si-AgBr collisions at 14.6 AGeV. (a) cosine space (b) ϕ-space.

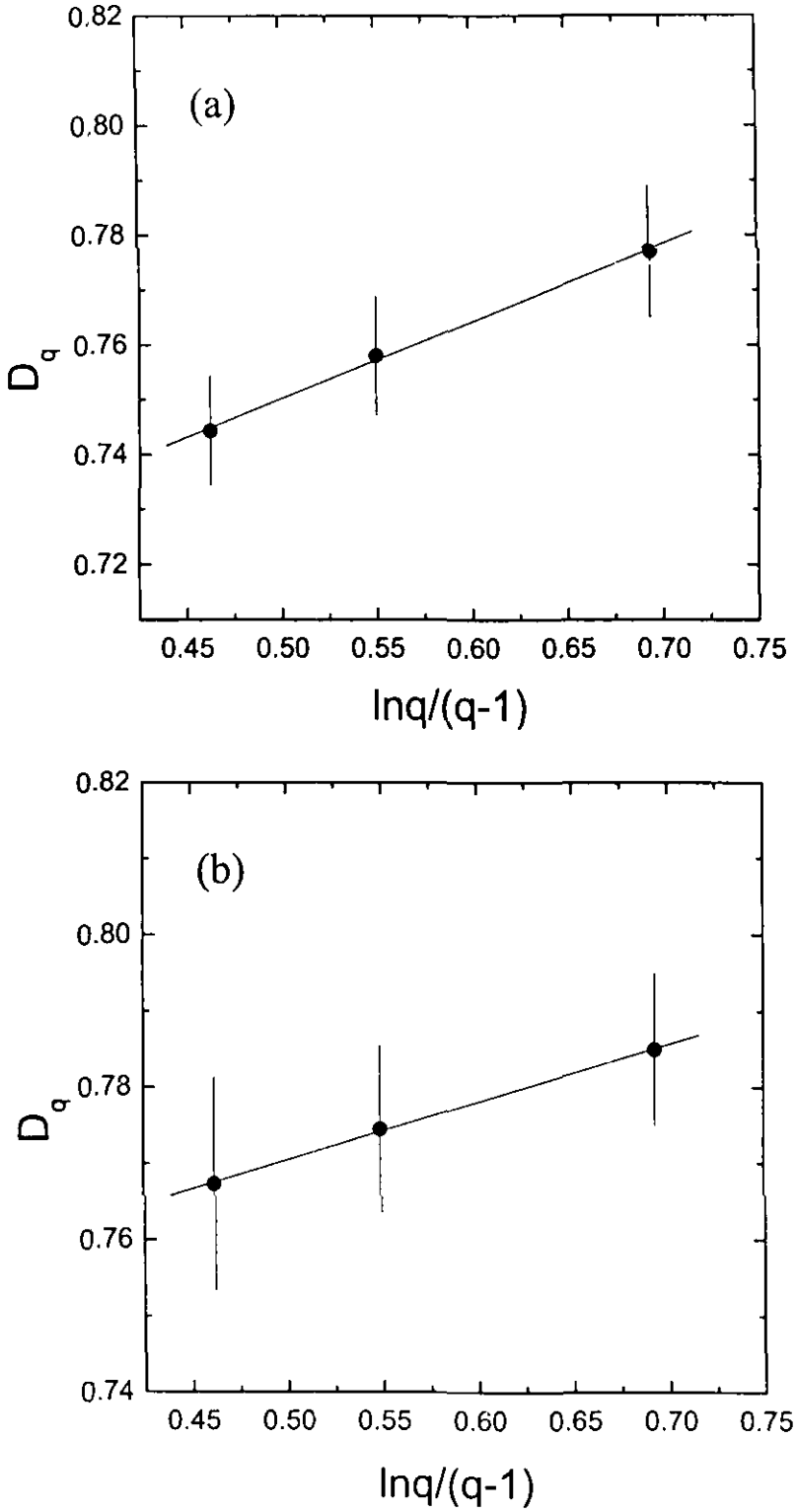

Fig. 5.5 Dependence of the generalized dimension D_q determined by Takagi method on lnq/(q-1) for ^{28}Si-AgBr collisions at 14.6 AGeV. (a) cosine space (b) ϕ-space.

two spaces respectively. Like D_q values, the values of c also depend on the method of analysis and the phase space in which the analysis is done.

Therefore, from the present investigation we conclude that fluctuations of non-statistical origin are present in the distribution of grey particles produced in ^{28}Si-AgBr collisions at 14.6 AGeV. By using the scaled factorial moment F_q and Takagi moment methods, fractal structures are observed in our data in the both cosine and ϕ spaces. This in turn reflects a self-similar behaviour in the production of these target protons. The generalized dimension D_q and the multifractal specific heat 'c' have been determined from both the analyses for both the spaces. Differences in the values of D_q as well as c from the two methods are mainly due to the difference in the definitions of these moments.

References

[1] C. F. Powel, P. H. Fowler and D. H. Perkins,
The study of elementary particles by Photographic method Pergamon, Oxford (1959) 450-464.

[2] M. Ploszajczak and A. Tucholski, *Phys. Rev. Lett.* **65**, (1990) 1539.

[3] Zh. S. Takibaev et al., *Sov. J. Nucl. Phys.* **47**, (1988) 282.

[4] D. Ghosh et al., *Europhys. Lett.* **48**, (1999) 508;
Int. J. Mod. Phys. **A13**, (1999) 2091.

[5] A .Bialas and R. Peschanski, *Nucl. Phys.* **B273**, (1986) 703.

[6] Fujio Takagi, *Phys. Rev. Lett.* **72**, (1994) 32.

[7] UA1 Collaboration, *Z. Phys.* **C43**, (1989) 357.

[8] TASSO Collaboration, *Z. Phys.* **C45**, (1989) 159.

[9] DELPHI Collaboration, *Z. Phys.* **C52**, (1991) 271.

[10] A .Bialas and M. Gazdzicki, *Phys. Lett.* **B252**, (1990) 483.

[11] D. Ghosh et al, *Phys. Rev.* **C66**, (2002) 047901.

[12] A. Bershadskii, *Phys. Rev.* **C59**, (1999) 364.

[13] R. C. Hwa, *Phys. Rev.* **D41**, (1990) 1456.

[14] E. Stanely and P. Meakin, *Nature* **335**, (1988) 405.

CHAPTER VI

Summary and conclusions

Relativistic heavy ion collisions provide an experimental setting for studying the exotic behaviour of the matter. It has been suggested that the strongly interacting matter at high energy densities produced in these collisions may undergo a phase transition to quark-gluon plasma (QGP). The QGP formation could cause large fluctuations in phase space, which in turn may result in large fluctuations in the measured particle densities. In the present work, we made an attempt to gain some insight into these density fluctuations of multiparticle production seen in the heavy ion collisions through the examination of factorial moments. Emulsion experiments are well suited for this type of analysis as the production angles of the produced particles are measured with high precision. Emulsion experiments also have the advantage that the same detector design can be used at all the experimental sites, so that experiments which cover a wide range of energies can be used without the use of differing detector corrections, which could affect the required signals.

From our systematic study of the scaled factorial moments of the pseudorapidity and azimuthal angle distributions of the secondary particles produced in silicon-emulsion collisions at 14.6 AGeV, a power law dependence of F_q on M, that is, an intermittency pattern is observed in both the spaces. A similar trend is followed in the two- dimensional space. The values of the intermittency indices ϕ_q obtained from the slopes of the plots increase with the increase in q for all the three cases and the two dimensional ϕ_q are larger than the one dimensional ϕ_q for all values of q. Further, the values of ϕ_q/ϕ_2 for both one and two dimensional phase spaces show an increase with the increase in q, which means that the factorial moments follow a generalized power law.

On investigating the behaviour of λ_q as a function of intermittency index ϕ_q for various M ranges, a λ_q minimum is observed in both the pseudorapidity and azimuthal spaces. This means that there is a certain value $q = q_c$ at which the multiparticle system behaves as a mixture of two states. On either side of this critical value, the multiparticle system behaves differently, which is an indication of non-thermal phase transition in the multiparticle production process in ^{28}Si-AgBr collisions at 14.6 AGeV.

Moreover, on studying the two dimensional $(\eta\text{-}\phi)$ $ln\langle F_2\rangle$ versus lnM plots with different values of Hurst exponent H, we found that the two dimensional second order factorial moment exhibits an upward bending as a function of partition of space. This upward bending, however, vanishes at H = 2.5 or 3.0. This means that only when we use the right value of H, that is, the proper partition along the longitudinal and perpendicular directions, in the analysis can the superposition of the contributions from the elementary collisions in the nucleus-nucleus collisions be correctly accounted for. A parameter 'a' is introduced to characterize the degree of upward bending. Using this parameter, it is found that the heavier are the colliding nuclei, the stronger is the upward bending, in consistence with the fact that the number of elementary collisions is larger for heavier colliding nuclei. If QGP is formed, then there will be no elementary collisions. This in turn will lead to vanishing of the superposition effect due to the contribution of elementary collisions in nucleus-nucleus collisions. Under such conditions, the upward bending in the two dimensional second order factorial moment plots is not likely to be seen. Thus study of the nuclear effect in nucleus-nucleus collisions could be used as another indirect test for QGP formation.

In the fourth chapter, we studied the erraticity behaviour of multiparticle production process through the moment of moments $C_{p,q}$ analysis. Erraticity measure is a capture of fluctuations that have been lost in the normalized factorial moments while averaging over all the bins and events. From this study we find that our data exhibit large fluctuations of factorial moments from event to event. A comparison of results on moment of moments $C_{p,q}$ and other erraticity parameters with those obtained for the generated uncorrelated events indicates that the contribution of the statistical fluctuations to the observed fluctuations in our data is very small. Further, a comparison of our results with those obtained for the FRITIOF events suggests that only a part of the observed fluctuations could be explained by the FRITIOF generator. There are additional fluctuations, which the FRITIOF generator fails to explain. At present we do not know what mechanism causes these fluctuations in heavy ion collisions. However, the method used in the present work is very effective in studying the non-statistical fluctuations in the event factorial moments in relativistic heavy ion collisions.

The fact that the values of the entropy index for different samples of our data are positive and very large as compared to the values obtained for the generated uncorrelated events indicates that the multiparticle production in ^{28}Si-emulsion collisions at 14.6 AGeV is chaotic in nature.

On studying the erraticity of rapidity gaps, the method proposed for low multiplicity events, we observe that both the erraticity measures S_q and Σ_q deviate significantly from 1 for both the pseudorapidity and azimuthal angle spaces and that both S_q and Σ_q increase linearly with the increase in q. This means that significant event-to-event fluctuations are present in the multiparticle production in ^{28}Si- AgBr collisions at 14.6 AGeV. The values of

erraticity measures obtained in the present investigation would provide valuable input to the models of multiparticle production.

In chapter five, we dealt with the non-statistical fluctuations in the angular distribution of target associated knockout protons. These particles are produced soon after the pions are produced and are believed to carry relevant information about the collision mechanism. By using the scaled factorial moment F_q and Takagi moment methods, fractal structures are observed in our data for both the cosine and ϕ spaces. This in turn reflects the self-similar behaviour in the production of target protons. The generalized dimension D_q and the multifractal specific heat 'c' have been determined from both the analyses for both the spaces. Differences in the values of D_q and c from the two methods used in our analyses are mainly due to the difference in the definitions of these moments.

Finally, we conclude that moment analyses of particle density distributions in one dimensional pseudorapidity space and two dimensional combined pseudorapidity–azimuthal angle space provide useful information about the mechanism of multiparticle production process. Experiments at RHIC and LHC will provide us interacting systems with much higher energy densities and larger formation times. If then large fluctuations induced in particle densities from the phase transition from QGP to hadronic matter are observed, then the comparison of moment analyses at RHIC and LHC energies with those at AGS and SPS energies may provide us one of the signals needed to establish the existence of the phase transition to a QGP state.